Technology Collaboration Programme
by IEA

Technology Collaboration Programme on Heat Pumping Technologies (HPT TCP)

Annex 49

Simulation of System integration, Design and Control for heat pumps in nZEB

Final Report Part 3

Editor:
Carsten Wemhoener
Institute for Energy Technology
Eastern Switzerland University
of Applied Sciences, Rapperswil
carsten.wemhoener@ost.ch

December 2020
Report no. HPT-AN49-4

Published by Heat Pump Centre
c/o RISE – Research Institutes of Sweden
Box 857, SE-501 15 Borås
Sweden
Phone +46 10 16 53 42
Website https://heatpumpingtechnologies.org

Production Heat Pump Centre, Borås, Sweden

ISBN 978-91-89385-30-6
Report No. HPT-AN49-4

Preface

This project was carried out within the Technology Collaboration Programme on Heat Pumping Technologies (HPT TCP), which is a Technology Collaboration Programme within the International Energy Agency, IEA.

The IEA

The IEA was established in 1974 within the framework of the Organization for Economic Cooperation and Development (OECD) to implement an International Energy Programme. A basic aim of the IEA is to foster cooperation among the IEA participating countries to increase energy security through energy conservation, development of alternative energy sources, new energy technology and research and development (R&D). This is achieved, in part, through a programme of energy technology and R&D collaboration, currently within the framework of nearly 40 Technology Collaboration Programmes.

The Technology Collaboration Programme on Heat Pumping Technologies (HPT TCP)

The Technology Collaboration Programme on Heat Pumping Technologies (HPT TCP) forms the legal basis for the implementing agreement for a programme of research, development, demonstration and promotion of heat pumping technologies. Signatories of the TCP are either governments or organizations designated by their respective governments to conduct programmes in the field of energy conservation.

Under the TCP, collaborative tasks, or “Annexes”, in the field of heat pumps are undertaken. These tasks are conducted on a cost-sharing and/or task-sharing basis by the participating countries. An Annex is in general coordinated by one country which acts as the Operating Agent (manager). Annexes have specific topics and work plans and operate for a specified period, usually several years. The objectives vary from information exchange to the development and implementation of technology. This report presents the results of one Annex.

The Programme is governed by an Executive Committee, which monitors existing projects and identifies new areas where collaborative effort may be beneficial.

Disclaimer

The HPT TCP is part of a network of autonomous collaborative partnerships focused on a wide range of energy technologies known as Technology Collaboration Programmes or TCPs. The TCPs are organised under the auspices of the International Energy Agency (IEA), but the TCPs are functionally and legally autonomous. Views, findings and publications of the HPT TCP do not necessarily represent the views or policies of the IEA Secretariat or its individual member countries.

The Heat Pump Centre

A central role within the HPT TCP is played by the Heat Pump Centre (HPC).

Consistent with the overall objective of the HPT TCP, the HPC seeks to accelerate the implementation of heat pump technologies and thereby optimise the use of energy resources for the benefit of the environment. This is achieved by offering a worldwide information service to support all those who can play a part in the implementation of heat pumping technology including researchers, engineers, manufacturers, installers, equipment users, and energy policy makers in utilities, government offices and other organisations. Activities of the HPC include the production of a Magazine with an additional newsletter 3 times per year, the HPT TCP webpage, the organization of workshops, an inquiry service and a promotion programme. The HPC also publishes selected results from other Annexes, and this publication is one result of this activity.

For further information about the Technology Collaboration Programme on Heat Pumping Technologies (HPT TCP) and for inquiries on heat pump issues in general contact the Heat Pump Centre at the following address:

Heat Pump Centre
c/o RISE - Research Institutes of Sweden
Box 857, SE-501 15 BORÅS, Sweden
Phone: +46 10 516 53 42
Website: https://heatpumpingtechnologies.org

Design and Integration of Heat pumps for nearly Zero Energy Buildings

Final report IEA HPT Annex 49 part 3

Simulation of System integration, Design and Control for heat pumps in nZEB

Carsten Wemhoener (Editor)
IET Institute for Energy Technology
OST - Eastern Switzerland University Applied Sciences, Rapperswil
carsten.wemhoener@ost.ch

Report Annex 49 part 3 Simulation

December 2020

International Energy Agency
Heat Pumping Technologies

Imprint

IEA HPT Annex 49 "Design and integration of Heat pump for nearly Zero Energy Buildings"

The work presented here is a contribution to the Annex 49 in the Heat Pumping Technologies (HPT) Technical Collaboration Programme (TCP) of the International Energy Agency (IEA)

Operating Agent (Switzerland):
IET Institute for Energy Technology, HSR University of Applied Sciences Rapperswil
(now: OST – Eastern Switzerland University of Applied Sciences, Rapperswil)
Prof. Carsten Wemhöner, carsten.wemhoener@ost.ch, Lukas Rominger

Austria:
Unit for energy efficient building UIBK, University of Innsbruck, Austria
Dr. Fabian Ochs Fabian.Ochs@uibk.ac.at, Mara Magni Mara.Magni@uibk.ac.at
IWT Institute of Thermal Engineering, Graz Technical University, Austria:
DI Dr. tech. Andreas Heinz andreas.heinz@tugraz.at
AIT Austrian Insitute of Technology
Philip Horn, Philip.Horn@ait.ac.at, Tim Selke, tim.selke@ait.ac.at

Belgium:
Institute of Aero-Thermo-Mechanics, ULB (Université Libre de Bruxelles), Brussels, Belgium
Prof. Dr. Patrick Hendrick, patrick.hendrick@ulb.ac.be

Germany:
Technical University Georg-Simon Ohm, Nuremberg
Prof. Dr. Arno Dentel, Arno.Dentel@th-nuernberg.de,
Christina Betzold, Christina.Betzold@th-nuernberg.de
Institute of Building Services and Energy Design IGS, University of Braunschweig,
(now: Steinbeis-Innovationszentrum energie+ (SIZ energie+))
Franziska Bockelmann, franziska.bockelmann@stw.de
TEB GmbH, Vaihingen/Enz
Dr. Thomas Dippel, dippel@teb-online.de

Norway:
SINTEF Community, Trondheim, Norway
Øystein Rønneseth, oystein.ronneseth@sintef.no, Maria Justo Alonso, maria.j.alonso@ntnu.no
NTNU
Prof. Dr. Laurent Georges, laurent.georges@ntnu.no, Dr. John Clauß, john.clauss@ntnu.no
COWI AS
Dr. Ing. Jørn Stene, jost@cowi.no

Sweden:
RISE Research Institutes of Sweden, Borås
Ola Gustafsson, ola.gustafsson@ri.se

United Kingdom:
Renewable Energy, Glen Dimplex, UK
Martin Betz, martin.betz@glendimplex.co.uk

USA:
Oak Ridge National Laboratory, Oak Ridge, Tennessee, USA
Van D. Baxter, baxtervd@ornl.gov, Ahmad Abuheiba, abuheibaag@ornl.gov
National institute of Standards and Technology (NIST), Gaithersburg, Maryland, USA
W. Vance Payne, Ph.D., vance.payne@nist.gov, Brian P. Dougherty, brian.dougherty@nist.gov
Center for Environmental Energy Engineering (CEEE), University of Maryland
Prof. Reinhard Radermacher, Ph.D., raderm@umd.edu, Jiazhen Ling, Ph.D., jiazhen@umd.edu
Center for Sustainability in the Built Environment (City@UMD), University of Maryland, College Park, Maryland, USA
Prof. Jelena Srebric, Ph.D., jsrebric@umd.edu

IEA HPT Annex 49 is a corporate research project on heat pump application in Nearly Zero Energy Buildings
The project is accomplished in the Heat Pump Technologies (HPT) Technology Collaboration Programme (TCP) of the International Energy Agency (IEA).
Internet: http://www.heatpumpingtechnologies.org/annex49

Abstract

The IEA HPT Annex 49 "Design and integration of heat pumps for nearly Zero Energy Buildings" deals with the heat pump application as core component of the HVAC system for nearly or Net Zero energy buildings (nZEB/NZEB) and is structured in the following Tasks:

- Task 1. State of the art in different countries
- Task 2: Integration options for multifunctional heat pumps in nZEB
- Task 3: Field monitoring of marketable and prototype heat pumps in nZEB
- Task 4: Design and control of integrated heat pumps for nZEB

A focus of the Annex 49 contributions of the participating countries was the detailed monitoring of heat pump system monitoring in more than 15 different types of nZEB which is documented in the Report Annex 49 part 2. For many of the monitored system, though, also accompanying in depth investigations by simulations have been performed, Results are given in this report based on the integration, design or control of the heat pump.

A focus of these accompanying investigations was set on smart integration of the heat pump with other building components, in particular thermal and electric storages. For the building Berghalde, a single family house with large PV installation, both self-consumption and grid supportive operation have been investigated by adapted control as well as thermal and electric storage design. Electric storage can notably increase the self-consumption, but is currently not economically feasible. Moreover, control strategies and thermal storage up to 2,500 l have the potential to increase self-consumption. Design diagrams have been derived based on the investigations.

For 8 single family terraced houses in the HerzoBase project, rule-based control has been applied for the load management of the central battery as well as central and decentralized thermal storages. Simulations confirm that grid load peaks could be reduced up to 24% in winter month. While direct use of PV electricity could be increased up to 21%, grid feed-in could be reduced by 10% and battery charging by 11%.

At the TU Graz, the storage of solar heat produced by solar thermal or solar PV in the building structure has been investigated. It was found that thermally-activated building system can offer a favourable option to reach high solar fraction both for PV and solar thermal yield.

At UIBK, two multi-family passive houses have been modelled in detail and validated with monitoring data of four year measurements. The validated models have been used to perform detailed investigations on desuperheater use, system configuration variants and optimization potentials of the nZE balance. Results confirm that with an extended PV-area instead of solarthermal, the nZE balance can be reached. A desuperheater use at low space heating demands of the building does not promise high performance increase in this configuration due to a reduced running time.

In Norway, the load management has been assessed from the grid perspective. By the control of the heat pump the CO_2-balance of electricity use can be improved, but this may counteract with electricity pricing.

At HSR Rapperswil, the design of capacity-controlled heat pumps for the application in nZEB has been investigated. It was found that a rather scarce design yield higher part load fractions at high COP values. Together with the NTNU, smart control has been tested. Results are ambiguous, since costs can be reduced, but at the same time energy use increases.

Results of the detailed analysis of heat pump application in nZEB underlines the suitability of the heat pump as heat generator in nZEB. In particular by the on-site electricity production in nZEB and the optimised building loads which can be covered with low supply temperatures increase the heat pump performance even more than in other buildings. Furthermore, as a main electricity consumer, the heat pump unlocks the potential to increase PV self-consumption and energy flexibility by demand response. However, meeting ambitious nZEB targets still need optimised building operation, which has been addressed by the accomplished detailed studies contributed to Annex 49.

Contents

System boundaries and characteristic numbers

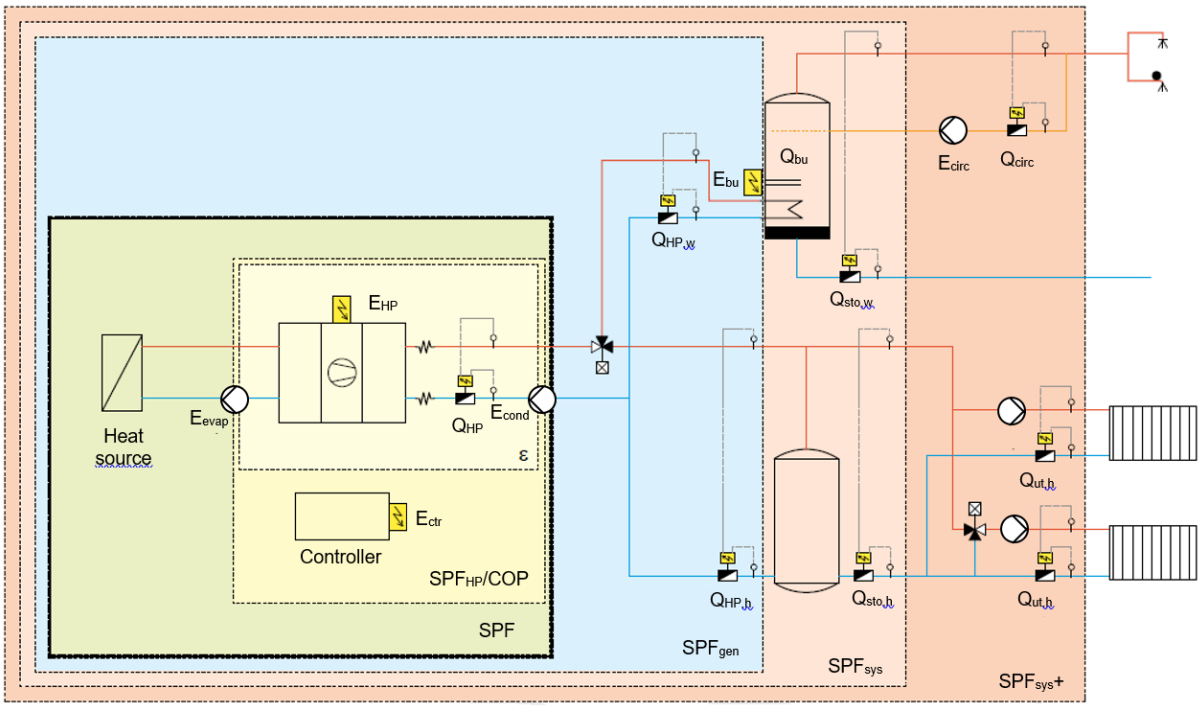

Power related

Performance Number (ε)

$$\varepsilon = \frac{\dot{Q}_{HP}}{P_{el}}$$

Coefficient of Performance (COP)

$$COP = \frac{\dot{Q}_{HP}}{P_{HP} + P_{evap,int} + P_{cond,int} + P_{ctr} + P_{defrost}}$$

Energy related

Seasonal Performance factor heat pump (SPF_{HP})

$$SPF_{HP} = \frac{Q_{HP}}{E_{HP} + E_{evap,int} + E_{cond,int} + E_{ctr} + E_{defrost} + E_{carter}}$$

Seasonal Performance factor heat pump (SPF_{HP})

$$SPF = \frac{Q_{HP}}{E_{HP} + E_{src} + E_{cond,int} + E_{ctr} + E_{defrost} + E_{carter}}$$

Seasonal Performance factor generator (SPF_{gen})

$$SPF_{gen} = \frac{Q_{HP} + E_{bu}}{E_{HP} + E_{src} + E_{sink} + E_{ctr} + E_{defrost} + E_{carter} + E_{bu} + E_{bu,aux}}$$

Seasonal Performance factor generator (SPF_{sys})

$$SPF_{sys} = \frac{Q_{sto}}{E_{HP} + E_{src} + E_{sink} + E_{ctr} + E_{defrost} + E_{carter} + E_{bu} + E_{bu,aux}}$$

Seasonal Performance factor generator (SPF_{sys+})

$$SPF_{sys+} = \frac{Q_{ut}}{E_{HP} + E_{src} + E_{sink} + E_{ctr} + E_{defrost} + E_{carter} + E_{bu} + E_{bu,aux} + E_{h,aux} + E_{w,aux}}$$

Figure 1: Definition of system boundaries for the seasonal performance factor (SPF) (source: SFOE)

The closest system boundary for the heat pump is the performance number ε, which is an instantaneous values of the ratio between the heating power and the electric compressor power.
The more commonly known value from standard testing is the Coefficient of Performance (COP) which additionally considers the auxiliary power inside the system boundary of the unit, namely the internal power of source and sink pump or fan to overcome the pressure drop inside the unit, the control, the defrosting in case of air-to-water heat pump and an additional carter heating. If the COP is integrated over time, the SPF_{HP}/COP results in the boundary of the COP.
The SPF_{HP} however, is also often defined with the external pressure drops on the source side, so the total source is included in the definition.
The heat generator seasonal performance factor SPF_{gen} considers the heat produced by all generator divided by the total electricity and back-up heaters and thus characterises the total heat production side without taking into account system losses.
The system seasonal performance factor SPF_{sys} in contrast relates the used heat, i.e. the produced heat minus storage, distribution and emission losses to the total expenditure for the heat generation. The SPF_{sys} only includes storage losses, while the SPF_{sys+} includes the total system losses including distribution and emission. Thus, the system seasonal performance factor gives the overall performance of the whole system.
The single boundaries for the SPF can also be separated by the energy use, i.e. according to the building services space heating, DHW, space cooling and dehumification.

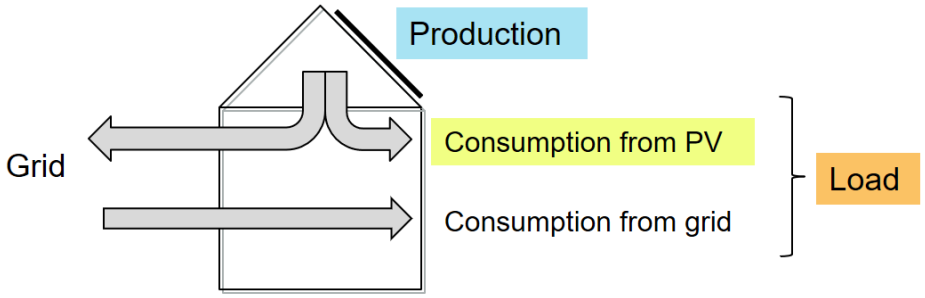

$$load\ cover\ factor = \frac{W_{el,\ consumption\ of\ local\ production}}{W_{el,\ total\ electric\ load}}$$

$$supply\ cover\ factor = \frac{W_{el,\ consumption\ of\ local\ production}}{W_{el,total\ local\ production}}$$

Figure 2: Definition of load cover factor and supply cover factor (source: FhG-ISE)

Figure 2 gives the definition of the load and supply cover factor. The supply cover factor (SCF) relates the on-site use of PV-electricity to the totally generated PV-electricity and is thus a characteristic for the self-consumption on the supply side. The load cover factor (LCF) relates the totally cover electrical load to the on-site generated PV-production and is thus the characteristic for the load or demand-side. It is also called autarky rate, since is describes the degree of autarky by on-site PV-production. The factors are based on the system boundary of total energy consumption. The supply cover factor has typically high values in winter time, since the PV-yield is low and nearly all the produced energy can be used on-site, i.e. the PV surplus in winter is low. In contrast, in summer, the PV production is high and the loads are lower due to less illumination and heating demand, so the PV surplus is high, and thus, the supply cover factor is low. The load cover factor has the opposite characteristic, since in winter only a small part of the total load can be covered by on-site PV production, but in summer, nearly all the load can be covered by on-site PV-production.

1 Investigated heat pump integration in Annex 49

Linked to the monitoring projects, detailed investigation of the heat pump integration with other building technology components have been carried out by simulation. Thereby, also design options and control strategies are analysed. The objectives of the accompanying simulations were on the one hand to approve options in order to reach ambition nZEB targets by optimisation of the system configuration, the design and control of the component. Another focus of investigations performed in different projects is on integration of the thermal and electric storages with the heat pump and PV system in order to optimise self-consumption of on-site PV electricity and to operate the system in line with grids requirement. That means that the on-site PV generation is considered on the one hand from building owner perspective regarding a more economic operation by on-site PV self-consumption, and on the other hand from the grid perspective regarding e.g. local storage operation in order to reduce peaks in the grid. Moreover, also simulation studies independent from the monitoring projects have been accomplished.

Table 1 gives an overview on the link to the respective monitoring project, the considered integration options as well as the focus of the investigation. Detailed information on results of the respective monitoring projects are found in the Report Annex 49 part 2. The photos of the buildings are also linked to the respective chapters of the report, so Table 1 can also be used as a table of contents. A click on the photo leads to the respective chapter.

Table 1: Overview of nZEB monitoring projects in Annex 49 regarding building type and other project features

Investigation link to monitoring			
Monitoring project	**Photo**	**Integration option**	**Particular research/ Investigations**
Social housing NTH 2 multi-family buildings Innsbruck-Vögelebichl Austria Contact Simulation study: UIBK, Fabian Ochs		• PV and solar thermal collectors • Storage design and integration • Desuperheater for DHW production	• Heat pump system modelling and validation based on monitoring results • Optimisation of system configuration in order to reach ambitious nZEB targets
Residential 8 terraced houses Herzo Base Herzogenaurach Germany Contact Simulation study: THN, Arno Dentei, Christina Betzold		• Integration of electri cal and thermal sto rage for self-con sumption optimisation • Integration for grid supportive operation	• Achievement of plus energy balance for group of buildings • Heat pump control by rule-based and model predictive (MPC) control strategies to increase PV self-consumption and grid support
Single family house Berghalde Leonberg-Warmbronn, Germany Contact Simulation study: SIZ+, Franziska Bockelmann		• Thermal and electric storage integration • Source integration by regeneration of the ground	• Control for increased PV self-consumption in single family houses • Storage design of thermal and electric storage for PV self-consumption in single family houses • Grid supportive operation by thermal and electric storage

Additional projects for source integration			
MFH Riedberg Frankfurt a. M. Germany <u>Contact results:</u> SIZ+ Franziska Bockelmann		• Integration of source storage with regard to source temperature and regeneration	• Achievement of plus energy balance for larger multi-family buildings • Optimisation of source storage
Willibald-Gluck-School Neumarkt in der Oberpfalz, Germany <u>Contact results:</u> SIZ+ Franziska Bockelmann		• Integration of energy piles and agrothermal field with regeneration	• Achievement of plus energy balance for non-residential buildings
Twin houses, Borås and Varberg Sweden <u>Contact results:</u> RISE Ola Gustafsson		• Integration of free-cooling function into the ventilation	• Evaluation of covering of residential cooling demands
Simulation projects			
nZEB Living lab Campus Gloshaugen NTNU, Trondheim Norway <u>Contact simulations:</u> NTNU Laurent Georges John Clauß		• Integration of PV and thermal storage for grid supportive operation	• Predictive rule-based control strategies for shifting peaks in the grid • CO_2-based and price based control strategies
Increase of solar fraction by TABS (SolSPONGEhigh) IWT, TU Graz Austria <u>Contact SolSPONGEhigh:</u> IWT, TU Graz Andreas Heinz	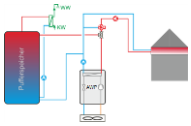	• Integration of PV and solar thermal collector with thermally activated building systems (TABS)	• Control investigation for the increase of solar fraction of solar thermal collectors and PV power2heat
Design of capacity controlled heat pumps in nZEB nZEB single family house <u>Contact simulation study:</u> OST Carsten Wemhoener		• Integration of speed controlled heat pump for nZEB application	• Design of speed control heat pumps for nZEB • Control of speed-controlled heat pumps • Price-based predictive rule based control (in collaboration with NTNU)

2 Integration on the source side

In this chapter investigated integration options on the source side of the heat pump are presented, which can comprise the upgrade of the heat source by preheating of another source, the regeneration of the source and the integration of different heat sources.

2.1 Regeneration of boreholes

2.1.1 Borehole heat exchanger and their regeneration in Berghalde project

In addition to natural regeneration of the borehole heat exchangers, “active” regeneration can also be easily implemented and at the same time the room comfort can be increased.

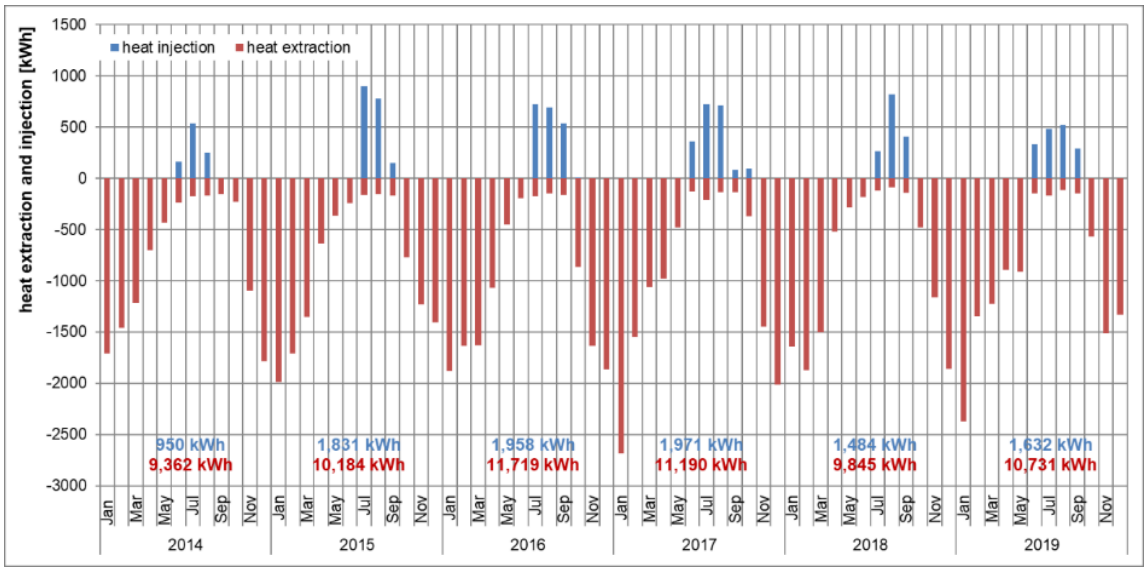

Figure 3: Monthly heat injection and extraction from borehole heat exchangers, 2014 to 2019

Figure 3 shows the monthly heat extraction and heat injection quantities for the years 2014 - 2019. On average, a heat extraction about 10,500 kWh/a can be found. The heat injection shown is based on free cooling by cooling with the floor heating system in the building. In addition to natural regeneration, free cooling contributes to improved regeneration of the geothermal borehole heat exchangers and reaches around 1,600 kWh/a.
The simple coupling of the underfloor heating system with the geothermal borehole heat exchangers in summer allows the ground to be regenerated and to generate more favourable temperatures for the space heating operation. On the other hand, the room comfort can be maintained at a pleasant temperature level in the summer months.

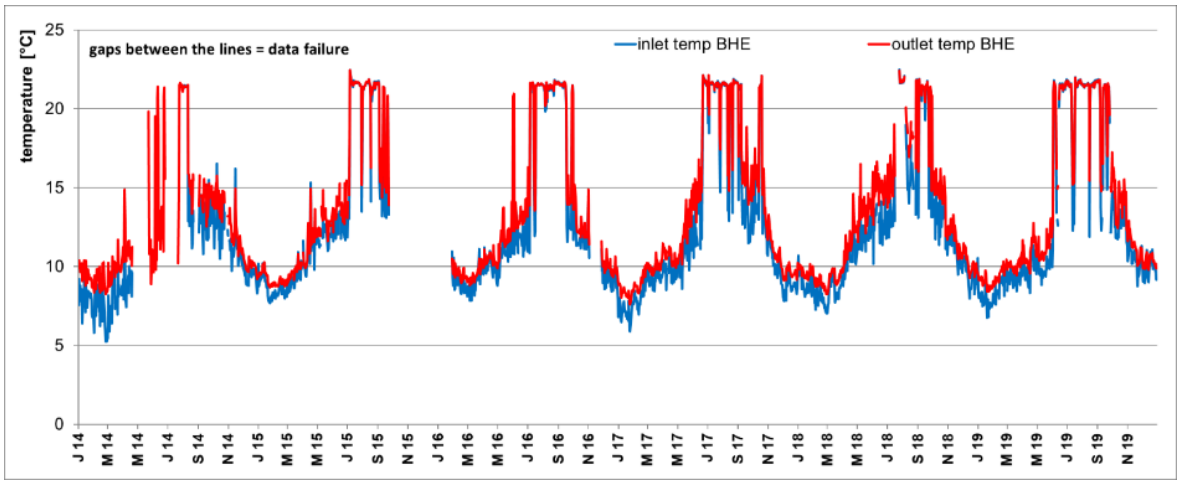

Figure 4: Daily mean values of the inlet and outlet temperatures of the borehole heat exchanger, 2014 to 2019

Figure 4 shows the daily averages of the inlet and outlet temperatures and the flow rate within the borehole heat exchangers. The inlet temperature corresponds to the return flow and the outlet temperature corresponds to the supply of the heating circuit between the heat pump and the borehole heat exchangers or between borehole heat exchangers and underfloor heating in cooling mode (free cooling). In the winter months, the temperatures are in the range of 6-10 °C and rise to around 23 °C in the summer months due to the reduced usage of heating energy and the use of free cooling.

2.2 Regeneration of source storages in Riedberg

2.2.1 Regeneration of source storages (ice storage)

In the multi-family house Riedberg, heat is supplied by an electric brine-to-water heat pump. Depending on the temperature level and availability, a solar thermal air absorber on the roof and an ice storage tank serve as heat source. The air absorbers are installed below the PV modules. The ice storage tank is regenerated in summer and the transition period on the one hand via heat conduction in the ground, by the solar air absorbers and by free cooling and parallel conditioning of the living areas in the summer months. In this way, the dissipated heat loads also contribute to regeneration in multi-family houses during the summer months in addition to improving comfort.
The supply concept is shown in Figure 5 left. The degree of ice formation in the storage tank can be estimated on the basis of the sensors and their measurement data. Due to the increase in volume when the aggregate state changes from liquid to solid, the distance between the water/ice surface and the lid decreases.

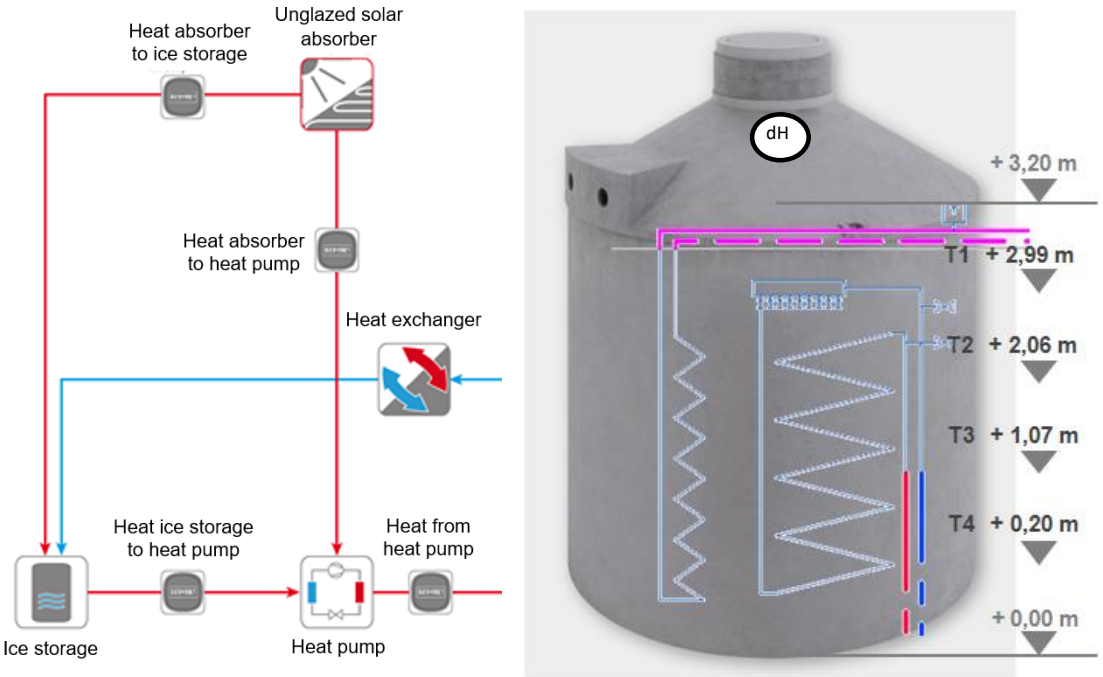

Figure 5: Supply concept winter and summer (left) and measuring points in the ice storage (right)

The following data from the ice storage is recorded as depicted in Figure 5 right:

- Temperature in the middle at 0.20 m height
- Temperature in the middle at 1.07 m height
- Temperature in the middle at 2.06 m height
- Temperature in the middle at a height of 2.99 m
- Distance (dH) from lid to water surface at 3.6 m height

It becomes clear that the regeneration of the ice storage tank cannot take place via free cooling alone, as the cold consumption is significantly lower than the heat extracted from the ice storage tank in the heating mode. Furthermore, the temperature level is limited in summer.

If the ice storage tank reaches a temperature above 18 °C, free cooling and thus the conditioning of the living areas is no longer possible.
The summer regulation therefore provides for the ice storage tank to continue to be used as a source for the heat pump for domestic hot water preparation and at the same time to regenerate the storage tank by free cooling. Cooling and warming in summer is shown in Figure 6 (fluctuation between 15 and 18°C in summer).
Figure 7 shows the amount of energy used as source energy for the heat pump. During the period under consideration (2017 - 2019) an average of 25.8 MWh (10.7 kWh/(m²a)) heat is extracted from the ice storage and 40.6 MWh (16.8 kWh/(m²a)) heat is made available from the absorbers on the roof for the heat pump. This means that the heat pump is supplied up to 60% by the absorbers. Conceptually, it has generally been assumed in the planning stage when implementing ice storage tanks, that the absorber, rather than the ice storage tank, is the main heat source.

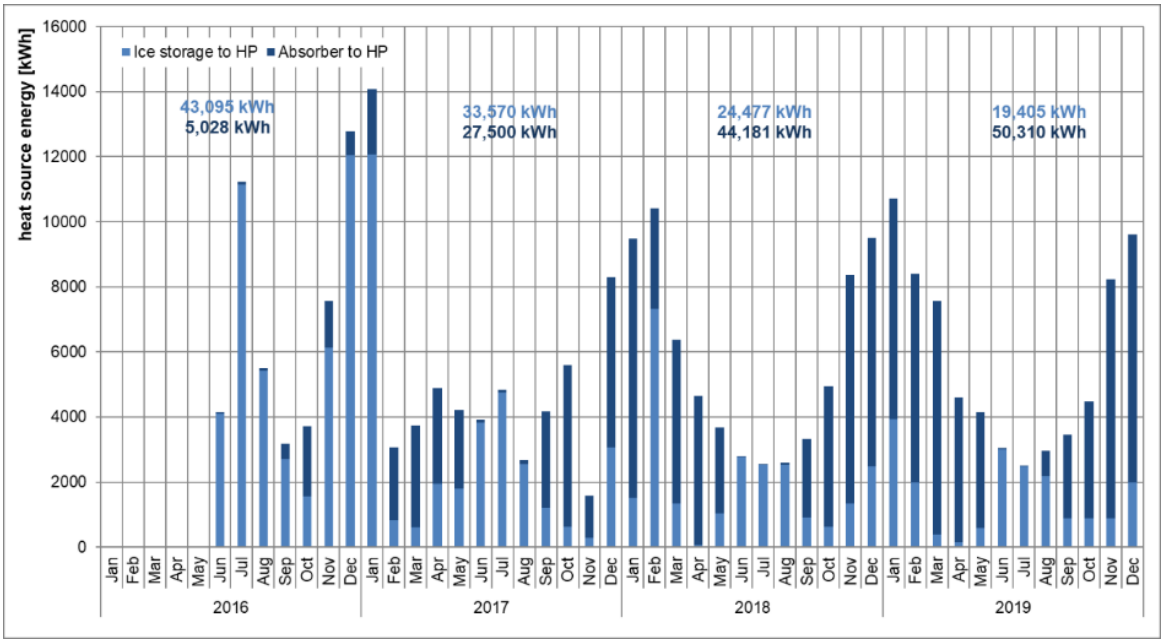

Figure 6: Heat from the ice storage or the absorbers to the heat pump, 2016 - 2019

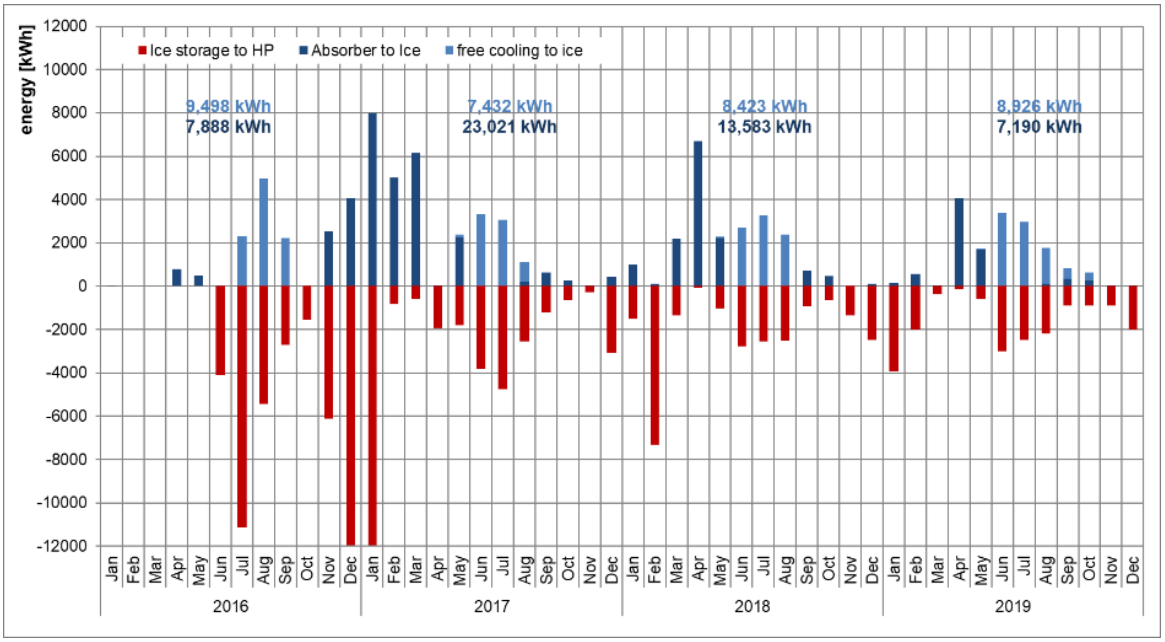

Figure 7: Heat balance ice storage, 2016 - 2019

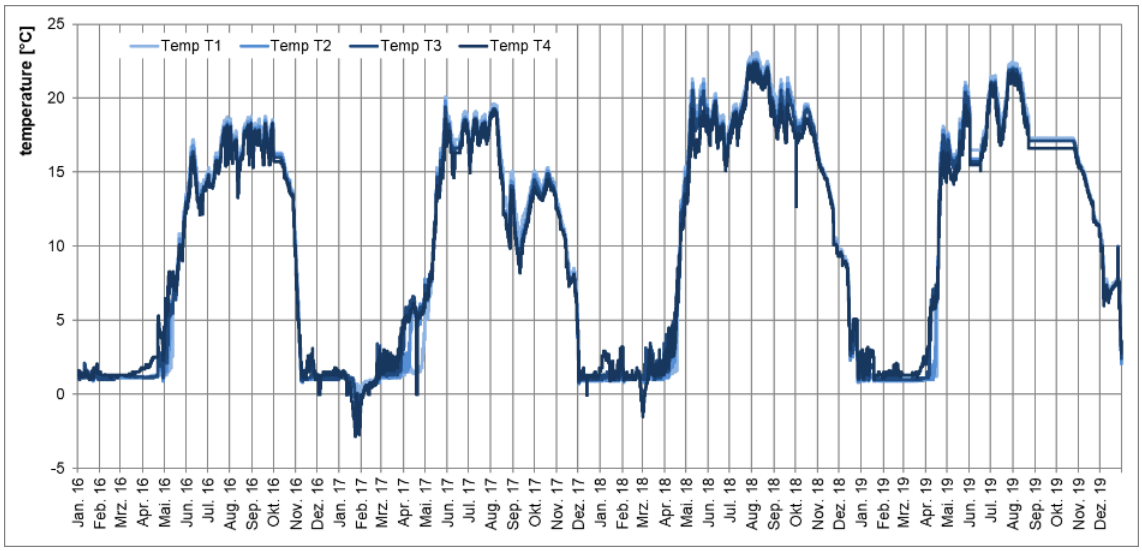

Figure 8: Temperatures in the ice storage (hourly average values), 2016 – 2019

The balance of the ice storage tank with regard to loading and unloading is shown in Figure 8. About 8.3 MWh (3.4 kWh/(m²a)) per year are supplied to the ice storage via free cooling in summer. In addition, 14.6 MWh (6.0 kWh/(m²a)) heat is conducted via the absorbers into the ice storage tank to regenerate it. The absorber loads the ice storage tank primarily during the heating period or in the transition period, when there is no cooling demand and the ice storage tank cannot be overheated.

On the basis of the temperature in the ice reservoir and the distance of the water surface to the lid of the ice reservoir, the freezing process could be observed and it could be determined that the icing had started too early and had already progressed too far in January, so that an additional heat generator was necessary. By completely freezing the ice storage tank before the end of the heating period, it can be concluded that the regeneration of the ice storage tank as well as the use of the solar absorbers as a direct heat source was not sufficient. It can be seen that there is no sensible heat in the storage tank already from November / December onwards, the temperatures reach 0 °C. Furthermore, the graph shows the regeneration in summer by solar absorber and free cooling.

2.3 Integration of heat sources

2.3.1 Agrothermal field and energy piles

In the annual balance 2017 to 2019, the heat extraction from the energy piles averaged 92.1 kWh/(m·a) (92.4 MWh/a), which corresponds to the planning value of about 100 kWh/m. The heat input amounted to 54.3 kWh/(m·a) on average, which corresponds to half the design value. For the agrothermal field, the annual heat extraction was on average 19.2 kWh/(m²a) and the annual heat input was about 10.9 kWh/(m²a). The heat input deviates slightly from the planning value of 16 kWh/(m²a). The energy balance for both heat sources shows that significantly more energy was extracted from the ground than was rejected to the ground. The ratio is around 63%.

The higher heat extraction of the agrothermal field in 2018 is based on an adapted regulation with regard to the determination of the agrothermal field output. In the 2018/2019 heating period, it was determined how long and with which withdrawal quantities the agrothermal field can supply the building as only heat source. For validation purposes, the energy piles were deactivated in the 2018/2019 heating period. The trial operation with the exclusive use of the agrothermal field has shown that the field can serve as the sole source for the heat pumps and supply the school building with heat, depending on the weather conditions from October to January inclusive. The brine inlet temperatures dropped to -2 °C. Due to the significantly higher brine temperatures, a switch to the bored piles was made in February 2019.

The brine inlet temperatures from the heat pump to the field/piles were on the monthly average between 2 °C and 27 °C. Due to the automatic frost protection circuit, the inlet temperatures for the bored piles were always > 3 °C.
In general, it can be stated that over the entire period under consideration both sources contributed about half of the heating and half of the cooling supply. The switch-over thus shows its functionality. However, it should be noted that the energy balance for both heat sources - also based on the optimisations and trial runs - shows that significantly more energy was extrated from the ground than is injected during the summer months. With the brine temperatures, however, it can be seen that, despite the unequal ratio of input to extraction, the temperatures do not fall. The natural regeneration currently ensures a sufficient annual heat flow.

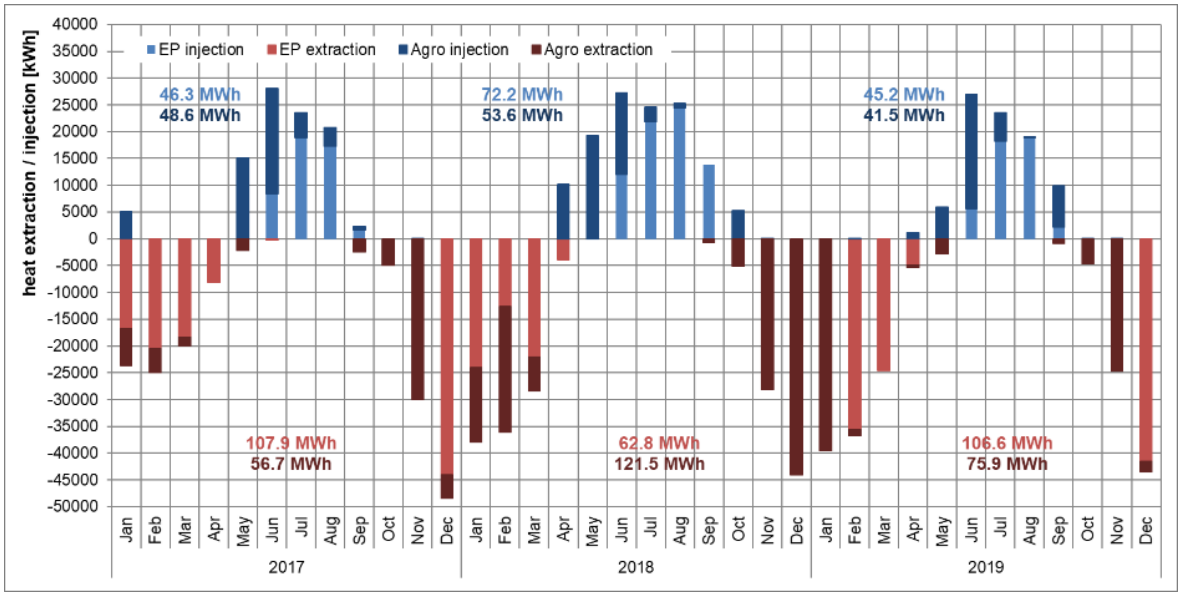

Figure 9: Monthly heat extraction and injection agrothermal field and energy piles, 2017 to 2019

For the future continued operation of both heat sources, however, care must be taken to ensure that a largely stable balance is achieved and that neither the soil of the agro-thermal field nor the soil surrounding the energy piles is cooled down too much.

2.4 Integration of free cooling operation with boreholes

Field measurements in Low Energy Buildings, for example in the so-called “Hamnhuset” in Gothenburg in Sweden, show that excess temperatures can easily occur during summertime in well-insulated houses, also in northern part of Europe (Gervind et al., 2011). In many cases, it is possible to lower the temperature by opening of windows, but this is not always desirable. The reason can be either noise or insecurity, or a desire from residents not to get too much pollen or air pollution for allergy or health reasons.
In a heating system with a ground source heat pump it is well known that the borehole can be used for free cooling in summertime (Zhou, Z. et al, 2016, Yuan, T. et al. 2017, Khilström, P. 2016). And if the house has a bidirectional ventilation system, the chilled air can easily be distributed throughout the building, which can be efficient from both an energy and cost point of view. However, such a solution requires that the heat pump and the ventilation system is linked and controlled together, which is rarely done today. The aim of this project was therefore to investigate the potential and to increase the knowledge of how a heat pump system can be integrated with a bidirectional ventilation system with heat recovery to enable free cooling.
The scope was thus to investigate the potential and to increase the knowledge of how a ground source heat pump system can be integrated with a bidirectional ventilation system with heat recovery to enable free cooling in a single family nearly Zero Energy Building (nZEB). This was done by simulation of the building and the building services engineering systems in IDA-ICE and by follow-up field measurements in a research villa.

2.4.1 Delimitations

Measurements were only performed during a part of one cooling season. It would have been beneficial to perform measurements during several full cooling seasons to be able to compare the different settings in a better way. In addition, the full range of the ventilation air flow rate used in the simulations could not be validated due to restrictions of fan capacity.
In this study, it has not been possible to predict the "cost" for the free cooling, in form of additional pumping and fan power. However, this should be taken into account when evaluating the "efficiency" of the free cooling. Even though less energy is most probably used compared to compressor driven cooling, there will still be a certain energy cost for the "free cooling".

2.4.2 Methodology

2.4.2.1 Simulation/measurement objects

In this study a reference house is used for the model. The house, situated at RISE's premises in Borås, Sweden, depicted in Figure 10 is a low energy single family house (average heat transfer coefficient, $U_{average}$ = 0.16 W/(m^2 K)) with a total floor area of 166 m^2 and two floor levels. Table 2 gives for more technical information of the building.

Table 2: Technical information about the nZEB and the heating and ventilations systems

Place	**Borås**
Size	166 m^2, 22 kWh/m^2/yr (projected space heating and DHW demand)
Ventilation	Balanced (bidirectional) ventilation system with heat recovery, design supply flow rate 60 l/s. Manufacturer efficiency data 82%
Heating source	Ground source heat pump (4.5 kW, on/off controlled) Storage tank 150 l. Borehole 90 m (81 m active) Dimensioning temperature: 0 °C
Heating system	Floor heating on upper and 1st floors Dimension temperature: 36 °C at dimensioning outdoor winter temperature
Solar	PV-panels 3000 kWh/yr
Habitants	Simulated family

Figure 10: The IDA model (left) and the reference house (right).

2.4.3 Simulations

A model of the single-family house is created in IDA Indoor Climate and Energy (ICE) 4.6 (IDA ICE, XX), and the construction and the configuration correspond to the reference house situated in Borås (see Figure 10 left). Result from the model for the heating demand is compared with measurements from the reference house and show good agreement (Ylmén, P. & Persson, J., 2017).
The program of IDA ICE is used to investigate the cooling demand and thermal conditions with different ventilation airflow rate, effects of window opening and a free cooling system. IDA is a dynamic simulation tool for studying indoor climate in the zones as well as energy use in the zones and the entire building for general-purpose.
It models buildings, systems and its controls, and it provides user interface to define, build up and simulate different cases which makes it possible to simulate a wide range of system designs and configurations (Equa Simulation Technology, 1999).

The climate data used in the model is for Gothenburg-Landvetter (45 km from Borås), which is fairly representative for Swedish conditions with a yearly average temperature of 8 °C. The weather data files are available in the IDA program and they are derived from integrated surface hourly weather data originally archived at the national climate data centre. Regarding the internal heat load, i.e. heat emission from lighting, equipment and appliance, 30 kWh/m^2 is used, suggested by SVEBY (2009) as a standard value for residential building energy simulation. The internal heat load is distributed to the rooms with specific schedules and unevenly distributed over the year, i.e. higher household electricity use in the winter and lower in the summer. Occupancy schedules are considered with a specific distribution. IDA simulations were performed for the cooling season, i.e. May to August.
To investigate the effect of different means of reducing the hours of overheating different cases were modelled. These cases included different ventilation flow rates, schedule for window opening and installation of a cooling coil (connected to borehole and placed after the air handing unit); see Table 3 for short descriptions of case studies. For each of these cases the number of hours that the temperature in three different rooms in the nZEB exceeded 24 °C was investigated.

Table 3: Descriptions of modelled cases

Case	Ventilation flow rate (l/s)	Schedule for **window** opening	Connected to cooling coil
1	60	No	No
2	100	No	No
3	60	Yes	No
4	60	No	Yes *
5	100	No	Yes *
6	60	Yes	Yes *

* The cooling coil starts to work when the room air and supply air temperature is above 21 °C and 16 °C, respectively.

The designed ventilation flow rate for the modelled house was 60 l/s (corresponding to 0.35 l/s/m^2), and the maximum flow rate was assumed to be 100 l/s. The schedule for window opening was made based on a literature study together with assumptions of opening window behaviour (when and how often people is likely to open window). A cooling coil was added to cool down the supply air temperature to 16 °C in warm days, i.e. case 4-6.
Furthermore, additional cases are modelled to obtain the required cooling capacity for maintaining the maximum room temperature below 24 °C at all times. This was done by adding fan coils in the living spaces, i.e., living room and kitchen and sleeping rooms for case 1, 2 and 3.
In addition, the maximum cooling capacity from free cooling system was investigated by estimation of the potential on the air side.

2.4.4 Measurements

2.4.4.1 System setup

The system setup is depicted in Figure 11, and consists of the following main components;

- A ground-source heat pump with a 2.3 kW electric compressor, operated in on/off mode. The heating power, excluding auxiliary resistive elements (blocked), is about 4.5 kW. The heat-pump is supplying both DHW and heating water for floor-heating.
- An air-handling unit with a rotating disk heat recovery. The electric power of the fans are about 170 W and delivers a max. flow of about the 90 m^3/h in the given installation (without additional cooling-coil).
- A cooling-battery dimensioned to give about 1 kW cooling power at the anticipated operation conditions.
- A separate frequency-controlled circulation pump on the brine circuit of the cooling battery.

The cooling battery was installed on the supply air duct, directly after the air-handling unit. A by-pass, operated by manual valves, allows for the cooling battery to be disabled when not needed.

The liquid circuit of the cooling battery was connected in parallel with the return pipe from the borehole to the heat pump. The additional circulation pump, along with a non-return valve, allow for brine to be circulated through the cooling battery, the heat-pump and the borehole (all in series) independently of the heat-pump operation.

2.4.4.2 Measurement system setup

The monitoring included PT100 and PT500 sensors for temperature readings for both the air- and brine side of the system. The flow-rate on the brine side was given by a volumetric flow sensor. Both brine temperature and flow rate were measured by a Kamstrup energy meter. The air flow was measured by differential pressure sensors. In addition, the electric power used by the equipment was logged with integrating energy meters. Data for evaluation the thermal system performance was recorded as 15 minutes averages. Some, but not all, measuring points are indicated in the system diagram in Figure 11.

2.4.4.3 Control system

The cooling power was controlled to reach a given set-point temperature on the supply-air to the living space. The control was achieved by regulating the speed of the circulation pump on the brine side of the cooling battery. A PID regulation was implemented to provide a feed-back from the supply air temperature to the operation circulation pump. The cooling was activated when the outdoor temperature exceeded 16.3 °C, and it turned off again when the outdoor temperature went below 15.0 °C (taking the temperature rise of the air due to the fan power into account).

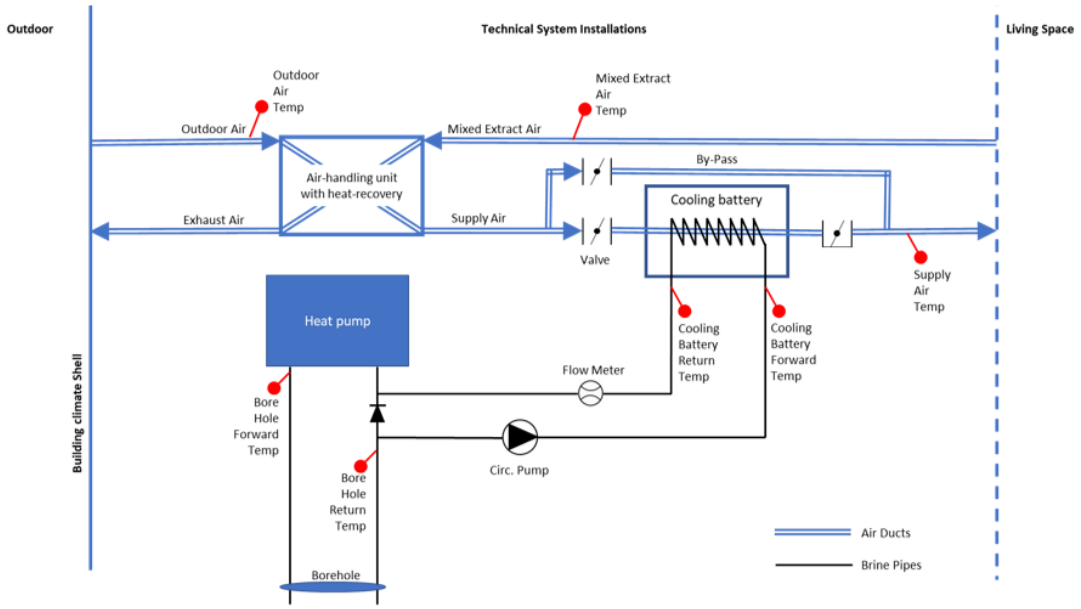

Figure 11: The system setup of the installation of the cooling battery in the Research Villa.

2.4.4.4 Operation settings

Three separate operation settings are presented here, which each has different effects on the final indoor air temperature of the house.

Operation setting 1 – Full ventilation, no cooling, HP in operation. The cooling battery was not activated, and the air went via the by-pass. The fans of the air-handling unit were running at maximum speed to give a supply air-flow of about 70 l/s. In this case a ventilation air flow of 100 l/s, was aimed for, but due to restrictions in fan capacity only 70 l/s was reached. The heat pump was running as normally, in an eco-mode setting. The measurement period for this operation mode was from 2017-06-19 to 2017-06-28.

Operation setting 2 – Full ventilation, 16°C cooling, HP in operation. The cooling battery was activated with a supply air temperature set-point of 16 °C. With an additional pressure drop over the cooling battery, the air-flow was reduced to about 60 l/s. The heat pump was running as normally, in an eco-mode setting. The measurement period for this operation mode was from 2017-08-22 to 2017-08-31.

Operation setting 3 – Full ventilation, 16°C cooling, HP turned off. The cooling battery was activated with a supply air temperature set-point of 16 °C. The air-flow was about 60 l/s. The heat pump was turned off. The measurement period for this operation mode was from 2017-08-11 to 2017-08-22.

2.4.5 Results and discussion

2.4.5.1 Simulations

Results from the IDA simulations are presented and discussed in this section.

2.4.5.2 Required cooling capacity

The required cooling capacity for case 1, 2 and 3 (see case description in Table 3) to keep the maximum room temperature below 24 °C during the whole cooling season is presented in Figure 12. As shown in the figure the peak cooling demand for all three cases is nearly the same, about 2000 W, while the number of hours required for the same amount of cooling demand is decreased by increasing ventilation flow rate or opening window.

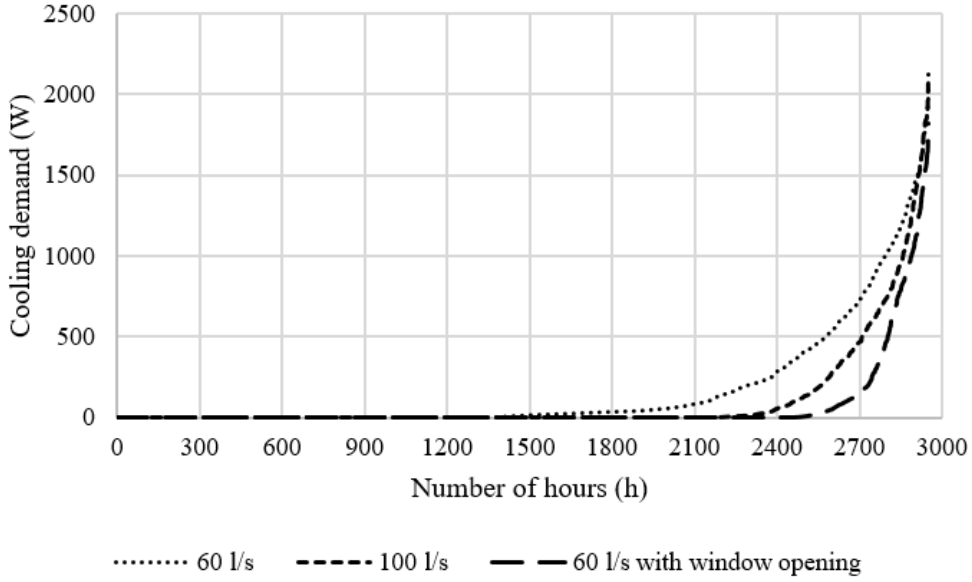

Figure 12: Duration diagram of cooling demand for case 1 – 3 during the whole cooling season.

2.4.5.3 Cooling potential in ventilation system

According to IDA calculation, the maximum cooling power (both sensible and latent) provided by the ventilation flow rate of 60 l/s and 100 l/s is about 1.2 kW and 1.9 kW, respectively. These values are valid for an outdoor temperature of 26 °C, relative humidity of 54% and supply air temperature of 16 °C. In the IDA model, the temperature for entering liquid and leaving liquid is assumed to be 5 °C and 10 °C (IDA default value), respectively.

2.4.5.4 Reduction of hours of overheating

In Figure 13 the indoor temperature of the modelled house is shown for a sunny day in July at 16:00. The contour plot of temperature is based on the simulation results for case 1 (base case). The temperatures for the living room and kitchen, bedroom 1 and bedroom 2 are at about 27, 29 and 30 °C, respectively. In general, the air temperature in the first-floor is lower than that in the second-floor; and bedroom 2 in the second-floor is warmer than bedroom 1 due to more incoming solar radiation in the afternoon. Therefore, bedroom 2 has a longer overheated period than bedroom 1 as shown in Figure 14.

Figure 13 shows the total number of hours when the room air temperature above 24°C during the whole cooling season for different cases, including increased ventilation flow rates (case 2 and 5), opening window (case 3 and 6) and using a free cooling system (case 4,5 and 6). As can be seen, increasing ventilation flow rate, opening windows, and connection to free cooling system helps to decrease extent of overheating in house, in terms of reducing the overheating hours. But of course, the changes also have in impact on the average room temperature.

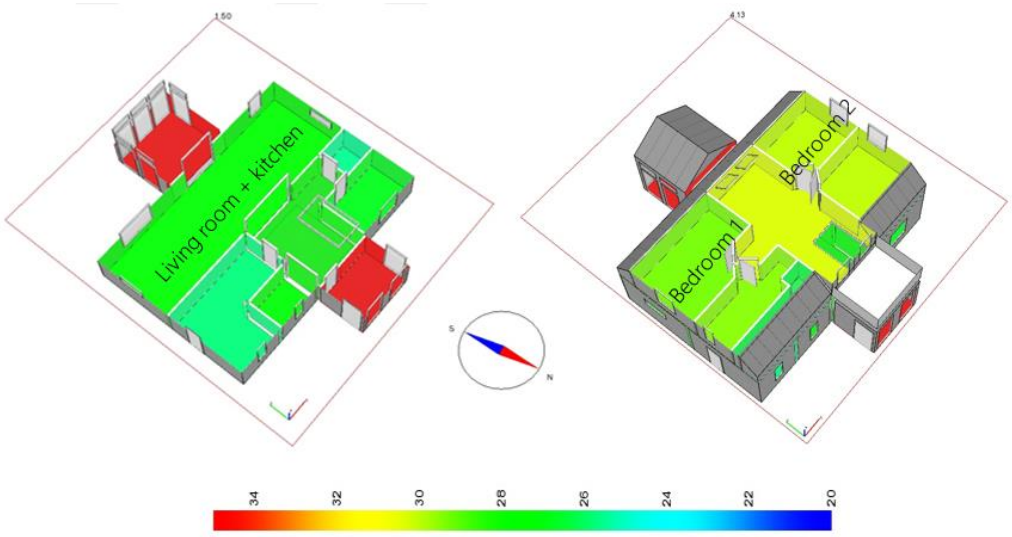

Figure 13: Contour plot of room temperature of the modelled house for a sunny day in July at 16:00

For example, the average room temperature for the living room and kitchen for case 1 and case 4 (with free cooling) is about 24 and 23°C, respectively; for bedroom 1, the average room temperature for case 1 and case 3 is about 25 and 23°C, respectively.

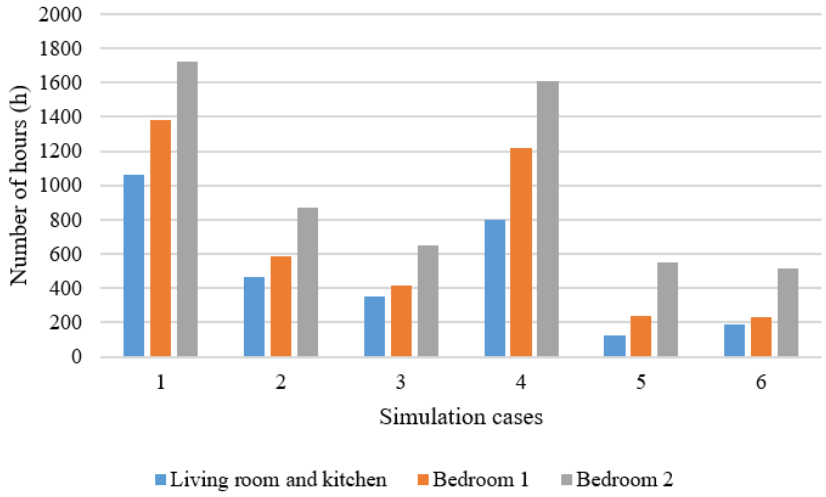

Figure 14: Total number of hours when the room temperature is above 24 °C for living room and kitchen and two sleeping rooms during the whole cooling season based on simulation.

2.4.6 Measurements

In Figure 15 the temperature of the mixed extract air is shown during the three different evaluation periods. This temperature is assumed to represent an average indoor temperature. No (or very few) window openings were done during the evaluation period since the measurements were performed in a research villa with no people living in the house. Occupancy is only simulated by electrical thermal loads. Due to restrictions in fan capacity, it was only possible to increase the air flow rate to 70 l/s (and not up to 100 l/s). As can be seen, temperatures over 24 °C are registered for a large amount of the time, even at moderate outdoor temperatures. After setting the cooling coil into operation, the temperature of the extract air is reduced significantly, even more than expected, since the ventilation air flow was reduced due to the additional pressure drop over the cooling coil. According to the default setting of the heat pump, the heat pump operates in heating mode during night time, if the outdoor temperature drops below a certain level.
It can be seen that lower temperatures are obtained if the heat pump operation is blocked, and nevertheless, the mixed indoor temperature never drops below 20 °C.

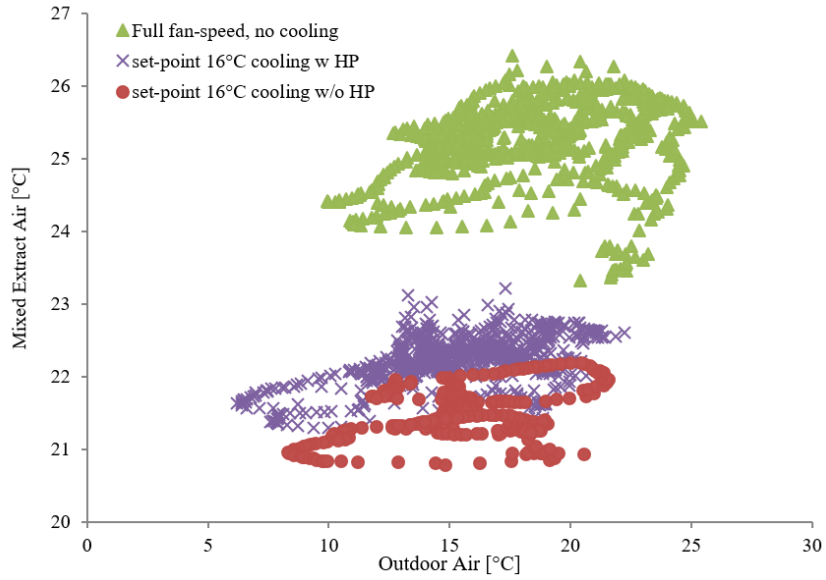

Figure 15: Temperature of the mixed extract air during different evaluation periods with and without free cooling and heat pump operation.

2.4.7 Lessons learned from measurements

Some lessons learned from the measurement evaluation periods are listed below.

- In order to limit the additional pump power, the cooling pump should not be oversized and equipped with variable flow control.
- In order to reduce the fan energy used during the whole year it is beneficial if the system has a bypass for the airflow to prevent the air from passing the cooling coil during the heating system.
- The control should include a summer and winter period to prevent the heat pump to heat the house during nighttime when there is a cooling need in the daytime.
- The system should have a valve to shut-off the cooling coil when the heat pump is operating. Otherwise there is a risk that too cold air (below 16 °C) is distributed by the ventilation system.

2.4.8 Discussion

As an alternative to distributing the chilled air through the ventilation system, separate fan coils could be installed in one or several rooms of the house. If only one is installed, it will be a challenge to distribute the cool air in the house, and if several are installed, it will lead to considerable extra cost, both for material, work and fan power. Therefore, the alternative if distributing the air by the already existing ventilation system is a cost-efficient alternative, even though the available cooling capacity is restricted by the ventilation air flow rate and a lowest permitted discharge temperature of 16 °C.

2.4.9 Conclusions

- It is possible to lower the indoor temperature significantly with a cooling connected to the borehole of a ground source heat pump and a bidirectional ventilation.
- The IDA model used in this study shows reasonable predictions of indoor thermal conditions for a typical summer based on the comparison results with the measurement data.
- Since the cooling capacity is limited in the free cooling system a good control scheme is required i.e. one must start cooling before the actual cooling need (high indoor temperatures) to prevent overheating.
- Increasing the ventilation flow rate is efficient to reduce the number of hours of overheating. Therefore, this should be the first step, if possible, before installing the cooling system.

3 System integration and optimisation by simulation

In this chapter the simulation and optimisation of the two multi-family passive houses in Innsbruck/Vögelebichl are described, which are supplied by the combination of a heat pump with a solar thermal system. The heat pump also incorporates a desuperheater for DHW production. In this chapter details on the system modelling, control and system optimisation by simuations are given while the monitoring data of the 4 years of field monitoring are documented in the
Report Annex 49 part 2 on Monitoring

3.1 Simulation Model

A simulation model of the building and heating, ventilation and air-conditioning (HVAC) system is developed to study alternative hydraulic designs and control strategies. The modelling approach begins parametrizing each component with monitoring data. The components are then simulated all together such that the simulated energy consumption reflects the measured one by fine-tuning the control settings. Note that the heating system model does not include the solar thermal panels, whose contribution is represented by the monitored inlet temperature and mass flow rate to the buffer storage (BS).
The simulation model is realized in MATLAB Simulink adopting the Carnot Toolbox (Solar Institute Juelich, 2019) for modelling the heating system, whereas the building is modelled based on the library carnotUIBK developed at the University of Innsbruck (Siegele et al., 2019). The following sections present the modelling assumptions and simplifications of each component and the results of the parameterized simulation model.

3.1.1 Buffer Storage Model

The BS model of the Carnot Toolbox is a one-dimensional multi-node model. Each node represents a portion of the storage volume at a homogeneous temperature. The temperature is determined solving the energy balance considering mass inflows and outflows, conduction between adjacent nodes, losses to the environment, and a heat transport term that models the mixing in case of inverse thermocline (i.e. node below or above respectively at a higher or lower temperature). It is suggested to set 50 to 100 nodes to achieve accurate representations, although the model is said to be stable with already 10 nodes (Solar Institute Juelich, 2018).
The simulated storage volume is divided into 75 nodes and has 8 pairs of inlet and outlet connections, which differs from the real number of connections (11 in total). The reason why is related to numerical stability and ease of modelling. Indeed, splitting, and merging signals could lead to algebraic loops and it increases the model complexity. Nevertheless, this required to model flow mixing and diverting within the storage. In some cases, this might not influence the energy balance point of view; for example, mixing of DSH and condenser (CND) flows in domestic hot water (DHW) priority mode. In others, it could lead to deviations, such as for the space heating (SH) flow branch that does not originate from the BS, but from the CND flow before the inlet to the tank. As a result, the storage model is always charged at full mass flow from the CND inlet. However, the fine discretization of the tank makes the mixing of heated water with a relatively small volume of stored water not influencing the SH flow temperature, thus limiting the error of this simplification.
The model is simulated with monitoring data inputs for CND, DSH and ST flow, and SH and DHW return, comparing the simulated outputs with the measurements. Figure 16 shows the monitored BS temperatures within the storage for a winter day compared to the simulated temperatures. As can be seen, the results are acceptably good as justified also by the root mean square error (RMSE) – and the corresponding coefficient of variation (CV) – computed for 10 days and reported in Table 4. The larger mismatch for the top-down sensor could be explained by its proximity to the separation metal sheet.

Although the model is not parametrized to the summer behaviour, the simulated storage temperatures appear also to match satisfactorily the monitored temperatures outside the heating season.

Table 4: Buffer storage (BS) temperatures root mean square error (RMSE) and coefficient of variation (CV).

	RMSE [K]	CV (%)
$\vartheta_{top\ up}$	4.4	8.0
$\vartheta_{top\ down}$	6.6	19.0
$\vartheta_{mid\ up}$	1.8	6.0
$\vartheta_{mid\ down}$	1.6	5.0
$\vartheta_{bottom\ up}$	1.1	4.0
$\vartheta_{bottom\ down}$	1.2	5.0

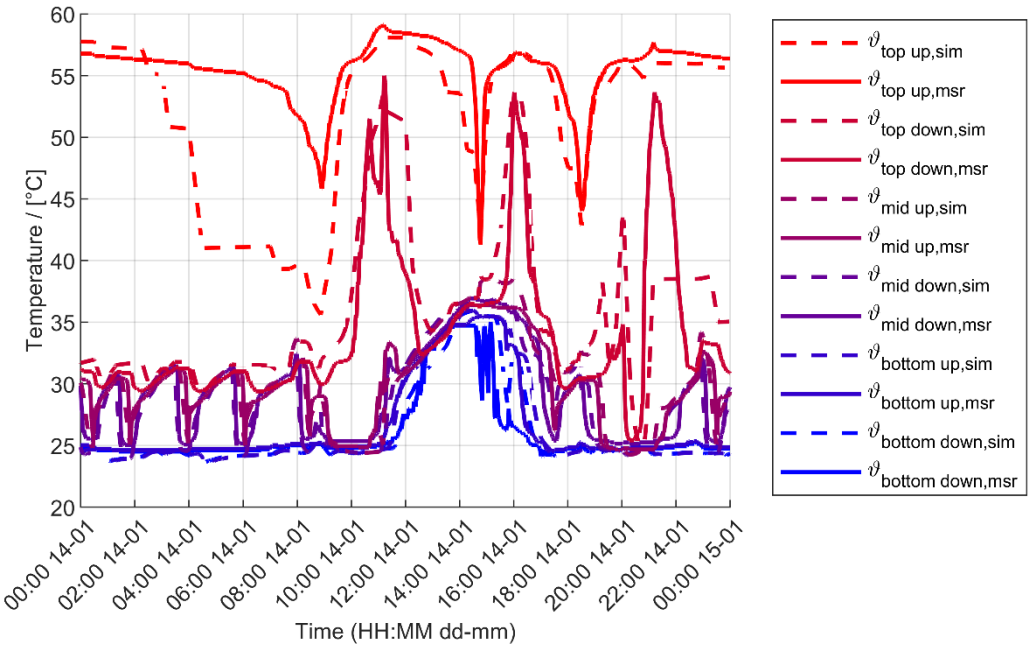

Figure 16: Buffer storage (BS) measured (msr) and simulated (sim) temperatures during a typical winter day in 2018.

3.1.2 Heat Pump Model

The HP model adopted was realized and parametrized by Monteleone (2019) starting from the block available in the CARNOT Toolbox. The dynamic model is based on an energy balance on the secondary side of the HP heat exchangers. The refrigerant cycle is represented by linear interpolation of performance maps obtained thanks to a parameterized model of the thermodynamic cycle in Monteleone (2019). For this kind of HP, three-dimensional tables were required to account for the presence of the desuperheater (DSH). Therefore, the look-up values are the source and the two sink temperatures (i.e. condenser and desuperheater).
The steady-state model of the HP solves the refrigerant cycle by iteratively searching for the DSH outlet enthalpy and evaporation and condensation pressures, such to minimize an error function, which is defined to ensure the solution found respects the laws of thermodynamics. The model receives as inputs the compressor efficiencies (isentropic and volumetric), the heat exchange coefficients of the heat exchangers, the subcooling and superheating temperatures difference, and the secondary sides (i.e. evaporator, condenser, and desuperheater) temperatures and mass flow rates. A sensibility analysis evaluated the weights of the assumptions on the results, guiding the proper choice of the parameters to calibrate the model to the measured values.
The parametrized steady-state model is then used to generate the performance maps of the HP to be used for the dynamic model. The performance maps represent both stage operations

and at source temperatures 0, 5 and 10 °C, and sink temperatures 35, 45, and 55 °C, with a fixed DSH outlet temperature of 55 °C.
The model proved to successfully represent the monitored behaviour of the heat pump as can be seen in Table 5 and in Figure 17, where respectively the steady-state and dynamic results are compared to measured values.

Table 5: Comparison of the outputs of the steady-state simulation with measured data in heating mode stage 2 (Monteleone, 2019).

	Measured	Simulated	Difference
$\vartheta_{source,out}$ [°C]	4.8	5.6	0.8 (+16%)
$\vartheta_{cond,out}$ [°C]	30.4	33.6	3.2 (+11%)
$\vartheta_{\mathrm{DSH,out}}$ [°C]	59.0	61.7	2.7 (+4)
$\dot{Q}_{EVP}$ [kW]	42.2	35.4	-6.8 (-16%)
$\dot{Q}_{CND}$ [kW]	47.0	42.4	-4.6 (-10%)
$\dot{Q}_{DSH}$ [kW]	3.1	1.2	-1.9 (-60%)
$\dot{W}_{EL}$ [kW]	9.2	8.3	-0.9 (-9%)
COP [-]	5.5	5.2	-0.3 (-4%)

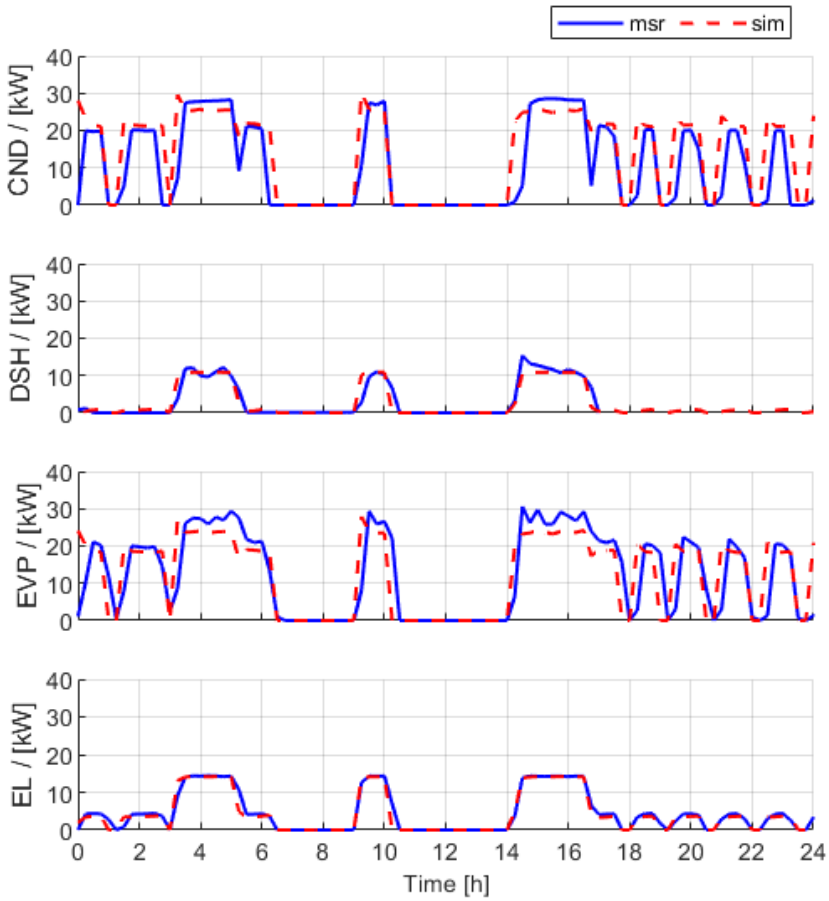

Figure 17: Heat Pump (HP) powers comparison between measured and simulated results over a day (Monteleone, 2019). From top to bottom: condenser (CND), desuperheater (DSH), evaporator (EVP), and electric (EL) powers.

3.1.3 Building Model

The CARNOT Toolbox is used to build the heat generation system model, whereas the building model is realized through carnotUIBK, a cross-validated tool (Magni et al., 2019) developed by Siegele et al. (2019) at the *Unit of Energy Efficient Building* of the University of Innsbruck. The tool is based on the *CARNOT Toolbox*, making it suitable for building and system simulation.
Opaque constructions are modelled by the *Beuken–model*, an RC thermal network, whereas windows are modelled with a transfer function and an incident angle adjusted solar gain coefficient Siegele et al. (2019). Heat exchange to the ground is modelled by considering a monthly average ground temperature determined according to standard (EN ISO 13370,

2017). Heat transfer within the thermal zone is calculated by a two-star thermal network where two nodal temperatures are defined: convective and radiative. All the surfaces exchange with the two nodes and gains are distributed to these depending on the convective-to-radiative ratio. Furthermore, carnotUIBK allows importing the building data directly from the Passive House Planning Package (PHPP). The building model was set-up by merging the information of the two buildings' PHPPs to realize a two thermal zones model, each representing one of the building blocks. The internal masses are not modelled by internal constructions, but their thermal capacity is accounted for by the heating terminal units, as described in the following. The monitored weather of 2018 from the weather station of the nearby airport is adopted for the simulations. All the simulations are run with 90 days initialization time. The building model includes a simplified ventilation system with heat recovery and summer by-pass. Schedules for night ventilation and shading devices are defined according to the PHPP, although they are representing a monthly average behaviour. Despite the presence of hydronic cooling, this is modelled as an ideal air-cooling system. Particularly, the ideal cooling is adopted not only in the months of actual cooling (i.e. June, July, and August) but also during the transition months from and to the heating season (i.e. April, May, September, and October), such that to simplify the parametrization of the building model, which focuses only on the heating demand (HD). The cooling system is set to achieve the monitored indoor temperatures. Having eliminated the dependence on shading and night ventilation schedules using ideal cooling, the only parametrization variable becomes the infiltration rate, which is used to account for user behaviour in window openings to match the building HD. Figure 18 shows the monthly HD of both buildings for the following cases:

1. Monitored in 2018 (msr).
2. Design HD computed by the PHPP used for the Passivhaus certification.
3. HD computed by a monthly energy balance according to ISO 13790 (PHPP) modified to account for the monitored climate of 2018, monthly measured indoor temperatures, and a value for the infiltration rate that makes the annual HD match with the annual monitored HD.
4. HD obtained by dynamic simulation (sim) of the building model presented in this section coupled to an ideal heating system to be consistent with the approximations of the PHPP. This case adopts the same parameters as the previous case (PHPP modified), i.e. monitored climate and indoor temperatures, infiltration rate.

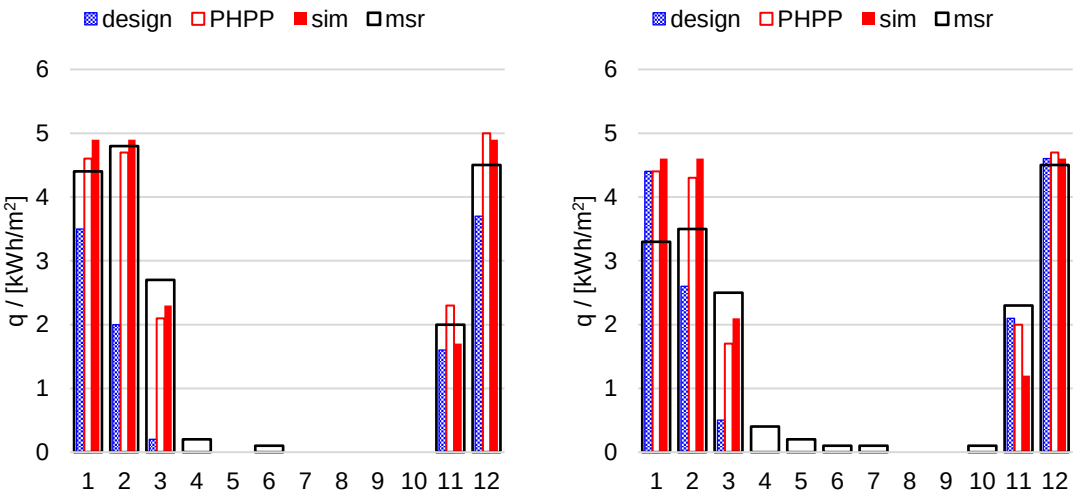

Figure 18: Comparison of monitored in 2018 (msr) and design monthly heating demand (HD) with PHPP adapted with monitored climate, indoor temperatures and parameterized infiltration rate predicted HD and with the dynamic simulated HD (sim) of the buildings (left north building, right south building).

The annual infiltration rates set to match the 2018 HD are n_{50} = 1.5 1/h and n_{50} = 0.6 1/h for the north and south building, respectively. The design HD for the north block is lower than the monitored HD, whereas in the south building this is not always the case. Particularly, in January

the measured HD for the south building is lower, and in November and December, they are practically equal. The modified PHPP HD (case 3) matches quite well with measured SH consumption, slightly overestimating in the coldest months, and underestimating the other months.
Simulated results (case 4) are close to those obtained by the modified PHPP, slightly higher, except for November that the HD is lower because of the accumulated heat during the summer that is considered by the simulation and not by the PHPP. Overall, the trend in cases 3 and 4 reproduces the measured trend, with minor deviations. The trend in January and February for the south building is hard to catch just by tuning the infiltration rate. Considering that in January also the design heating demand is higher, the reason for this mismatch could be related to user behaviour, e.g. flats not heated in these months since they are unoccupied. However, an annual average infiltration rate coefficient seems restrictive and unable to represent the different user behaviour as the seasons change. Indeed, the degree of ventilation by window openings is expected to decrease during the coldest months because of decreasing outdoor temperatures. Therefore, for the simulation of the building with the actual HVAC system, the model is parameterized employing monthly varying infiltration rate coefficients shown in Table 6. The results with the actual HVAC system follows in the next section.

Table 6: Infiltration rates that yield the best match between measured (msr) and simulated (sim) heating demand.

	Jan	Feb	Mar	Apr	May	Jun	Jul	Aug	Sep	Oct	Nov	Dec
n_{50} North [1/h]	1.0	1.5	1.5	1.5	1.5	1.5	1.5	1.5	1.5	1.5	1.5	1.4
n_{50} South [1/h]	0.4	0.4	0.6	0.6	0.6	0.6	0.6	0.6	0.6	0.6	0.6	0.5

3.1.4 Building and Heating System Model

The components so far presented are coupled together to realize the simulation model of the building and its heating system.
To couple the building and the heating system it is necessary to model the radiant floor panels. This is performed by using the radiator model of the Carnot Toolbox, which is a one-node model implementing the equation of standards (EN 442, 2015) and by setting a high thermal capacity and the radiator exponent to n=1.1 as specified by Dott et al. (2013). The capacitance includes the thermal mass of the floor; therefore, no additional internal masses are added.
The SH mass flow separation to the two buildings is modelled according to the average ratio of monitored mass flow rate to the building south to the SH pump nominal flow rate, which is 35%. Figure 19 shows the comparison between monitored and building with an actual heating system simulated HD. The difference is low during the heating season, whereas it increases during the months where some heating demand is measured even though normally not expected. The annual HD for both buildings is achieved and a good distribution of it into months is obtained thanks to the monthly variable infiltration rates. Still, the HD in March for both buildings, and in January and February for the south building, differs from the measured value.

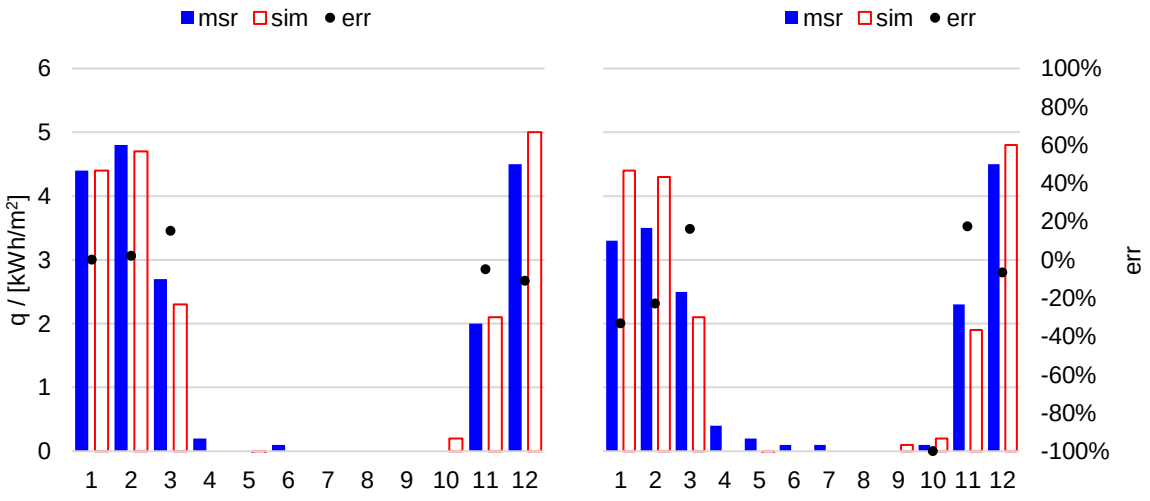

Figure 19: Comparison of measured in 2018 (msr) and simulated (sim) building north (left) and building south (right) monthly heating demand (HD), with relative errors (err).

In Figure 20, the difference between measured and simulated total electric energy consumption is highlighted. The annual relative error (err) for total electric consumption is around 15%, which is acceptable considering the simplifications introduced (e.g., not parametrized thermal losses). Furthermore, on a monthly basis, the error is larger than the 20% only for the months that the anomalous behaviour of the auxiliaries' consumption has been observed.
The simulation model is representing the monitoring behaviour accurately enough that it could be used as a reference point for the analysis of the heating system alternative hydraulic designs.

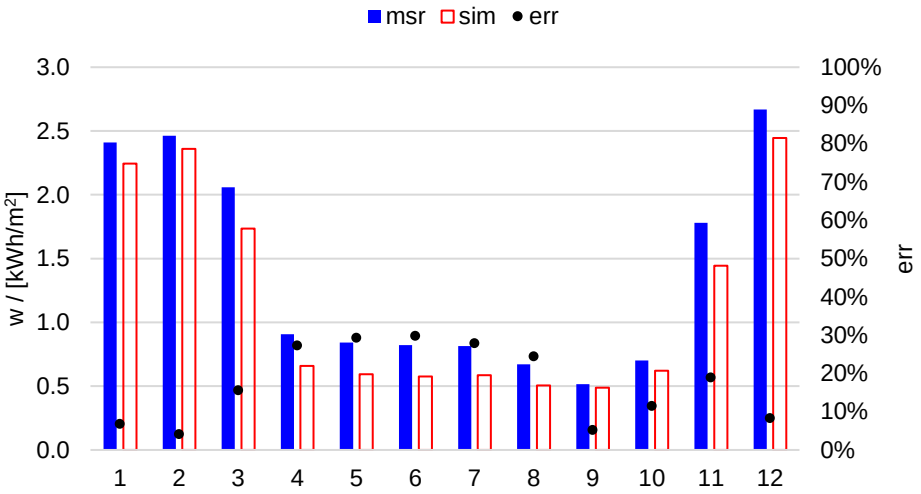

Figure 20: Measured in 2018 (msr) and simulated (sim) total electric energy consumption (HP+Aux).

3.2 Optimization and Alternative System Designs

The simulation model so far developed allows testing different control strategies and alternative hydraulic system designs to minimize energy consumption. In the following, the simulation results of some variation to the control strategy and some alternative system designs are presented. Firstly, the control strategy suggested in section 3.2.1 is tested. The heating system is also simulated without the contribution of ST panels. The section concludes presenting two alternative schematics.

3.2.1 Control Strategy Improvement Simulation

A slight modification of the control strategy allows the DSH to be always on. As a result, it is expected that the DSH contribution will increase, leading to an energy-saving. To test this, the reference model is simulated applying the improved control strategy to estimate its benefit.
Particularly, the DSH is in operation in all HP conditions (i.e. heating in stage 1 and 2, and DHW mode) and the water flow is controlled by a mixing valve that ensures the supply water reaches the buffer storage temperature at the inlet, increased by 1 K to avoid the inverted thermocline.
This modification to the control strategy leads indeed to an electric energy saving, though just of the 1% because of the high DHW-to-SH demand ratio (i.e. for the case study in 2018 it was 60%).

3.2.2 Reference without Solar Thermal Panels

As Ochs et al. (2014) highlighted, full coverage of PV panels might be economically optimal, and the energetic difference should be negligible.
The energetic impact of replacing the ST panels with additional PV panels can be studied by simulations of the reference model neglecting the contribution of ST. In the absence of ST, the storage volume and the height of the connection should be also changed.

However, this analysis aims to provide an estimate of the increase in energy consumption, with particular regard to the heating season, rather than determining the optimal configuration of the reference system without ST.
Figure 21 shows the comparison of the monthly HP electric energy consumption. The HP electric energy consumption without solar thermal increases considerably (38% more annual total electric energy consumption), mainly because DHW demand in summer must be covered by the HP. There is also a slight increase in energy demand during the coldest months, with a maximum increase of 6% in January.
Considering that the configuration without ST is not optimized, there is room for performance improvement such to diminish energy consumption. Moreover, the surface covered now by ST could be instead covered by additional PV panels such to compensate the added consumption.
Table 7 presents the annual values of consumption, generation, and the balance for the cases considered. The electric balance from the case with more PV panels results slightly lower than the reference, suggesting that, for this case, ST might not be necessary. However, for a complete comparison, the grid round-trip efficiency must be accounted and on-site (thermal, electric) storage must be considered and optimized.

Table 7: Annual electric energy consumption, PV yield, and balance for the reference case, the reference without ST, and the latter case with a larger PV area.

Annual values [kWh/(m²a)]	Reference	Reference w/o ST	Reference w/o ST + PV scaled
Annual consumption	14.3	19.7	19.7
Annual PV yield	12.0	12.0	17.5
Annual Balance	2.3	7.7	2.2

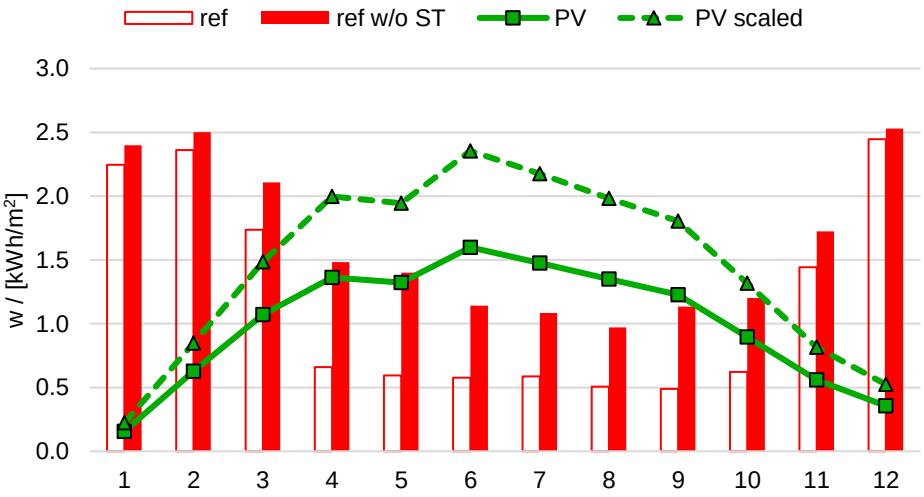

Figure 21: Comparison of monthly total electric energy consumption (HP+Aux) of the reference model (ref) and the reference without the contribution of solar thermal panels (ref w/o ST). The lines represent the electric energy yield by PV panels at the actual state and scaled considering exploiting the area left free by ST.

3.2.3 Theoretical Potential of Desuperheater

The theoretical electric energy saving thanks to the DSH is estimated by Ochs et al. (2019) between 1% and 9%. This is obtained for different DHW to heating demand ratios and DSH contribution factor f_{DSH} (typically ranging between 5% and 15%), considering the reference electric energy consumption

$$W_{tot,ref} = \frac{Q_{DHW}}{SPF_{DHW}} + \frac{Q_H}{SPF_{SH}}$$

and the consumption with the DSH

$$W_{tot,DSH} = \frac{Q_{DHW} - Q_{DHW,DSH}}{SPF_{DHW}} + \frac{Q_H + Q_{DHW,DSH}}{SPF_H}$$

with the contribution of the DSH computed as

$$Q_{DHW,DSH} = f_{DSH} \cdot Q_H$$

Figure 22 (left) shows a scheme of the typical load duration curve with share of SH and DHW and highlights possible DSH contribution.
Figure 22 (right) gives the trend of the electric energy saving, highlighting the typical values of heating to DHW energy demand ratios for low energy house (LEH), Passive House (PH) standard for single-family house (SFH) or multi-family building (MFB). As it is clear from Figure 22, the energy-saving thanks to the DSH is larger as the DHW to heating demand is lower; therefore, the largest benefit is expected for buildings less performing than Passive houses.

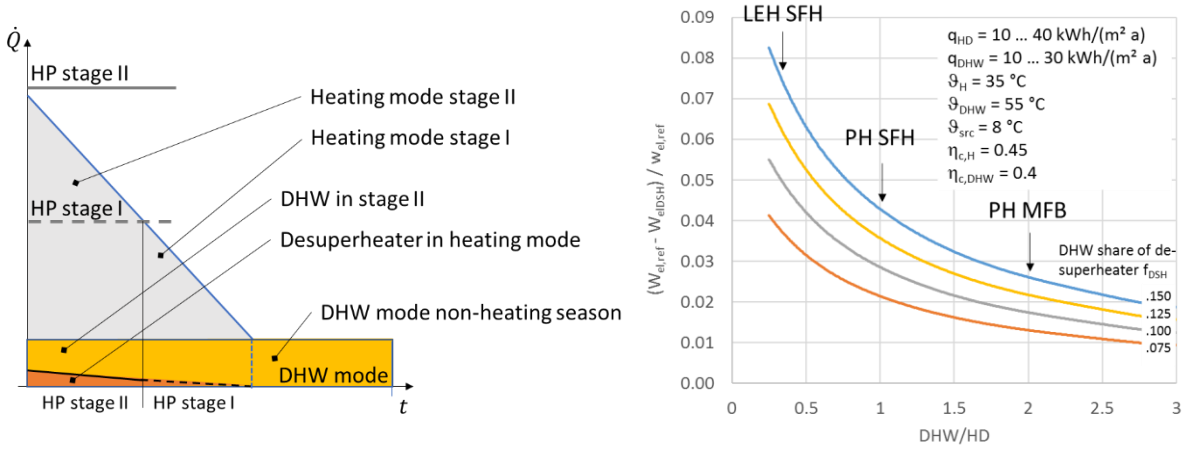

Figure 22: Left: schematic sorted load duration curve (baseload DHW and peak load heating) with double stage HP with possible share of DHW contribution from DSH in heating mode. Right: theoretic reduction of electricity consumption by using a DSH depending on the ratio of domestic hot water (DHW) and heating demand (HD), corresponding to low energy house (LE) and Passive House (PH) standard for single-family house (SFH) or multi-family building (MFB) with the DHW share of desuperheater f_{DSH} as parameter acc. to Ochs et al. (2019)

3.2.4 Alternative System Designs

This section is dedicated to the presentation of possible simplifications to the hydraulic scheme. The aim is to think of system schematics that address education of thermal losses as well as reduction of auxiliary energy consumption and improved HP performance. Even though thermal losses are not accurately modelled in this work, reasonably they are related to the high number of connections to the storage and its large volume. Considering that half of the storage volume is spare space for ST contribution during summer, one possible solution to the reduction of losses would be removing ST, with the effect of reducing also thermal bridges due to connections. Other reasons for removing ST are their little contribution to heating, as emerged in the previous section, and the large photovoltaic panels (PV) energy surplus during summer, which could be effectively exploited for DHW preparation. Therefore, the common aspect of the optimization configurations is the absence of ST in favour of a larger PV area. The increased PV energy yield can be estimated scaling proportionally to the surface ratio of the actual monthly electric energy supply by PV. However, also in this case sufficiently large on-site thermal storage is required in order to avoid strong grid interactions. It is further noteworthy that in case of limited sources for the heat pump (e.g. limited size of ground heat exchanger or limited ground water withdrawal rate), solar thermal can have a positive influence. The excessive auxiliary energy consumption could be tackled simply by reducing the number of circulation pumps and implementing temperature control through variable speed pumps – rather than mixing valves – that save electric energy when the needed mass flow rate is lower than nominal conditions.
Additionally, the benefits of a double staged HP remain unclear, and despite the theoretically advantageous presence of a DSH, there is no such evidence in the monitored data. Figure 22 right, by testing various HP with DSH configurations, showed that the DSH might lead to performance improvement, but as shown above it is very limited in case of high-performance buildings such as the Passive House. Anyhow, it is instructive to test the HP in different configurations.

All these arguments considered, the alternative configurations that best tackle these issues are:

a) direct space heating (SH);
b) condenser-de-superheater (CND-DSH) series;

which are shown in Figure 23 left and Figure 23 right, respectively, and described in the following sections. Note that in these cases the electric grid is used for daily storage, which needs to be evaluated in comparison to a thermal (or electrical) storage on-site in a further step.

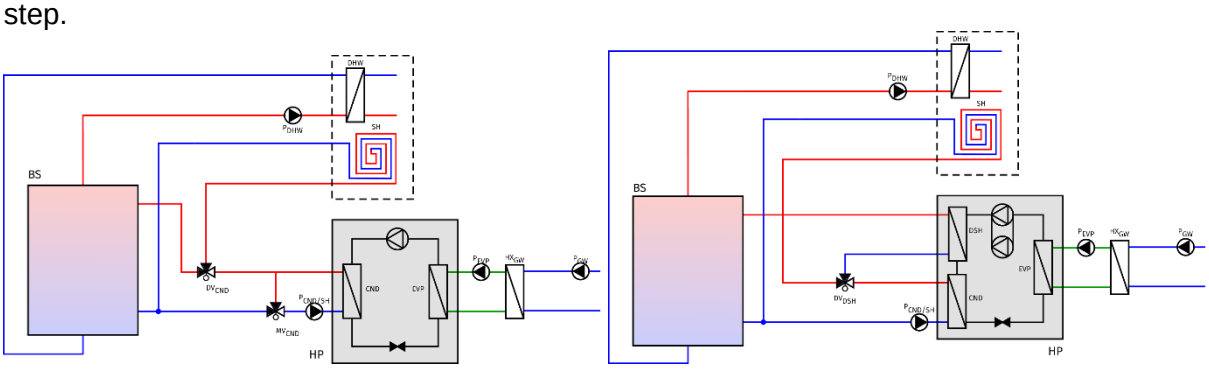

Figure 23: Case A: Heat pump (HP) directly connected to space heating (SH) and buffer storage (BS) for domestic hot water (DHW), without solar thermal panels (ST) ("direct SH") (left) and Case B: Heat pump (HP) with condenser (CND)-desuperheater (DSH) series connection and buffer storage (BS) for domestic hot water (DHW), without solar thermal panels (ST) ("CND-DSH series").

3.2.4.1 Case A: Direct Space-Heating

In this configuration, the HP is directly connected to SH, and through a diverting valve, the HP can load the BS, which is dedicated only to DHW and provides the control variables to trigger DHW priority mode. A mixing valve controls the CND flow temperature to reach the DHW setpoint. Figure 23 shows this schematic.
An alternative version of this configuration uses a variable speed pump instead of a mixing valve to control the flow temperature in DHW mode. The pump drives at maximum power in SH mode, whereas it modulates to reach the flow temperature setpoint when charging the storage. Furthermore, the use of a variable speed pump allows adjusting the flow rate based on the SH demand of the building. Though this case is not considered. Therefore, this optimization case includes two variants:

1. direct SH with mixing valve for temperature control in DHW mode;
2. direct SH with a variable speed pump for temperature control in DHW mode.

The HP in SH mode is controlled based on the indoor air temperature by a hysteresis control (±0.5 K), and there is no control of the flow temperature, which therefore varies based on the return temperature. It must be highlighted that being each simulated building modelled as a single thermal zone, the temperatures to be controlled are just two, which in reality, when several flats are present, is not the case, and care should be put on the choice of a correct control parameter. Several alternatives are available e.g., ventilation exhaust temperature or floor heating return temperature, and it would be interesting to test these strategies; however, for this work, the simplification of controlling based on average air temperature is accepted.
The control for DHW is based on the storage temperature with a top sensor that turns the HP on when the temperature falls below the setpoint and a sensor at the bottom that stops the BS charging. Both the top-most sensor and connection are located lower than the actual top of the BS to ensure the reserve volume required to guarantee the comfort conditions. The DHW set-point is 52 °C, which is the current DHW average flow temperature of the actual case-study. Accordingly, the mixing valve controls the CND flow temperature to reach the set-point. The storage is charged to reach 48 °C at the bottom.
The new storage tank is assumed to have the same thermal characteristics as the original one. With volume equal to 1.5 m^3 and the diameter set such to minimize the lateral surface.

The HP unit is substituted with a simpler unit without DSH and with a single compressor. Another reason for selecting a new HP is that the original HP is oversized for the required heating power. The new HP is modelled as presented in 3.1.2, where the performance maps adopted are provided by the manufacturer and reported in the appendix.

3.2.4.2 Case B: Condenser- Desuperheater Series

The parallel loop connection for CND and DSH connection is not beneficial in DHW mode. Indeed, being the loops separated, the condensation temperature must be raised to the DHW setpoint (e.g. 55 °C), resulting in an HP performance decrease. A better option would be allowing the series connection between condenser (CND) and DSH on the secondary side, at least for DHW preparation, which would guarantee a lower condensation temperatures (Monteleone, 2019, Ochs et al., 2019).
The series connection is thus investigated. To keep the schematic simple, a diverting valve is installed on the CND flow branch, which deviates a part of the CND flow into the DSH providing simultaneously SH and DHW. The fraction of the mass flow rate to be circulated in the DSH depends on the DSH outlet temperature set-point. In this case, this is controlled such to achieve the storage temperature at the height of inlet increased by 1 K to ensure stratification. In DHW priority mode, the valve diverts the flow completely to the DSH. Unless temperature control was performed, at the beginning of DHW priority, the storage would be loaded with the flow at a lower temperature, causing mixing, and thus requiring longer loading time. Consequently, there must be temperature control, which is in this case performed by varying the pump flow rate, as in the second variant of the “direct SH” optimization case. The BS has the same characteristics as the previous case.
The HP unit adopted for this case is the same as the reference model, slightly modified to use the mass flow rate fraction as look-up value rather than the DSH inlet temperature. The new performance maps were developed through the steady-state model developed by Monteleone (2019) adapted as presented in Franzoi (2020).

3.2.4.3 Alternative System Designs Simulation Results

Figure 24 shows the monthly HP, auxiliary, and total electric energy consumption of the reference case and the alternative designs.

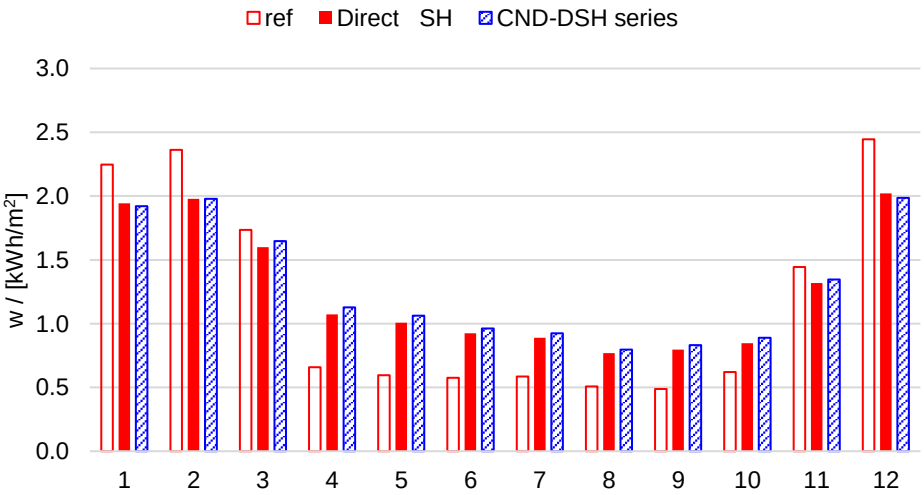

Figure 24: Comparison of total electric energy consumption (HP+Aux) for reference case (ref), direct space heating (SH), and condenser-desuperheater (CND-DSH) series alternative system design cases.

In “Direct SH” with temperature control performed by the mixing valve, the energy consumption results in a 2% higher consumption than in the case with the variable speed pump, therefore it is not considered in the comparison. However, the increase in energy consumption is related only to the higher auxiliary energy demand, whereas the HP consumes equally. Therefore, in this case, mixing valve or variable speed pump-driven temperature control does not influence the performance of the HP.

It is also important to notice that the heating demand (HD) of the building with the alternative hydraulic designs decreases slightly (3 %) when compared to the reference case. This is a consequence of the different connections between terminal units and the HP. The difference in HD reduces also the electric energy required, though insignificantly.
For both alternative cases, the energy consumption is higher in summer due to the absence of solar thermal contribution. Nonetheless, the consumption during the heating season is decreased with respect to the reference case. The “CND-DSH series” performs slightly better than the “direct SH” configuration during the coldest months, thanks to the DSH. Indeed, when the HD is high, the simultaneous preparation of DHW is also higher, reducing the time for DHW priority only, which harms the performance of the HP. In the other months, the original HP is less efficient than the unit installed in the “direct SH” configuration (i.e. SPF = 3.2 instead of SPF = 3.4 outside the heating season). The annual seasonal performance factors (SPFs) for “direct SH” and “CND-DSH series” are in both cases equal to 4.1, whereas for the reference case is SPF = 3.9. The share of auxiliaries on the total consumption is decreased thanks to the reduced number of circulation pumps for both the optimized schematics.

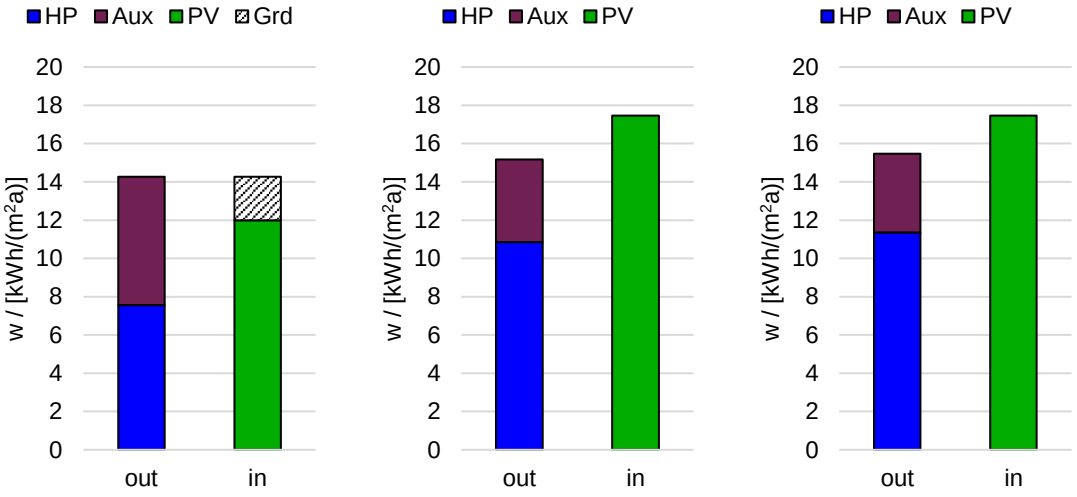

Figure 25: Annual electric energy balance for reference case (left), direct space heating case (centre), and condenser-desuperheater series case (right).

Considering that the annual electric energy consumption is slightly larger for ”CND-DSH series” (11.4 kWh/(m^{2}a)) than “direct SH” (10.9 kWh/(m^{2}a)) and that the “direct SH” configuration is simpler in terms of hydraulic schematics and components to be installed, the suggested alternative design for the case studied is the latter.

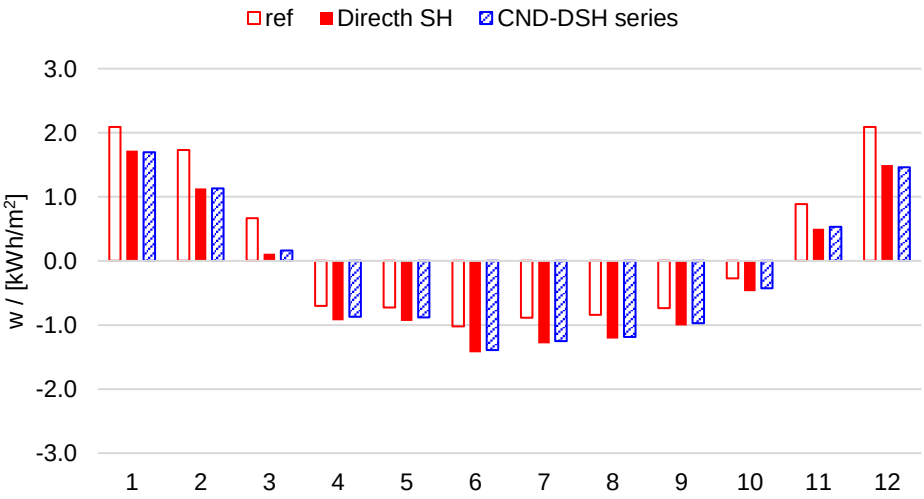

Figure 26: Monthly electric energy balance for reference case (ref), direct space heating (SH), and condenser-desuperheater (CND-DSH) series alternative system design cases.

Nevertheless, it must be noted that the performance of heating systems in buildings with a higher SH-to-DHW demand ratio could benefit from the presence of the DSH.
Thanks to the larger PV energy supply and the reduced share of the auxiliaries, the annual net-zero electric energy balance can be achieved in both the optimized schematics, as shown in Figure 25, despite the larger HP energy demand than the reference case.
Figure 26 shows the monthly balance. The alternative cases outperform the reference in all months. However, the net-zero balance is far from being achieved during the winter months also for the alternative cases, and the annual balance is less than zero thanks to the large energy surplus in summer.

3.2.5 Critical Discussion of Net-Zero Energy Buildings

Through the analysis of the simulation results, some conclusions on the achievement of net-zero energy balance can be made, particularly regarding the effectiveness in reducing the building-specific CO_2 emissions and the calculation boundary for the energy flows.
As previously discussed, the achievement of the net-zero energy balance in the alternative cases is achieved mostly thanks to the large energy generation surplus during the summer months. Being the renewable energy share on the grid low during winter – and the opposite in summer months, the achievement of the net-zero energy balance on an annual basis is misleading and does not provide a unique mean to ensure lower CO_2 emissions. An alternative evaluation criterion to quantify the *decarbonization effect* of a building might be the annual non-renewable primary energy balance neglecting surplus energy sold to the grid, obtained assuming monthly-dependent conversion factors as by Ochs and Dermentzis (2018) (Table 8). This emphasizes the importance of maximizing the performance of the building during the winter months when on-site renewable energy generation is at its lowest, rather than considering beneficial the energy surplus during summer.

Table 8: Monthly variable non-renewable primary energy factors for two generation scenarios considering the different share of hydro, wind, and photovoltaic energy as by Ochs and Dermentzis (2018). The non-renewable primary energy factors assumed for hydro, wind, PV and fossil are respectively $f_{nren,hydro} = 0.01$ kWh$_{PE}$/kWh$_{el}$, $f_{nren,wind} = 0.05$ kWh$_{PE}$/kWh$_{el}$, $f_{nren,PV} = 0.1$ kWh$_{PE}$/kWh$_{el}$ and $f_{nren,hydro} = 2.4$ kWh$_{PE}$/kWh$_{el}$. The monthly values are computed as $f_{nren} = \sum_i f_{nren,}/W_{el,tot}$.

Scenario	Jan	Feb	Mar	Apr	May	Jun	Jul	Aug	Sep	Oct	Nov	Dec
A (10-10-10)	2.01	1.96	1.89	1.60	1.33	1.20	1.18	1.28	1.53	1.78	1.92	2.01
B (10-30-30)	1.53	1.42	1.23	0.50	0.08	0.08	0.08	0.08	0.33	0.98	1.33	1.54

Table 9 presents the annual primary energy consumption for the reference and alternative cases considering the “scenario A” of Table 8, together with the total annual electric energy consumption, the PV yield, and the balance. Both the optimization reduces the primary energy consumption of the reference case by one third, because of the lower consumption and the larger PV yield during winter.

Table 9: Annual total electric energy demand, photovoltaic panels (PV) yield (referred to the floor area), electricity balance, and non-renewable primary energy balance.

	W_{el} [kWh/(m^{2}a)]	W_{PV} [kWh/(m$_{flr}^2$a)]	ΔW_{el} [kWh/(m^{2}a)]	PE_{nren} [kWh/(m^{2}a)]
Reference	14.3	12.0	2.3	14.8
Direct SH	15.2	17.5	-2.3	9.9
CND-DSH series	15.5	17.5	-2.0	9.9

Figure 27 shows the monthly electric energy demand if household consumption is considered in the energy balance. For the estimate of appliances’ consumption, a quite optimistic value of 1500 kWh/a per flat – as opposed to an estimated consumption in the European Union (EU) of 3200 kWh/a per flat – is chosen as in Ochs et al. (2017) (common-area electricity such as for the lift is disregarded). In this case, the PV yield is hardly enough to cover the monthly electricity demand, particularly for the heating months. This enforces once more the importance of focusing the design effort in minimizing demand and maximizing the performance of the heating system during winter, to limit its dependence on the grid.

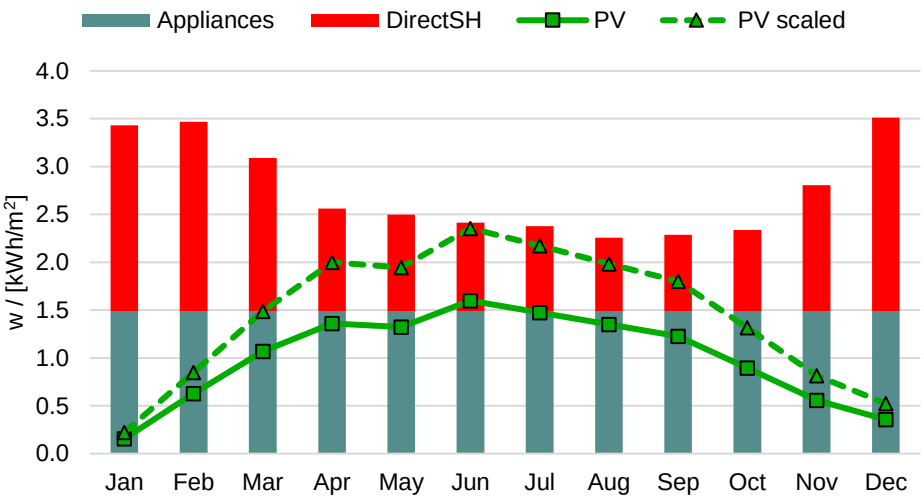

Figure 27: Total monthly electric energy consumption with appliances for direct space heating (SH).

Furthermore, this poses the question of whether the effort of optimizing the control for PV self-consumption would be relevant considered that it could be directly used for household energy needs. Therefore, for correct analysis, a reasonable assumption for appliances usage schedule and consumption should be included.

3.2.6 Conclusions

This report shares the experience so far gained by the group of Energy Efficient Building of the University of Innsbruck during the years-long monitoring and analysis of the multi-family passive house “Vögelebichl”, built to achieve the ambitious goal of a net-zero energy building. The monitoring data provided insight into the main design and commissioning issues. Parametrized simulation model firstly of the HP and the buffer tank, then of the building and heating system allowed to perform testing of preliminary improvements, which guided the proposal of alternative system designs and control strategies. The sound sizing of the components adapted to the buildings can be furthermore derived from these models.
The work will continue further analysing the critical aspects that emerged from the monitoring analysis. The simulation model will be adopted to study optimal control strategies of the actual heating system, particularly regarding the control of the double-staged HP. The study on the trade-off between ST and PV will be expanded accounting for costs and different heat generation units e.g., air-source HP as well as accounting for the grid interaction.
The results presented in this work and those that will follow, are a valuable source for guiding the proper integration of HPs in nZEBs to ensure maximum exploitation of the technology to achieve the highest performance and minimize the environmental impact of the building within the constraint of cost-optimal solutions.

4 Integration and control of thermal and electric storage

4.1 Integration of thermal and electric storage at SFH Berghalde

In smaller buildings, the heat pump is often one of the main electricity consumers and has a potential for load shifting, since thermal energy can be stored or the inertia of the thermal systems can be used by overloading. Thus, the heat pump in combination with the building-integrated or technical storages can be used for a smart operation to either increase the self-consumption of on-site PV electricity or to use the demand response capability of the heat pump for grid supportive operation.

The single family plus energy house Berghalde of 260 m^2 energy reference area and an installed PV system of 15.3 kW_p was used as example to investigate smart controls as well as the use of thermal and electric storage for load management strategies. Detailed monitoring data of the building of four the years 2016-2019 are documented in the Report Annex 49 part 2 on Monitoring.

4.1.1 Control strategies for increasing self-consumption

Within the framework of the research project documented in Bockelmann et al. (2015) control strategies and optimisations for increasing supply and load cover factor by on-site PV electricity in connection with electrical and thermal storage were tested and approved on the Berghalde single-family house using simulations.
Within the framework of the variant and parameter study, the aspects and approaches listed in Table 10 were examined in a first step in order to be able to delimit the influence on the increase of the supply cover factor. In a second step, the results of the individual parameter analyses were then combined into targeted components for increasing the supply cover factor.

Table 10: Combination of variants and parameters

Abbreviation	Variant
A	Activation heating and cooling mode
B	Adaptation buffer storage control
C	Night setback
D	PV surplus control - PV power
E	PV surplus control - temperature increase

4.1.2 Variant A –Activation of heating and cooling mode

Within the framework of the variants "Activation of the heating and cooling case" it is intended to show that the activation control for the heating and cooling case can and should be kept simple.

Table 11: Parameter change Variant A – Activation heating and cooling mode

	Heating mode		Cooling mode	
	ON	**OFF**	**ON**	**OFF**
Basis	$T_{amb,72h}$ < 12°C AND 2 days < 17 °C General heating from T_{amb} < 6°C	$T_{amb,72h}$ >15°C	$T_{amb,72h}$ > 26°C AND 2 days > 24 °C General cooling from T_{amb} > 30°C	$T_{amb,72h}$ < 22°C
A1	$T_{amb,72h}$ < 12°C	$T_{amb,72h}$ > 15°C	$T_{amb,72h}$ > 26°C	$T_{amb,72h}$ < 22°C
A2	$T_{amb,48h}$ < 14°C	$T_{amb,48h}$ > 16°C	$T_{amb,48h}$ > 20°C	$T_{amb,48h}$ < 18,5°C
A3	$T_{amb,24h}$ < 14°C	$T_{amb,24h}$ > 16°C	$T_{amb,24h}$ > 20°C	$T_{amb,24h}$ < 18,5°C
A4	$T_{amb,72h}$ < 12°C General heating from T_{amb} < 6°C	$T_{amb,72h}$ > 15°C	$T_{amb,72h}$ > 22°C General cooling from T_{amb} > 30°C	$T_{amb,72h}$ < 20°C

Furthermore, the influence of a shift of the temperature limits and averaging on the self-consumption is to be examined.
Compared to a complicated control via an average value as well as additional conditions over further time intervals, a simple average value control has a negligible influence on the heating demand as well as on an increase of self-consumption.
The implementation of simple controls is therefore preferable. A change in the averaging from an average outdoor temperature over 72 h to 48 h and 24 h with a simultaneous increase in the switch-on temperature leads to an increase in heating demand of about 2-3%. The PV supply cover factor and load cover factor increases only very slightly < 1%. The total electricity requirement increases by around 1%. As a result, the grid electricity supply remains almost identical to the basic variant.

For future regulations a simplification to a simple average regulation should be foreseen, e.g. regulation on T_{amb24h}.

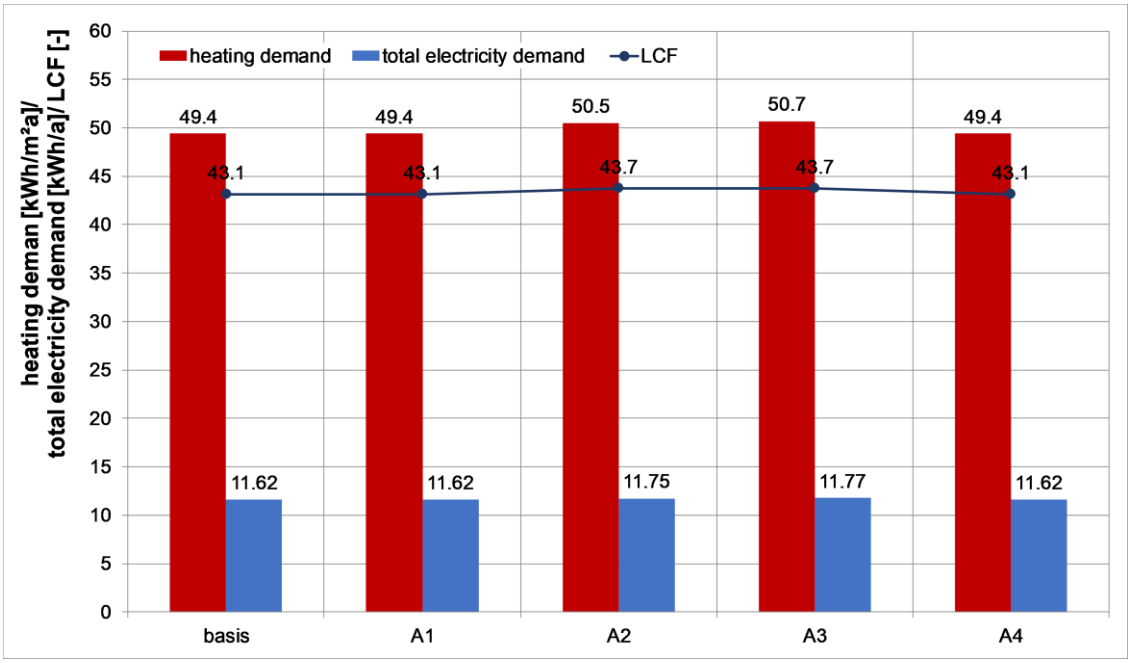

Figure 28: Heating demand, total electricity demand and PV load cover factor of variant A – Activation of heating and cooling mode

4.1.3 Variant B - Adaptation of storage tank control

Within the variant study for storage tank control, it is to be elaborated to what extent the specification of the storage tank temperature has an influence on the further operation of the system and which temperature limits are to be determined. The buffer storage tank control is the temperature in the thermal storage tank that must be provided to supply the floor heating system. Adaptation of the buffer storage tank control from a heating curve of the storage tank temperature with respect to the floor heating flow temperature to a fixed setpoint control and consideration of a hysteresis does not have any significant effect on the domestic electricity share. The share of self-consumption remains almost constant. The supply cover factor decreases minimally up to 1%.
The decisive factor in this case is the effect of the specified temperature levels to be achieved on the annual performance factor and thus on the efficiency of the heat pump. By increasing the supply temperature, the performance factor of the heat pump decreases accordingly and the electricity consumption and energy costs increase. The supply temperature for the floor heating system in the thermal storage tank is permanently maintained at a higher temperature level than would be necessary for heating the building (depending on the outside temperature). Operation with night setback from 10 p.m. to 6 a.m. results in a saving in the heating requirement of around 0.6%. Due to the lower system temperatures at night, the annual performance factor and thus the efficiency of the heat pump system increases.

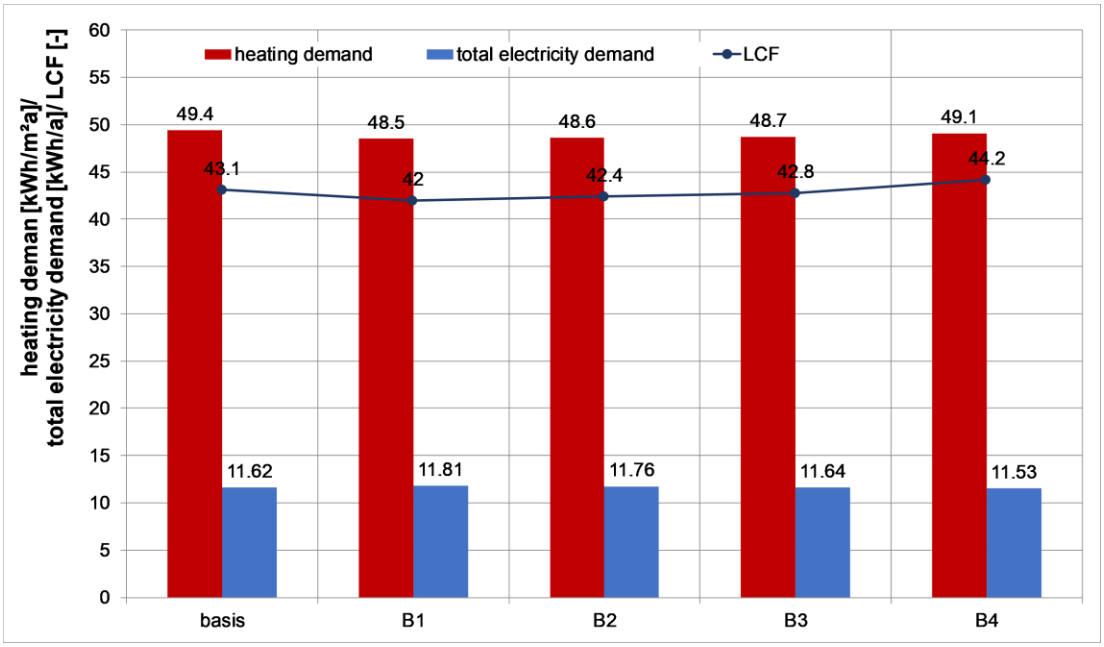

Figure 29: Heating demand, total electricity demand and load cover factor of variant B - Adaptation of buffer tank control

The most reasonable variant is a control via the heating curve with night setback. However, a reduction of the storage tank temperature must be followed by a simultaneous reduction of the set flow temperature and the set surface temperature.

Table 12: Parameter change Variant B - Adaptation of storage tank control

Basis	Heating curve (red, without hysteresis) for the storage temperature of the floor heating system 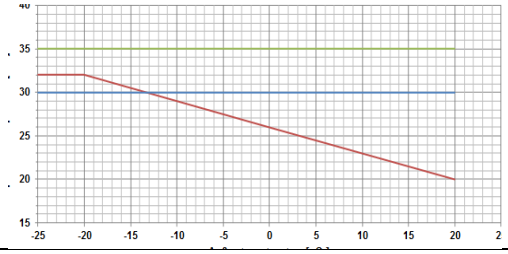
B1	Fixed setpoint temperature in the buffer tank of 35 °C (without hysteresis)
B2	Fixed setpoint temperature in the buffer tank of 30 °C with 5 K hysteresis (HP ON < 30°C and HP OFF > 35°C)
B3	Fixed setpoint temperature in the buffer tank of 30 °C without hysteresis
B4	Control via heating curve with night setback (eco and comfort mode) comfort: 6.00 to 22.00 and eco: 22.00 to 6.00 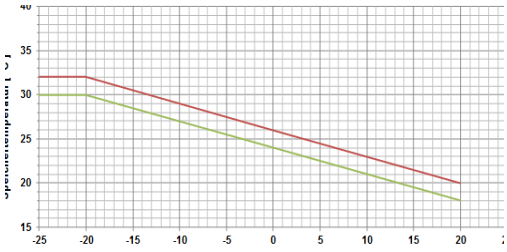

4.1.4 Variant C - night setback

In this variant, the influences of a reduction of the flow temperatures in the period from Mon - Sun from 22:00 to 5:00 o'clock on the different heating curves and thus system components, storage tank temperature, flow floor heating and target surface temperature are to be determined.

Table 13: Parameter change Variant C – night setback

Basis	No night-time reduction and all-day operation of the heat pump
C1	The heating curve (return flow control) for the buffer tank is reduced by 2 K as night setback.
C2	Reduction of the target surface temperature during the night to a minimum of $T_{surface}$ = 19 °C, corresponding to a minimum room air temperature T_{room} = 17 °C
C3	Night setback of the set surface temperature + floor heating flow temperature: Set surface temperature at night to minimum $T_{surface}$ = 19 °C and Shifting the heating curve floor heating flow from max. 38 °C to max. 33 °C.
C4	Night setback of the set surface temperature + floor heating flow temperature + buffer / HP return control. Variants C1 to C3 together.

With regard to room comfort, no room temperature below 18 °C can be recorded when implementing the night setback in all variants. The heat is stored in the massive building structure and released overnight. The room comfort is therefore not impaired.
Lowering the heating curve of the thermal storage has no significant effect on the heating demand. The total electricity demand drops slightly by 0.6%. Due to the shift in the heat pump's operating times to daytime operation, the amount of electricity drawn from the grid is reduced and the PV load cover factor can be increased by 0.7%. The implementation of a night setback of the target surface temperature results in the highest savings. The heating requirement is reduced by 6.3% or 3.0 kWh/(m²a). A saving of 2.4% is achieved in terms of total electricity consumption. Grid electricity purchases were reduced by 5.9% as result of the increase in the load cover factor from 41.6% to 43.8%. A lowering of the heating curve of the floor heating flow temperature as well as the combination of all individual variants does not achieve additional savings on heating demand, total electricity demand and/or main power supply. The supply and load cover factor remains almost the same.

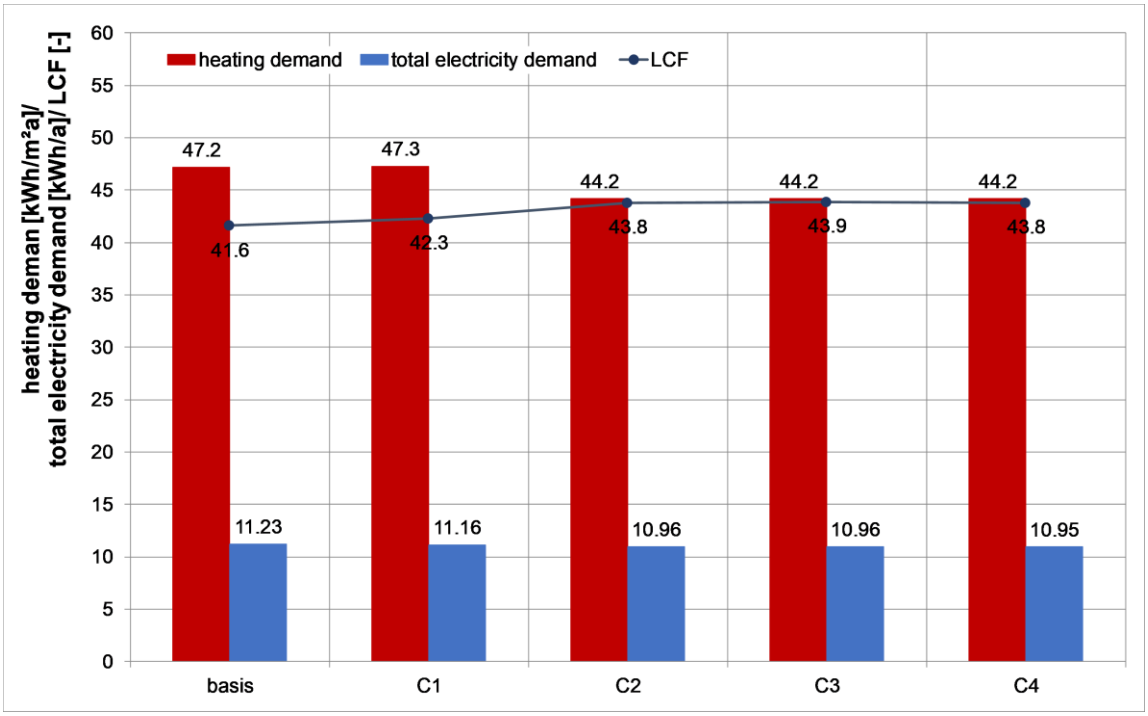

Figure 30: Heating demand, total electricity demand and load cover factor of variant C – night setback

The simulation result also clarifies that a night setback in heat transfer must take place first. Lowering the floor heating flow temperature or the buffer tank temperature without simultaneously lowering the target room temperature (target surface temperature) does not lead to any savings. On the other hand, there is a risk of an increased heating demand, due to the longer running times of the circulating pumps with lower system temperatures in order to reach the target temperature in the room.

The lowering of the surface temperature is implemented, since a further lowering of the buffer storage or flow temperature does not achieve any further reductions.

4.1.5 Variant D - PV surplus control - PV power

In the course of the parameter study on PV surplus control, it is to be determined from which PV yield capacity a control for forced operation of the heat pump becomes decisive in order to increase the inflow share. The PV surplus control occurs when the PV system exceeds a defined PV production capacity during the heating period. In this case, the increase of the surface temperature, the storage tank and the heating curve for the underfloor heating are activated. As far as the scheme is concerned, this means that

- the surface temperature setpoint increases by +2 K,
- the storage tank is heated to 55 °C and
- the floor heating flow temperature is raised by +2 K.

The individual variants and steps result from the marginal PV income payments for the activation of the surplus regulation. The limit values "PV surplus for PV output" > 2 kW, 3 kW, 4 kW and 5 kW are assumed.
By increasing the surface temperature of the floor, the operative room temperatures in the zones rise, a warmer room climate is created. The PV surplus control - PV capacity leads to an increase in the heating demand. This increases between 3.7% and 7.3% for the variants examined. This is also due to the increase in storage losses of ~2% to 5%. The share of PV own use increased by 3.8% to 6.0%. At the same time, the load cover factor rose between 3.8 % and 5.6 %.

When selecting the activation value, ensure that it is higher than the sum of the base load (household electricity / user electricity) and heat pump electricity. Below the demand, additional electricity would have to be drawn from the grid to operate the heat pump, in order to cover the then existing electricity demand by the forced operation of the heat pump.

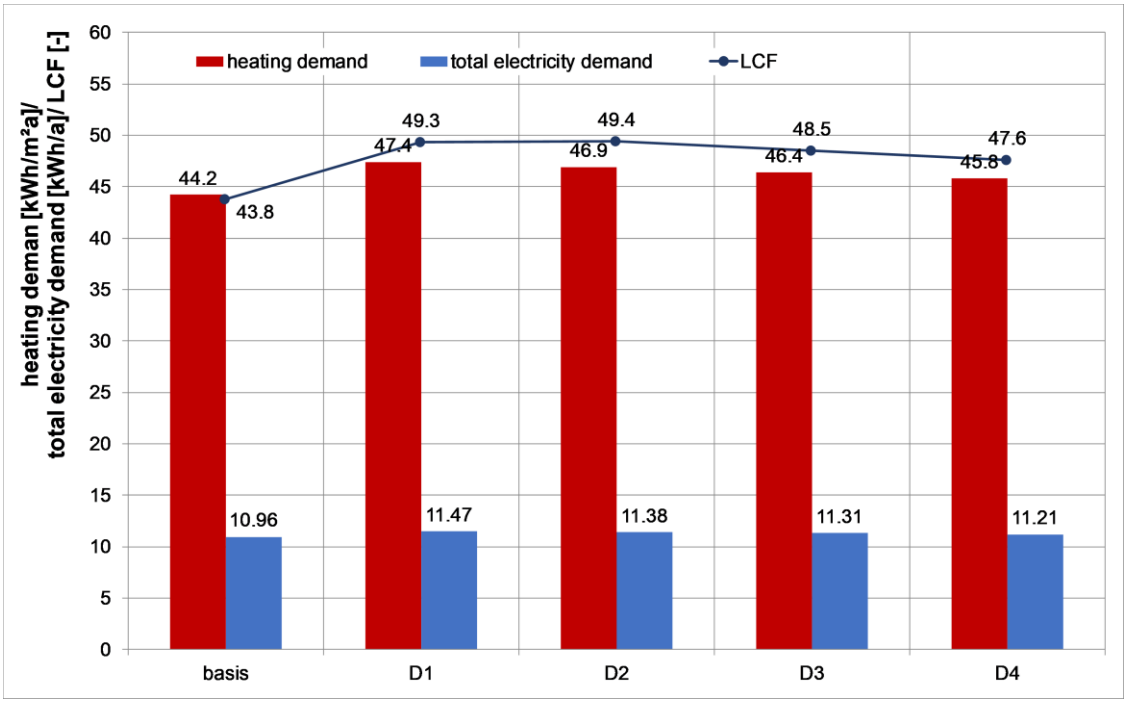

Figure 31: Heating demand, total electricity demand and load cover factor of variant D - PV surplus control - PV power

4.1.6 Variant E - PV surplus control - temperature increase

In the course of the parameter study on PV surplus control, it is intended to determine not only the PV output, but also, in how far the target temperature increase can be beneficially used without compromising comfort. The PV surplus control occurs when the PV system exceeds a defined PV production capacity during the heating period. In this case the overheating of the surface temperature, the storage tank and the increase of the heating curve for the floor heating is activated.

Starting from the basic variant (overheating +2 K), a further increase in the overheating temperature leads to a negative influence on comfort due to excessive operative temperatures. A reduction of the superheat to 1 K leads to a reduction in the use of own electricity and an increase in the use of main electricity.

It is recommended to maintain the 2 K surface temperature overheat and the floor heating flow temperature for PV surplus control.

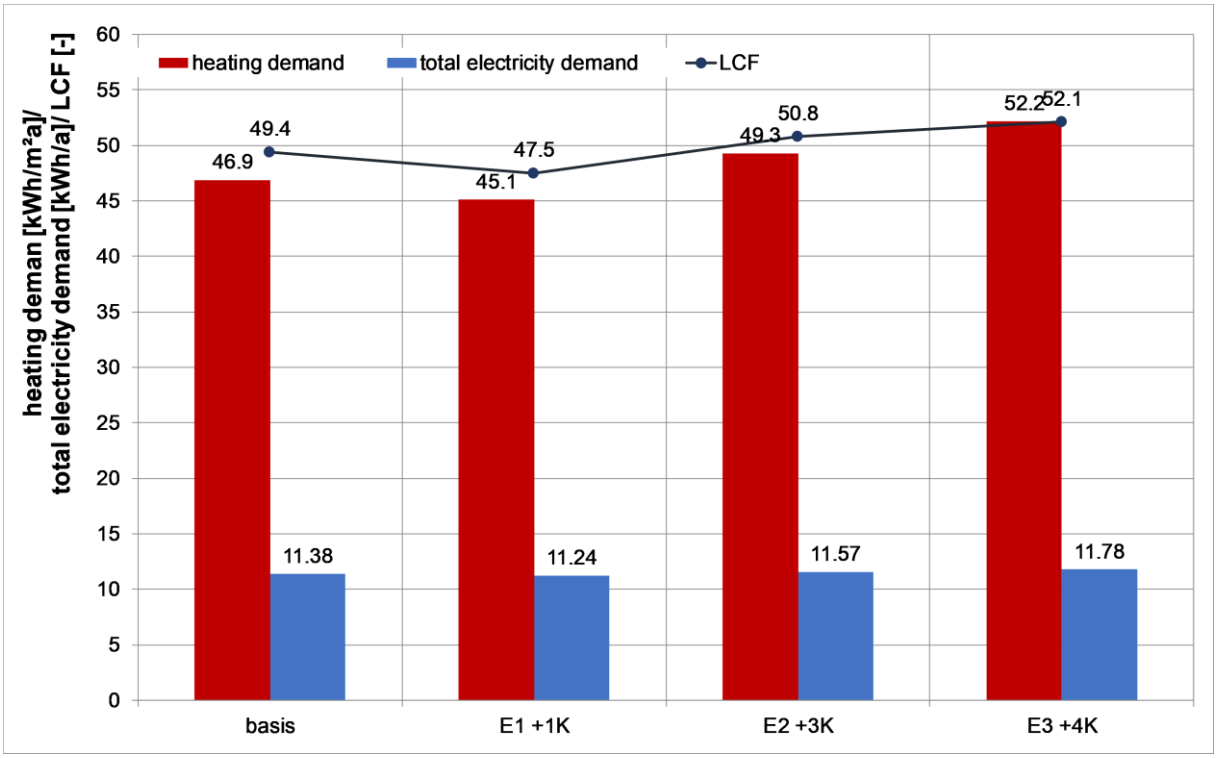

Figure 32: Heating demand, total electricity demand and load cover factor of variant E - PV surplus control - temperature increase

4.1.7 Concept variants for increasing self-consumption

Based on the above-mentioned findings of the various individual influences with regard to heating requirements, total electricity demand, load cover factor and total annual costs, eight variants were considered to be target-oriented and were then examined and evaluated in more detail. The variants are based on the one hand on simple implementation without major technical effort and on the other hand on optimization measures that entail further investment costs.

In order to increase the load cover factor, eight other strategies were examined in addition to normal operation. The selected system variants for the increase of self-consumption are based on a thermal and electrical storage of the self-produced power yields, control strategies and can be combined with each other.

When implementing the PV control, as soon as sufficient PV yield is available by the PV system, all available thermal storage capacities such as the underfloor heating and the hot water storage / buffer storage are used.

The scheme provides that

- the buffer storage temperature is increased, so that the storage potential can be increased and thus a sufficient heat storage tank is generated for the time without electricity production
- the setpoint value of the surface and flow temperature of the underfloor heating is raised. In the course of this, the structural storage mass is used as an intermediate storage. This is stored in the solid components surrounding the room to counteract the drop in temperature in the evening and night hours below the comfort limit.

The buffer storage expansion is only carried out in the heating period from (September - May). During this time, a second buffer storage tank (700 l) is connected to the existing buffer storage tank (825 l) and the storage volume is coupled, so that a total volume of 1,525 l is available.
In principle, the following applies: User comfort should not or must not be restricted by the planned measures.

Table 14: Variant Analysis Simulation

Basis	no battery and optimizations for self-consumption -> "normal operation" of the house
1	Night setback of the flow temperature (surface temperature min. 19°C)
2	Night setback + PV control (PV power > 3 kW)
3	Integration of a 7 kWh - battery
4	Battery (7 kWh) + night setback
5	Battery (7 kWh) + night setback + PV control (PV power > 3 kW)
6	Night setback + PV control + buffer storage expansion (27.09. - 10.05.)
7	Battery (7 kWh) + night setback + PV control + buffer storage expansion (27.09. - 10.05.)
8	Integration of a 27 kWh battery + night-time reduction + PV control + buffer storage expansion

The simulation results show that by using the different components (battery, buffer storage, etc.) the PV supply cover factor can be increased from 27% (base) to over 45% and the PV load cover factor from 34% (base) to over 50%. Furthermore, the proportion of electricity supply by the grid can be reduced by up to 30%, when the variants are integrated and implemented. However, the measures will increase electricity demand by up to 4.5%. This is due to the increased running time of the heat pump as well as the higher flow temperature within the PV control (Figure 33 and Figure 34).

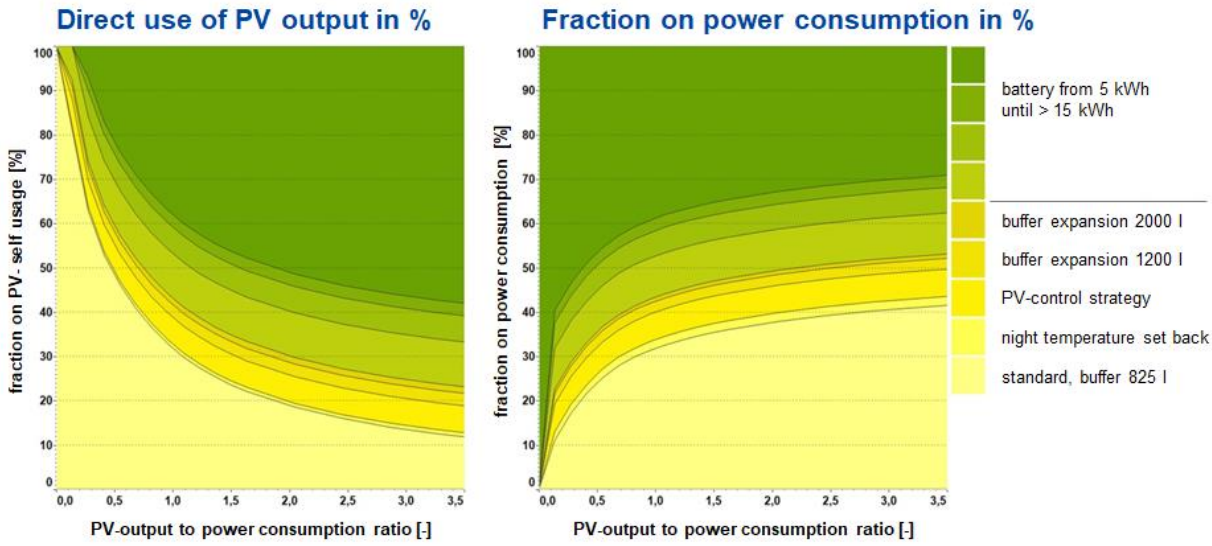

Figure 33: Results of system simulation: direct use of PV and fraction on power consumption

On the basis of the selected component variants, it can already be shown that the supply cover factor and the load cover factor can be increased with only a small amount of effort and a few technical components. Even the implementation of a night setback or the implementation of the PV surplus control will result in an increase of the shares up to 40%. Without the use of an electrical storage unit, but with adaptation of the control strategy for electricity self-consumption and a buffer storage extension, the supply cover factor can be increased to 38% and the load cover factor to 45%. At the same time, grid purchases are reduced by around 13%.

Figure 34: Results of system simulation increase of electricity self-consumption

4.1.8 Integration and design of electric storage

Various studies, tools and programs are currently available on the German market for the design, dimensioning and determination of the load cover factor and supply cover factor of batteries. A comparison shows that all applications give similar results and do not show large deviations. It can therefore be assumed that the available tools and programs can be used for the initial design and dimensioning of the plants.
It should be noted that the supply cover factor as well as the load cover factor according to the definition on page 8 describes the share of the total electrical energy in the building that can be covered by locally generated PV electricity. A full feed-in of the PV system would mean that the load cover factor is 0%, while 100% expresses that the building can be completely supplied by PV electricity. A load cover factor of 100% could only be achieved with very large batteries (high storage capacity). Particularly in the winter months, most households in Germany cannot cover their needs with PV electricity. In principle, however, the higher the nominal output of the installed PV system, the higher the load cover factor of a typical private household.
With regard to a limit value consideration of the supply and load cover factor, the following can be stated for a single-family house without electricity storage (Kley, 2018):

- With increasing PV output, the PV supply cover factor and load cover factor develop in opposite directions. While the supply cover factor decreases with increasing PV output, the load cover factor increases. The decrease or increase decreases with increasing performance (diminishing marginal utility).
- Over the power range considered, an increase in the power of the PV system has a higher effect on the decrease in the supply cover factor than on the increase of the load cover factor.

As a basis or parameter study for the determination and limit observation of the battery size to achieve 100% supply- and load cover factor, simulation studies were implemented on the building and system model of the Berghalde single family house. The results show that a nominal storage capacity of around 6,000 kWh would be required to achieve a load cover factor of 100% (full autarky).
The results of the analysis to achieve self-sufficiency of the building show that it is questionable and unrealistic to achieve self-sufficiency for single-family houses. On the one hand, a battery with a capacity of 6,000 kWh would not fit into a single-family house (too much space required), and on the other hand the control or loading would have to be considered. Moreover, current marketable batteries are not suited for seasonal storage, but for daytime storage.

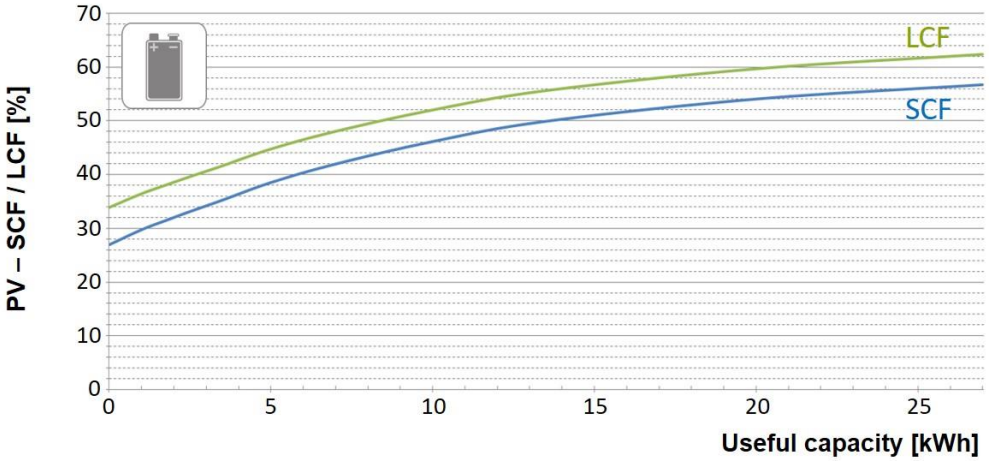

Figure 35: Results of system simulation Increase of PV self-consumption as LCF and SCF

It would take months to years until the installed battery is fully charged. In addition, there are high storage losses and a high maintenance charge would be necessary in the winter months. The aim of the conversion and implementation of batteries should therefore be to increase the load cover factor and to reduce energy costs, but self-sufficiency cannot be the goal. Reasonable capacities of battery storage are well below 50 kWh for single-family houses.

A coverage ratio of max. 50-60% is to be achieved. The goal of self-sufficiency and thus coverage of 100% of the electricity demand cannot be implemented in an economic solution in central European latitudes and in the less productive winter months. The battery would have to be oversized and the PV system would therefore be uneconomical.

By means of a sensitivity analysis, the influences and sizes of individual plant components and consumers on the load cover factor and supply cover factor are examined. The simulations carried out on the "Berghalde" building (Kley, 2018) and consider the essential design parameters for energy supply to achieve a high supply and load cover factor. The results are used to develop design diagrams that can be used to plan electricity storage facilities and maximize the load cover factor. The diagrams apply to locations in Germany and can be used for single and two-family houses as well as apartment buildings with monovalent electric heat pumps. Taking into account the usable electricity storage capacity, the PV yield as well as the electricity demand of the building, the diagrams enable an optimization of the supply cover factor (SCF) and the load cover factor (LCF) by minimisation of grid supply.

With a ratio of PV yield to annual electricity demand of 1 MWh/MWh and no electricity storage in single-family houses, a coverage ratio > 30% can be achieved for both the supply and the load cover factor. The dimensioning of an electricity storage unit, which is integrated into a system to increase the electricity self-consumption, can be based on the installed capacity of the PV system and the electricity demand. The isolines of the PV self-consumption show a steeper curve above 1.25 kWh of usable capacity per MWh PV yield. With a specific solar yield of 1,000 kWh/kW_p, this results in a characteristic value related to PV output of 1.25 kWh of usable capacity per kW_p of PV output.

From the progression of the share of own electricity use, it can be seen that from a ratio of storage capacity to electricity demand of > 1.25 kWh/MWh, a further increase in the electricity storage is of little benefit and the load cover factor cannot be further increased significantly.

This can be explained by the fact that larger electricity storage units cannot be completely discharged during the night and thus not the entire storage capacity is available the following day. With a storage capacity of 1 kWh/MWh and a PV yield of 1 MWh/MWh, the load cover factor is 50%. By doubling the storage capacity to 2 kWh/MWh, the load cover factor can only be increased to 55%.

In addition, an increase in the size of the electricity storage unit has little added value. This relationship becomes even more apparent when looking at the isolines of the load cover factor. An expansion of the storage capacity beyond the diagonal generally causes only a slight increase in the load cover factor. In order to achieve a high load cover factor, both the storage capacity and the PV output must therefore be increased.

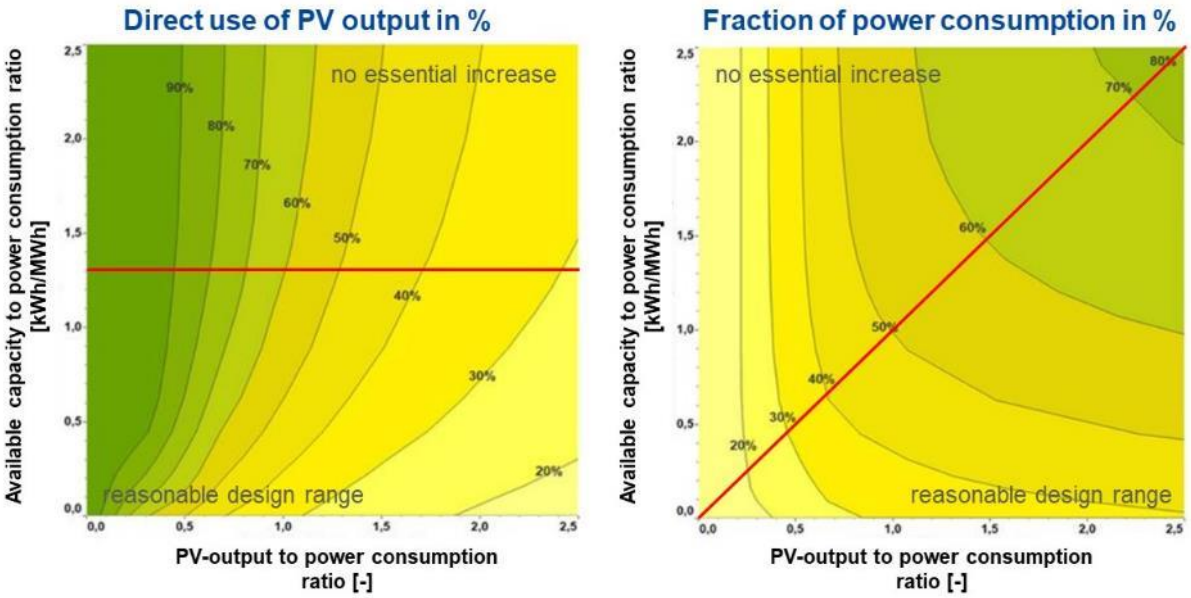

Figure 36: Share of PV owner-occupancy and coverage of single-family houses (Kley, 2018)

4.1.8.1 Comparison between Power-to-Heat and electrical storage

Further sensitivity analyses are used to analyse and compare the influences of the thermal and electrical storage systems on the cover factors as well as on the profitability.
In the first step, it is determined to what extent the increase in supply cover factor by increasing the storage volume of the thermal storage is reasonable. Subsequently, the electrical storage units are evaluated and the costs for storing the electrical energy are determined. Finally, a comparison of the two storage systems is made.

4.1.9 Thermal storage

With the system variants (see above) it has already been shown that an interaction between the PV surplus control and an increase in the buffer storage by 700 l to a total of 1,525 l a coverage of 50% can be achieved in the project building (PV system 15 kW_p).
The extent to which the storage volume of the buffer storage has an influence on the increase of the supply cover factor is shown in Figure 37. The calculations assume a specific PV yield of 922 kWh/kW_p. Up to a buffer storage tank size of 2,500 l, the PV supply cover factor and the load cover factor are constantly increasing. Subsequently, an optimum is achieved with a coverage ratio of about 46%. A further increase leads to a marginal reduction in the load cover factor. The supply cover factor continues to rise steadily as the buffer storage volume increases (Kley, 2018).

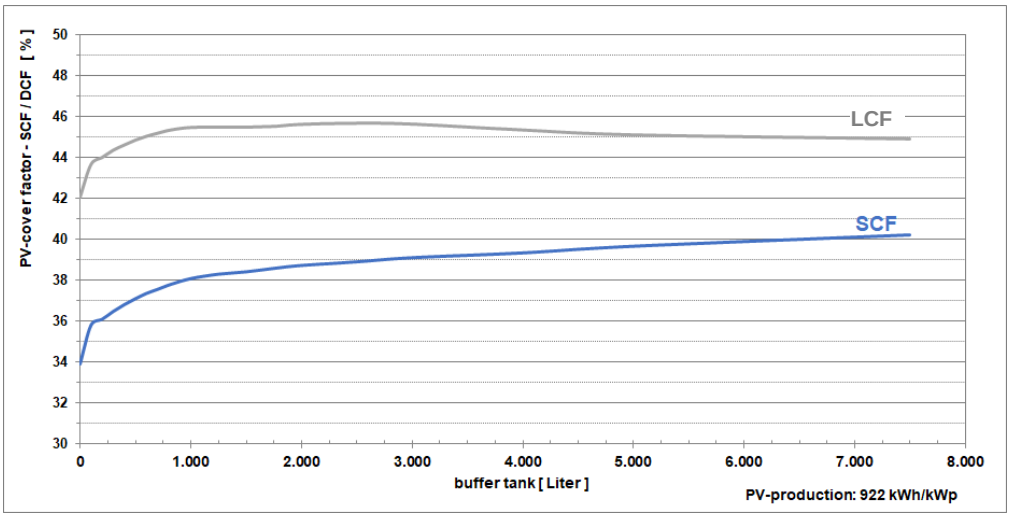

Figure 37: Influence of the storage volume on the supply and load cover factor (PV yield 922 kWh/kW_p) (Kley, 2018)

On the basis of the sensitivity analysis on thermal storage combined with a PV surplus control, it can be determined with regard to the increase of the supply cover factor and load cover factor (Kley, 2018):

- It makes sense to increase the buffer storage volume in combination with a PV surplus control up to a total volume of 2,500 l maximum.
- In order to increase the solar fraction, the buffer storage tank size should be 100 l/kW$_p$ to 130 l/kW$_p$ or 110 l/MWhPV yield to 140 l/MWhPV yield in relation to the size of the PV system and its solar yield.
- With the usual yields of PV systems in Germany in the range of 700-1,200 kWh/kW$_p$, supply cover factors of 32% to 45% and load cover factors of between 41% and 49% are realizable.

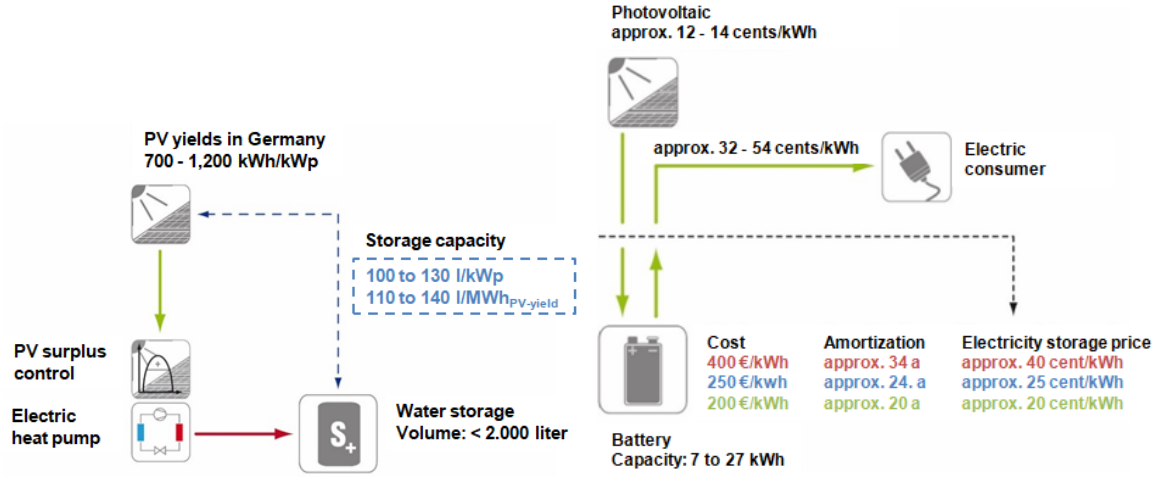

Figure 38: Enlargement of the water storage in combination with a PV surplus control (Kley, 2018) and economic evaluation of a power storage unit (Kley, 2018)

4.1.10 Electrical storage

In summary, it can be said that the implementation of an electrical storage unit in the energy supply of a residential building increases both supply and load cover factor. The cost of simply storing one kWh of electricity would be reduced to around 20 cents (net) if the investment costs for electrical storage could be reduced to around ~200 €/kWh. With generation costs of a photovoltaic system of 12 to 14 €cts/kWh (net), the electricity generation costs are 32 to 54 €cents per kWh of stored solar electricity.

4.1.10.1 Comparison

In the following, a total annual cost comparison between the electricity storage system and the PV surplus control strategy with increase of the buffer storage volume is evaluated. The aim is to achieve the same PV load cover factor. The following costs (net) are taken into account:

- PV system
- Current storage system with lead-acid batteries
- PV surplus control
- Buffer storage

In order to achieve a load cover factor of 45%, variant 1 requires a PV surplus control in combination with an increase in the buffer storage tank by 700 liters (total volume 1,525 l). Alternatively, variant 2 requires the use of an electricity storage system with 10 kWh nominal storage capacity.

A comparison of the annual and capital costs shows cost differences in the capital cost of around 29%. Also in terms of the total annual costs, the enlargement of a water storage tank is cheaper than an electrical battery storage. The cost saving is up to 10%, Figure 39. (Kley, 2018). The evaluations and analyses show that it may be currently energetically sensible to operate a heat pump directly with surplus PV electricity and thus to load thermal storage tanks as well as building masses (screed of the underfloor heating) with heat (power-to-heat). This strategy also helps to increase the supply cover factor. Thermal storage tanks are often present in heating concepts.

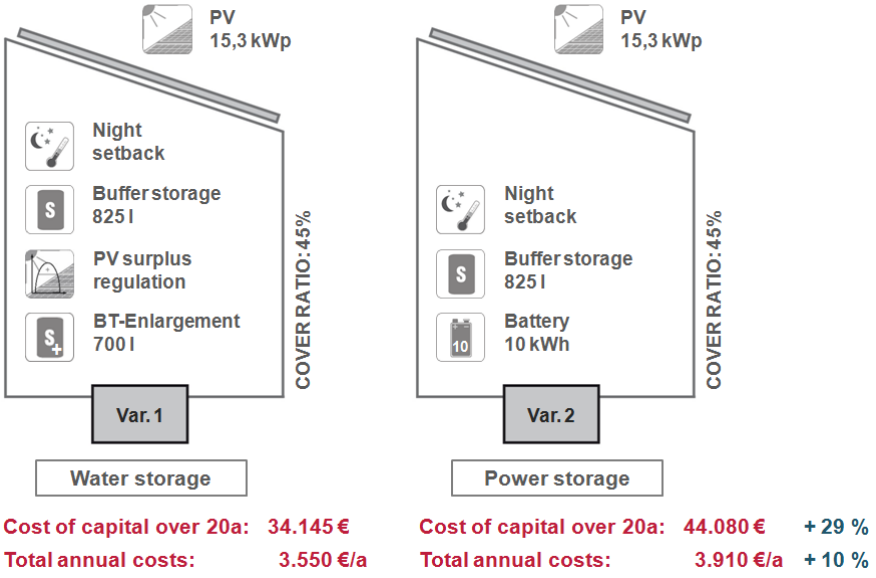

Figure 39: Cost comparison of PV surplus control with buffer storage enlargement and battery (Kley, 2018)

An increase in the storage volume is thus given and, according to the results, currently also considerably cheaper than corresponding energy storage in a battery. Electricity storage systems are generally not economical at current investment costs (Kley, 2018).

4.1.11 Load management and demand response

4.1.11.1 Operating strategies for charging the electrical storage and grid supportive operation

In order to maximize the use of PV supply cover factor and to relieve the public grid, three different charging strategies for the electricity storage are considered in Table 15.

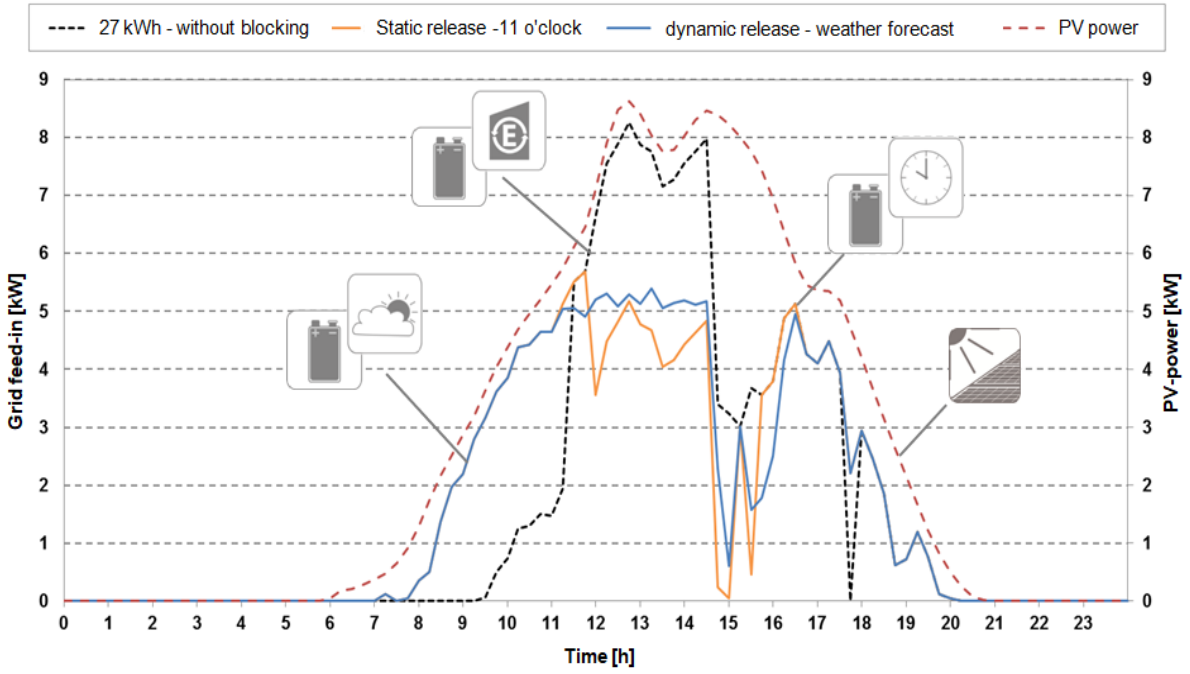

Figure 40: Influence of the charging strategies on the load curve of the feed-in on 24 July (Kley, 2018)

Using the example of a daily load profile, the reduction and shifting of the feed-in peaks through the different operating strategies can be illustrated by comparing the charging strategies with regard to PV grid feed-in in Figure 40. The red dotted line represents the PV yield that is generated on that day.

In the static and dynamic mode of operation, blocking the battery charge results in an increase in the grid feed in the morning hours. At the same time, the peaks in feed-in at noon and in the afternoon can be significantly reduced. In the period from 11:00 to 17:00 h, the weather forecast-guided operation of the battery charge results in a significant relief of the power grid - the grid load becomes more even and daily peaks can be significantly dampened. The morning feed-in peaks can be reduced by a weather forecast-guided charging strategy.

Table 15: Charging strategies for electricity storage devices

Operating mode for priority increase of supply cover factor	
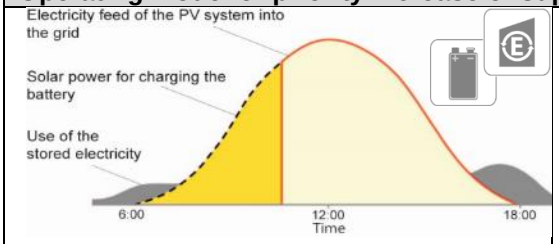	The battery is charged when there is surplus yield from the PV system and the maximum charge level of the battery has not yet been reached. Only if the electricity storage tank is fully charged the generated surplus of solar electricity is fed into the grid. The difference between the current PV generation capacity and the current load is decisive for the amount of electricity fed into the grid.
Static battery charging - operating mode with time-based activation of the battery charge	
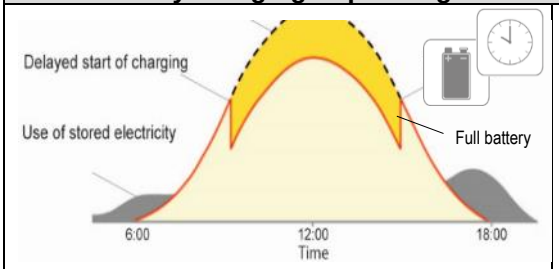	After blocking the charging in the morning hours, the battery charge is activated depending on the time of day. By blocking the charging in the morning, feed-in peaks at midday and in the afternoon are to be damped by a higher available storage capacity. The charging strategy is based on the previous one, except that a fixed start time (here 11 am) is given.
Dynamic charging strategy - operating mode with weather forecast-controlled battery charging	
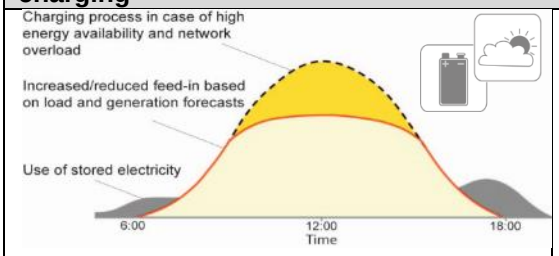	With the dynamic charging strategy, the battery is charged according to a weather forecast. The operating mode controls the charging of the battery depending on the available storage capacity and the predicted PV output over the next 24 hours.

Table 16 shows the three operating strategies in terms of their advantages and disadvantages. It can be seen that the operating strategies can be differentiated significantly with regard to their grid support. Although fixed feed-in limits relieve the grid by reducing the feed-in peaks, they do not address the high feed-in gradients. In order to be able to operate a PV storage system in the long term both to maximize its supply cover factor and to serve the grid, while minimizing control losses and steep feed-in gradients, forecast-based operating methods are required.

Using the example of the Berghalde project building with a 15 kW_p PV system and a battery with 27 kWh storage capacity, the influence of the charging strategies on the grid feed-in as well as on the supply cover factor will be investigated. The simulations and evaluations show that in comparison to conventional loading (supply cover factor), a damping of the feed-in peaks is generally possible through the static activation after a fixed time or the dynamic battery charge. The maximum feed-in peaks at lunchtime and in the afternoon can be significantly reduced. With the dynamic operation mode of battery charging, a further reduction of the feed-in peaks is possible.

If the feed into the electricity grid is considered, it can be seen, that compared to a charging strategy that is exclusively oriented towards the supply cover factor and which results in feed-in peaks (grid feed) of about 70 to 80% of the nominal output of the PV generator, a static mode of operation reduces the feed-in peaks by about 5%.

Table 16: Evaluation of the operating strategies

Business strategy	Advantages	Disadvantages
Electricity self-consumption 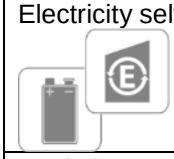	• Control losses are kept to a minimum • Optimized supply cover factor	• high input peaks • steep feed-in gradients
Static battery charging 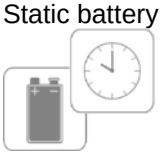	• Main relief by capping the feed-in peaks	• Danger that the storage is not fully loaded at the end of the day • Supply cover factor optimization no longer has top priority • Losses due to control partly unavoidable
Dynamic battery charging 	• Potential to address and fulfil all desired aspects • Losses in yield due to control can be minimized by means of a forecast-based energy management system	• Depending on the quality of the forecast data

With the dynamic operation mode of battery charging, a reduction of the feed-in peaks by about 10% to approx. 60% of the nominal output of the photovoltaic system is possible, see Table 17. In the case of static loading, there is a decrease in the PV supply and load cover factor of around 2% each compared to the charging strategy according to supply cover factor, resulting in an increase in grid electricity purchases of up to 5%.

The reason for the decreases is, among other things, that the electricity storage unit often cannot be fully charged during dynamic loading on cloudy days, which means that both supply and load cover factor decrease. For the example, the dynamic battery charge based on a weather forecast results in a reduction of supply and load cover factor of about 6% each. At the same time, annual grid electricity purchases will increase by around 16%. A prerequisite for implementing the dynamic charging strategy is knowledge of the future course of PV generation. Nowadays, this can be predicted with good accuracy for the coming hours via external providers, see Table 17 (Kley, 2018).

The example shows that the grid support has a negative effect on the performance within the buildings. The higher the grid support, the higher the losses in supply cover factor. The priority of a private operator in particular is usually on the "inner" performance, since this correlates directly with the consumption costs. If the weather forecast-guided, dynamic operation strategy is compared to a static loading of the electricity storage, no significant additional gain is shown with regard to grid support (Kley, 2018).

Table 17: Influence of battery charging strategies on the supply and load cover factor and grid interaction

PV system with 15 kW_p and electric storage with 27 kWh	**Use of on-site electricity** 	**Static loading** 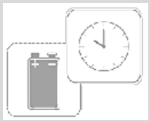	**Dynamic loading** 
Supply cover factor	54.4%	52.5% **-2%**	47.8% **-6%**
Load cover factor	61.2%	59.4% **-2%**	55.2% **-6%**
Grid feed-in/feed-in peaks	70-80%	65-75%	60-70%
Grid usage	4.41 MWh/a	4.41 MWh/a **+5%**	5.10 MWh/a **+16%**
Grid support			

4.2 Integration of thermal and electric storage at Herzo Base Project

4.2.1 Simulation and control strategies at Herzo-Base Project

The project Herzo Base comprises 8 single family terraced houses designed to a plus energy balance. The 8 houses are connected by a thermal grid and equipped with two modulating central ground source heat pump and a central thermal buffer storage as well as an electric battery. The DHW is produced decentrally with booster heat pumps in 8 DHW storages in the houses. Monitoring results of the project are documented in the Report Annex 49 part 2 on Monitoring.
The terraced houses and the energy system are analysed in an annual simulation and the thermal and electrical storage units are dimensioned within a parametric simulation study. Especially, the PV optimized control (PVC) is developed and tested in simulations in order to determine the potential of increase PV self-consumption compared to heat-controlled (HC) operation. Furthermore, a model predictive control (MPC) was developed and compared to the PVC and two different HC for the modulating heat pumps (MHPs). In a first test phases in the terraced houses, the MPC operates the MHPs and 5 of 8 DHW-HPs.

4.2.1.1 Annual simulation

In order to verify the targets of the PVC, the terraced houses and the energy system are modelled in the simulation program TRNSYS. A details description of the process is in Dentel and Betzold (2017). The modular structure of TRNSYS allows a high flexibility for modelling building structures and plant systems. As the terraced houses are built in Northern Bavaria, Germany, the weather data from the test reference year for region 13, defined by the Deutsche Wetterdienst (DWD), was chosen. The simulation period is one year with a time step of 5 minutes.
In the simulation the effect of the PVC is clearly visible. Compared to the HC operation the results of the simulation show an increase of direct PV and also a decrease of grid consumption. Figure 41 shows the energy distribution of PV production and consumption for the simulation of HC and PVC as well as the results of the first (and second) monitoring period from 01. April 2018 (2019) until 31. March 2019 (2020). In general, the assumptions in the simulation have deviations to the monitoring results. In the monitoring period the PV production was 41% higher and the energy consumption was 32% less than in the annual simulation. The supply cover factor differs a lot from the simulation results of PVC, but the load cover factor is quite good.

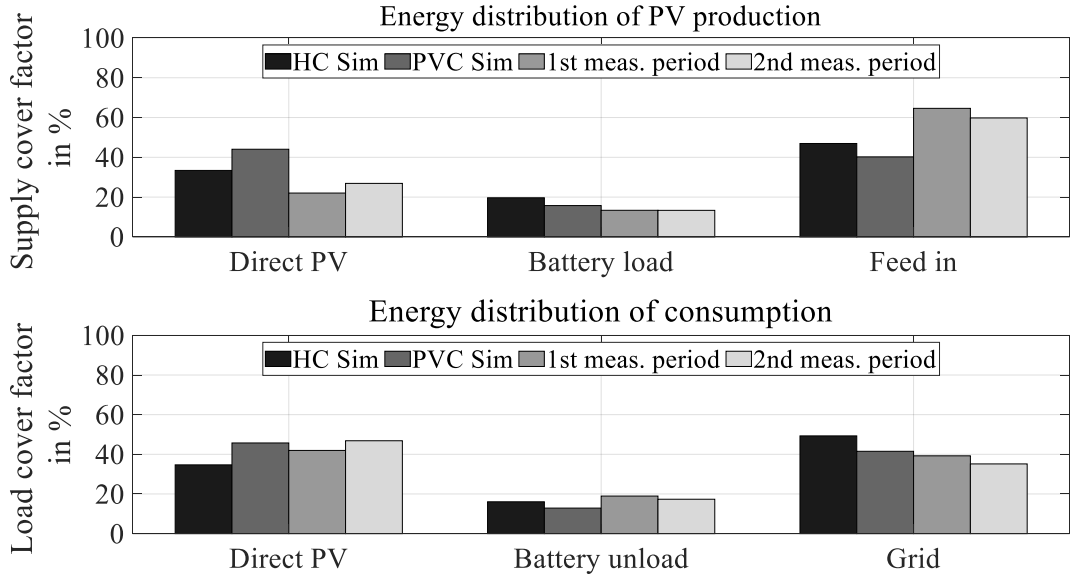

Figure 41: Supply and load cover factor for simulation of HC and PVC as well as monitoring results from April 2018 until March 2019

The DSM was adapted and optimized to the real energy system during the implementation in the building automation, so that the further development of the control (Betzold and Dentel, 2019) led to a PV-optimized control (PVC). The PVC controls two MHPs, five of eight DHW DHW-HPs and has been in operation since October 2018 for the MHPs and since February 2019 for the DHW-HPs. Due to the user settings of the DHW-HPs, the other three DHW-HPs cannot be controlled by the building automation.

4.2.1.2 Parametric study

Another main aspect of the annual simulation was the design of the thermal and electrical storage units. A parametric simulation study (Dentel & Betzold, 2017) investigated the interaction between design parameters, control settings, and energy consumption. The study examined different capacities of battery and thermal storage tanks as well as the temperature level of the thermal storage tanks and its impacts on the grid consumption of the terraced house including the household electricity. The battery capacities were 40 kWh, 50 kWh and 60 kWh. The storage volumes of the thermal buffer storage included 3.2 m³, 5.3 m³, 6 m³, and 7.2 m³. The temperature levels were 35 °C, 45 °C, and 55 °C during PV operation. The parametric study produced 36 combinations and results.

Figure 42 left shows the dependencies for the different storage volumes (3.2–7.5 m³), electrical storage capacities and set point temperatures in the thermal storage tanks. Less grid consumption is characterized by configurations with a high electrical storage capacity and a low set point temperature in the storage tanks. The buffer storage volume itself does not have a large impact on the results.

Another result of the design study is the identification of optimal cost and high self-consumption of the storage capacity for the battery system. In this investigation, the battery has a capacity from 0 kWh to 60 kWh with 10 kWh steps, while the thermal storage size is 2.8 m³ and the temperature level is 35 °C. Figure 42 right shows that the grid consumption can be reduced significantly by 41% for a battery size of 40 kWh. Between the maximum size of 60 kWh and a size of 40 kWh is only an additional 8% reduction of grid power, while costs increase by 40%.

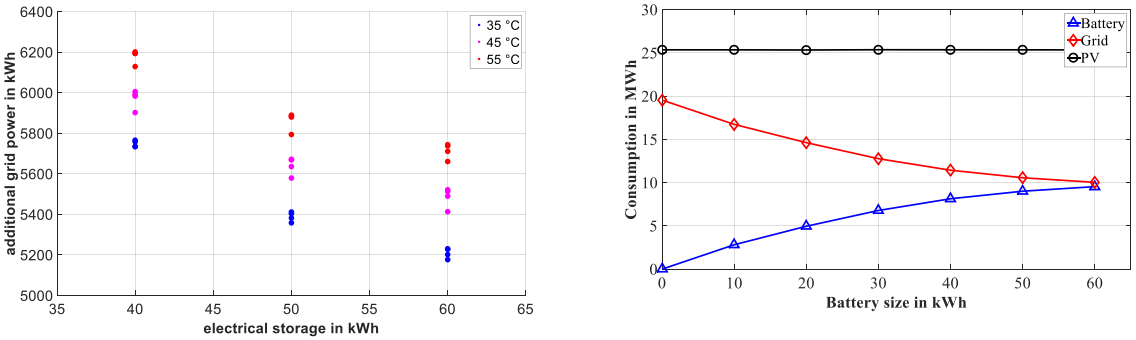

Figure 42: Dependencies of capacity of electrical and thermal storage and set point temperature (left) and dependencies of capacity of the electrical storage on PV feed in, grid consumption and battery load (right)

4.2.1.3 Model predictive control (MPC)

The MPC is based on numerical optimization and on weather and load forecasts. A mixed-integer linear optimization algorithm (MILP) was used. The MPC was created in MATLAB (R2019a) with the additional software GUROBI (version 8) to use the Special Ordered Set (SOS) option. The SOS option enables interpolation between operating points so that the polynomial of the MHP can be mapped at variable compressor speeds at B5/W35. Thus, the thermal output of the MHP can be between 4.8 kW and 18.1 kW and the electrical output between 1.0 kW and 4.7 kW. DHW heating has a constant thermal output of 2.2 kW and an electrical output of 0.5 kW. The mapping of the energy system is based on simplified models and is represented by an energy balance of energy supply and discharge.

In a simulation study (Betzold et al., 2021) in MATLAB (R2019a), two advanced control strategies, PVC and MPC, are developed and compared to two different heat controlled strategies.

As main result, the MPC increase PV self-consumption with low effect up to 2.1% and reduce operating costs up to 36.1% compared to a heat controlled strategy with on/off heat pumps (HPs). However, the cost savings mainly result from less energy consumption due to a more efficient operation of modulating HPs in part load during MPC. A heat controlled strategy with the ability to modulate the HPs can compete with the advanced control strategies, and even gets partly better results as the PVC regarding energy consumption, operating costs and SPF. In Betzold et al. (2020) a detailed description of the MPC and the PVC operation in the terraced houses is analysed. The real operation of the MPC takes place over several hours in test phases in order to be able to monitor the results of the MPC and the behaviour of the heat pumps. The sliding optimization horizon is 23 hours with a new optimization run every 15 minutes. For the evaluation, a test operation is analysed over a period of seven hours. The MHPs and five of the eight DHW-HPs are targeted in operation. Due to user settings of the DHW-HPs, the other three DHW-HPs cannot be controlled by the building automation. The targeted operation of the battery is not used in the test period, but modelled in the energy balance.

Forecast data is received from a weather forecast station over a period of 24 hours to create the heat pump operating plan. The PV power is determined using the forecast solar radiation and a physical model in MATLAB. Thermal, electrical and DHW load forecasts are determined using Artificial Neural Networks (ANN). These were created in MATLAB using the Deep Learning Toolbox. The network is a two-layer feedforward network with 20 neurons and layers each and was trained with the Levenberg-Marquardt algorithm. Monitoring data over the past 12 months served as training data. The input values for creating the load forecasts are outside temperature, hour of day, solar radiation on the horizontal and the distinction between day of the week and working day. Previous comparisons of prognosis and measured values gave moderate results.

The MHPs are operated by setting the set return temperature at the condenser inlet in order to influence the thermal output. It is not possible to set the compressor speed directly. Setting the current return temperature higher or lower leads to an increase or decrease in the compressor speed.

First test phases shows good operation of MHPs during the charging process. Figure 43 shows the thermal and electrical power of the MHPs by MPC specification and measurement. The state of charge, also seen in Figure 43, is well done by MPC specification and measurement. The first MPC specification (black line) for the next 7 hours also shows that the forecast was quite good. However, the internal control of the MHPs influences the operation as internal settings lead to a switch-off under certain conditions. Also, varying temperature spread of condenser during different compressor speed (2-5 K) leads in same cases to a temperature reduction in the thermal storage.

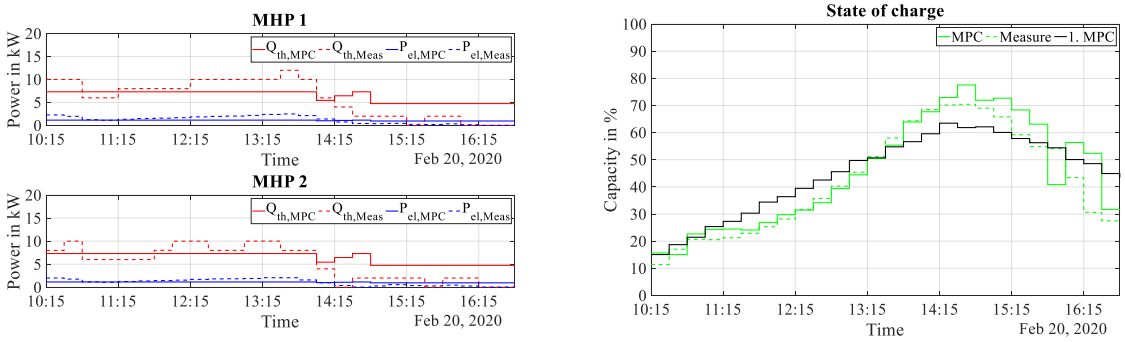

Figure 43: Thermal performance of MHP1 (left, top) and MHP2 (left, bottom) in comparison of MPC specification to measurement as well as state of charge in comparison of continuous MPC specification to measurement and first specification of the MPC (right)

4.3 Energy flexible buildings by storage integration

4.3.1 Outline

Heat pump systems are a competitive and mature heating technology. They offer the possibility to deploy the demand side flexibility provided by buildings. This chapter summarizes the findings from three research studies that investigated the control of heat pump systems to activate the energy flexibility of Norwegian residential buildings. In this context, it is shown that Norway is a special case in the European power grid since (1) the electricity generation is almost fully based on hydropower and (2) the lowest $CO_{2eq.}$ intensities usually occur simultaneously with the highest daily electricity spot prices. However, a main concern in Norway is the capacity of the electricity distribution grid with continuously increasing electricity use in households. As most residential buildings are heated using electricity, congestion problems can occur due to too much stress on the grid, especially during very cold winter days and peak hours. The flexibility potential generated from (predictive) rule-based controls applied to heat pump systems in Norwegian residential buildings has thus been investigated.
When applied to both space-heating and domestic hot water (DHW) production, it is shown that price-based and $CO_{2eq.}$ intensity-based controls fail to decrease operational costs or CO_2 emissions in Norway, respectively. Higher fluctuations in hourly electricity prices or hourly $CO_{2eq.}$ intensities (like in Denmark) are necessary to benefit from these demand response measures. Schedule-based control proved to be very effective for load shifting towards grid off-peak hours, but at the risk of creating new peaks in these off-peak hours. Applying time-varying set-point temperatures to the heating system, it has also been shown that the DHW prioritization of the heat pump has a strong influence on the operation of the electric auxiliary heater for bivalent monoenergetic heat pump systems. It strongly affects the overall electricity use for heating throughout the year and subsequently the energy costs and CO_{2eq} emissions.
When applied to the DHW production only, price-based controls can reduce operational costs and CO_{2eq} intensity-based controls can reduce emissions. This is due to the higher storage efficiency of the water tank.
This chapter summarizes the research work accomplished within the IEA HPT Annex 49 as well as the IEA EBC Annex 67 on building energy flexibility.

4.3.2 Introduction

More intermittent renewable energy sources are required for the transition towards a more sustainable energy system. The introduction of renewable energy sources implies several challenges for the energy system operation that requires new solutions. Typically, electricity generation plants are operated to satisfy the electricity demand. However, to make full use of the electricity generated from intermittent renewable sources, like wind and solar energy, demand side flexibility is essential. Furthermore, demand side flexibility can help to mitigate the stress on the distribution grid, a stress that will arise from an increasing electrification of the building, industry and transport sector.
The Scandinavian power system is highly interconnected enabling to trade electricity between Scandinavian bidding zones and with the continental European power grid. On an annual perspective, Norway is a net electricity exporter, but, during a year, it also imports electricity at times. Electricity generation in continental Europe often relies on thermal power plants.
It is therefore more carbon-intensive than the electricity generation in Norway, which is almost fully based on hydropower. At times of electricity imports to Norway, the Norwegian electricity mix becomes usually more carbon intensive. Greenhouse emissions from the building operation phase can be reduced by avoiding electricity use during those periods.
Electricity-based heating systems can be controlled based on the carbon intensity of the electricity mix. Heat pump systems are recognized as a promising technology to contribute to a decarbonization. This potential for decarbonization is high in Norway, since the electricity generation is almost entirely from hydropower. Heat pumps bridge the electricity and the heating sectors, and they provide the possibility to decouple the electricity demand for charging thermal storages and the actual heat demand of a building

In other words, residential heat pumps can be connected to thermal energy storages and thus enable flexible operation. Regarding buildings, demand side flexibility is also called building energy flexibility.

"In the broadest sense, an energy-flexible building can be understood as a building changing its energy use to react to an external signal."

4.3.3 Energy flexibility of buildings

In the broadest sense, an energy-flexible building can be understood as a building that can react to an external signal (meaning received from outside the building). *Building energy flexibility* can be seen as an *ability*, a *building property* and/or a *service*.
Two components are essential to deploy the energy flexibility potential of buildings:

- A *smart meter* or a *building management system* to receive external signals. These input signals typically correspond to the current and future operating conditions of the building (i.e. forecast of weather data, electricity prices or $CO_{2eq.}$ intensity).
- *Thermal energy storages* in the building. This is usually done using water storage tanks. However, it has been shown that the building thermal mass can be an efficient and inexpensive energy storage, if fluctuations of the indoor temperature are allowed by occupants. This strategy is also called thermal mass activation.

Thermal storages can be controlled in a way that they temporarily get loaded to higher temperatures (in case of heating), in other words the thermal storages are *activated*. Depending on the control objective, this activation often leads to an increased total energy use for heating, but at the same time a decrease of total operational costs or total CO_2 emissions. On top of this, a service to the electricity grid can be provided.

4.3.4 Norwegian context

In 2015, the building sector accounted for 36% of the energy use in Norway. Out of these 36%, approximately 75% were covered by electricity, which is due to the widespread use of direct electric heating. Historically, direct electric heating has been a feasible technology since the total domestic electricity generation is almost fully covered by hydropower, which is a rather cheap technology.
However, the extensive use of direct electric heating can contribute to grid congestion problems, especially during the coldest winter days. Demand side flexibility in combination with demand response measures can be deployed to avoid grid congestions and to delay the necessity of upgrading the distribution grid. Demand response measures can be based on any kind of external signal. However, as a starting point, it is worth to consider the electricity spot price or the $CO_{2eq.}$ intensity of the electricity mix as external signal.

4.3.4.1 Spot price vs. $CO_{2eq.}$ intensity

Regarding the correlation of electricity spot prices and the $CO_{2eq.}$ intensity of the electricity mix, Norway is a special case in Europe because low $CO_{2eq.}$ intensities occur at times of high spot prices and vice versa. Exemplary, Figure 44 shows the average $CO_{2eq.}$ intensity and electricity use in the Norwegian bidding zone NO2 for five days in January 2015.

"Norway is a special case in Europe because low $CO_{2eq.}$ intensities of the electricity mix occur at times of high spot prices and vice versa."

The opposition of electricity use and average $CO_{2eq.}$ intensity poses a problem for control because it seems obvious from the graph that it is not possible to minimize costs and emissions at the same time.

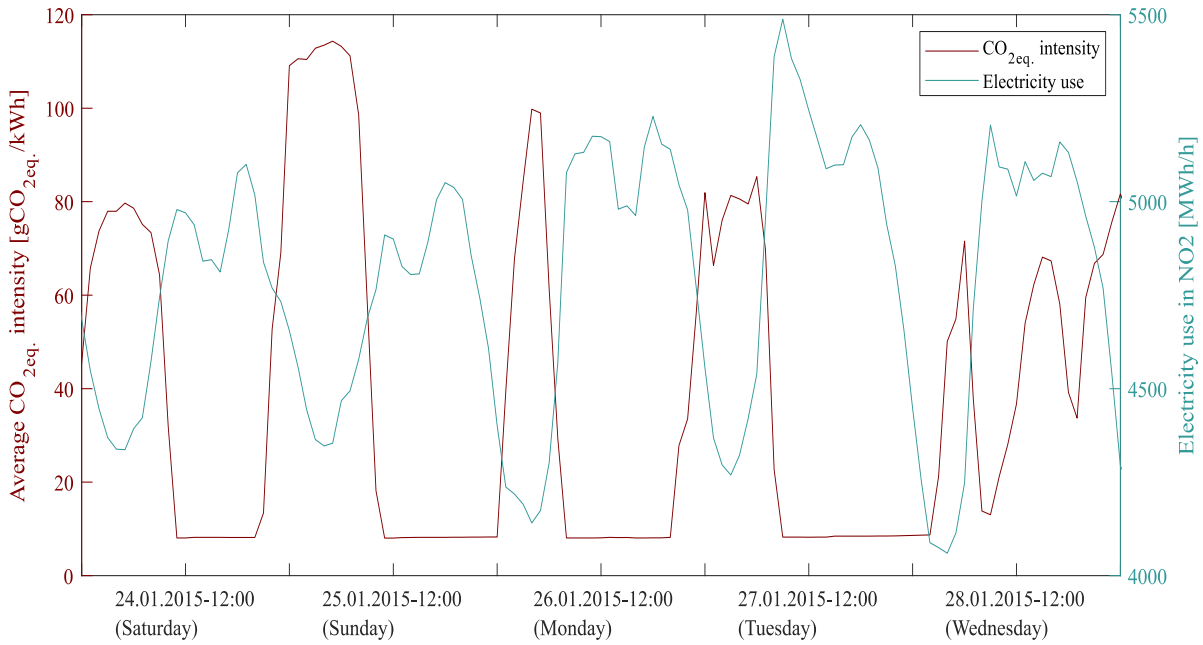

Figure 44: Average $CO_{2eq.}$ intensity and electricity use in NO2 for five exemplary days in Jan. 2015 (Clauß et al., 2019)

4.3.4.2 Energy efficiency vs. flexibility

Another fact that deserves attention is that energy efficiency and energy flexibility are most often two conflicting objectives. Making use of the energy flexibility means an activation of thermal energy storages, for example water storage tanks or the building thermal mass. This activation to higher temperatures also leads to increased thermal losses from these storages, meaning that a flexible operation comes at the cost of a lower energy efficiency of the system. In other words, the essence of energy efficiency is a reduction/minimization of energy use, whereas energy flexibility often addresses other objectives, like providing a service to the grid, minimizing CO_{2eq} emissions or reducing the risk of grid congestion.

4.3.4.3 Building insulation level and thermal mass

The energy flexibility potential differs between building insulation levels and thermal masses. For a same increase of the indoor temperature, higher thermal mass, like in concrete buildings, can store more heat in the structure so that the operation of the heating system can be delayed for longer periods. For a same amount of heat stored in the building, the indoor temperature will be lower with a higher thermal mass which results in lower storage losses. This also favours longer periods of load shifting. Most of the Norwegian residential buildings are lightweight wooden constructions with rather low thermal mass.

Furthermore, the building insulation level also affects the flexibility potential. Building from the 1980s have lower insulation requirements than buildings built according to the latest building regulation, TEK17. Lower building insulation level means higher heat losses through the envelope and thus a shorter time period of delayed heating system operation. On the contrary, buildings with a lower insulation level have higher energy needs, which means that the amount of energy that could be shifted for rather short time periods is higher compared to buildings with a higher insulation level.

4.3.5 Control strategies

Control strategies should operate these thermal storages in real time to make the building energy flexible. Heating control strategies often follow a rule-based approach. It can also be based on more sophisticated control strategies that solve an optimization problem (e.g. optimal control or model-predictive control). Predictive rule-based controls (PRBC) rely on a set of pre-defined rules to control the energy system.

It is predictive because it takes forecasts into account in the control algorithm. The rules continuously evaluate the temperature set-points for space heating (SH) and DHW heating (i.e. the charging and discharging of the thermal storages) and thus start or delay the operation of the heating system. The temperature set-points are varied depending on the external control signals. (P)RBC is often analysed using building performance simulation (BPS) tools because their implementation in these tools is rather straightforward. A drawback of PRBC is the necessity of careful (and usually time-intensive) design and fine-tuning of the control rules.

"Predictive rule-based controls rely on a set of pre-defined rules to control the energy system. It is predictive because it takes forecasts into account in the control algorithm. The rules aim to vary temperature set-points for space heating and DHW heating to delay or start the operation of the heating system. The temperature set-points are varied depending on external signals."

Model-predictive control (MPC) is an optimal control strategy and is briefly described here. MPC has been used for decades in many industries but has only recently got a lot of attention for controlling heating systems in buildings. MPC does not rely on rules, but on optimizing a mathematical problem, such as minimizing the operational costs. Its major drawback is the identification of a control model, which often is time-consuming (Killian and Kozek, 2016). Where PRBC requires a careful tuning of rules, MPC requires a careful identification of the control model and tuning of the objective function, more specifically the weights for each term in the objective function need to be carefully chosen.

By nature, the results achieved by MPC are optimal (or close to it as they remain modelling and uncertainty errors), whereas PRBC leads to non-optimal results. Nevertheless, it has been shown that PRBC can reduce operational costs and carbon emissions effectively. Therefore, it can be a decent compromise to more advanced controls. Both, PRBC and MPC can deal with time-varying operating conditions and can interact with the energy system as well as the grid (De Coninck and Helsen, 2016). Both control approaches have the potential to contribute to peak shaving and load shifting of the electricity consumption (Haghighi, 2013).

A control strategy always requires an external signal (see section 1.1), also called penalty signal. Frequently used signals are the electricity (spot) price, the $CO_{2eq.}$ intensity of the electricity mix or the share of renewables in the electricity mix.

In this work, PRBC is implemented into the building performance simulation tool IDA ICE Version 4.8. The control strategies address the following objectives (directly or indirectly):

- Load shifting away from peak hours, as well as peak shaving to reduce the power peaks by using a pre-defined schedule to control the operation of the heating system,
- Reducing energy costs for the end-user by using time-varying spot prices as a control signal,
- Improving the energy use from low-carbon energy sources, typically renewable energy sources, by using the hourly average $CO_{2eq.}$ intensity as a control signal.

For this purpose, three control strategies are investigated in this work:

- Price-based control strategy (CSP),
- $CO_{2eq.}$ intensity-based control strategy (CSC),
- Schedule-based control strategy (CSS).

The basic idea is a variation of the temperature set-points for heating. More particularly, the set-points for SH in the rooms, the supply water temperature (for example to floor heating) and the temperatures that the heat pump has to supply to the water storage tank are varied with time. The principle for the control signal determination based on the hourly average $CO_{2eq.}$ intensity is illustrated in Figure 45.

The determination for the price-based control signal follows the same principle. The illustrated principle aims at charging the thermal storages right before peak hours, thus highest $CO_{2eq.}$ intensities or highest spot prices, by increasing the temperature set-points before the peak periods, also indicated in red in Figure 44. A detailed description of the control algorithm is provided in Clauß et al. (2019).

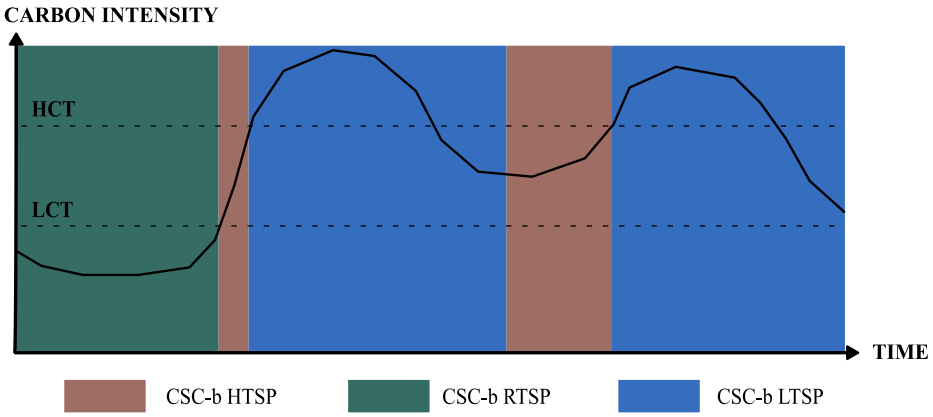

Figure 45: Illustration of the principle for determining the control signal based on the CO2eq. intensity.

4.3.6 Heat pump system and simulation setup

The case study building, the Living Lab, is located at the Gløshaugen Campus in Trondheim. Figure 46 shows the building and its floor plan. A detailed multi-zone dynamic model of this zero emission residential building (ZEB) has been implemented into the BPS package IDA ICE. In this framework, detailed dynamics of the energy supply system can be investigated and indoor climate and building energy use can be studied. The building has a heated floor area of approximately 105 m^2. It has a lightweight timber construction and a highly-insulated building envelope with energy-efficient low-emissivity windows.

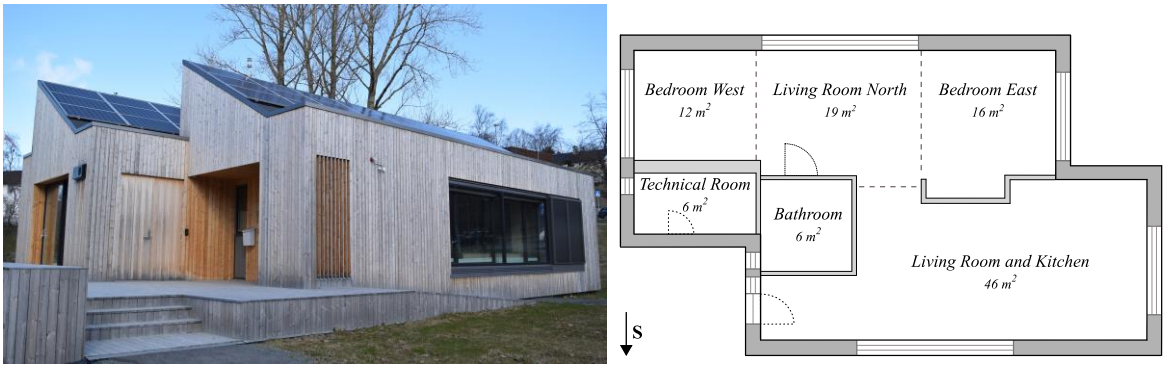

Figure 46: Living Lab at Gløshaugen Campus in Trondheim, Norway.

The energy system of the building is shown in Figure 4. A modulating air-source heat pump has been considered for this study while the real Living Lab is equipped with a ground-source heat pump (shown in Figure 47). Except the heat pump, the other technical aspects have been taken directly from the Living Lab. For instance, the heat pump is connected to a water storage tank which supplies DHW and heating to a floor heating system. The building is also equipped with 4 m^2 of solar thermal collectors to preheat the water storage tank and with photovoltaic panels of 12 kW_{el} capacity. This combination of the technical solutions is in line with typical Norwegian ZEB concepts (Kristjansdottir et al., 2018).
The heat pump is an air-source heat pump with a capacity of 5.1 kW and COP 4.57 at nominal conditions (A7/W35). The key features of the simulated heat pump are:

- It is controlled using a tuned PI-controller with anti-windup control
- It can modulate between 30% and 100% of the nominal capacity
- A minimum heat pump cycle time of 10 min is enforced
- It can supply heat to both DHW and SH
- DHW heating is prioritized over SH

The water storage tank is modelled as a one-dimensional stratified tank where heat conduction and convection are considered. The water tank is divided into ten horizontal layers, where the DHW part consists of the upper four layers and the SH part of the six lower layers.

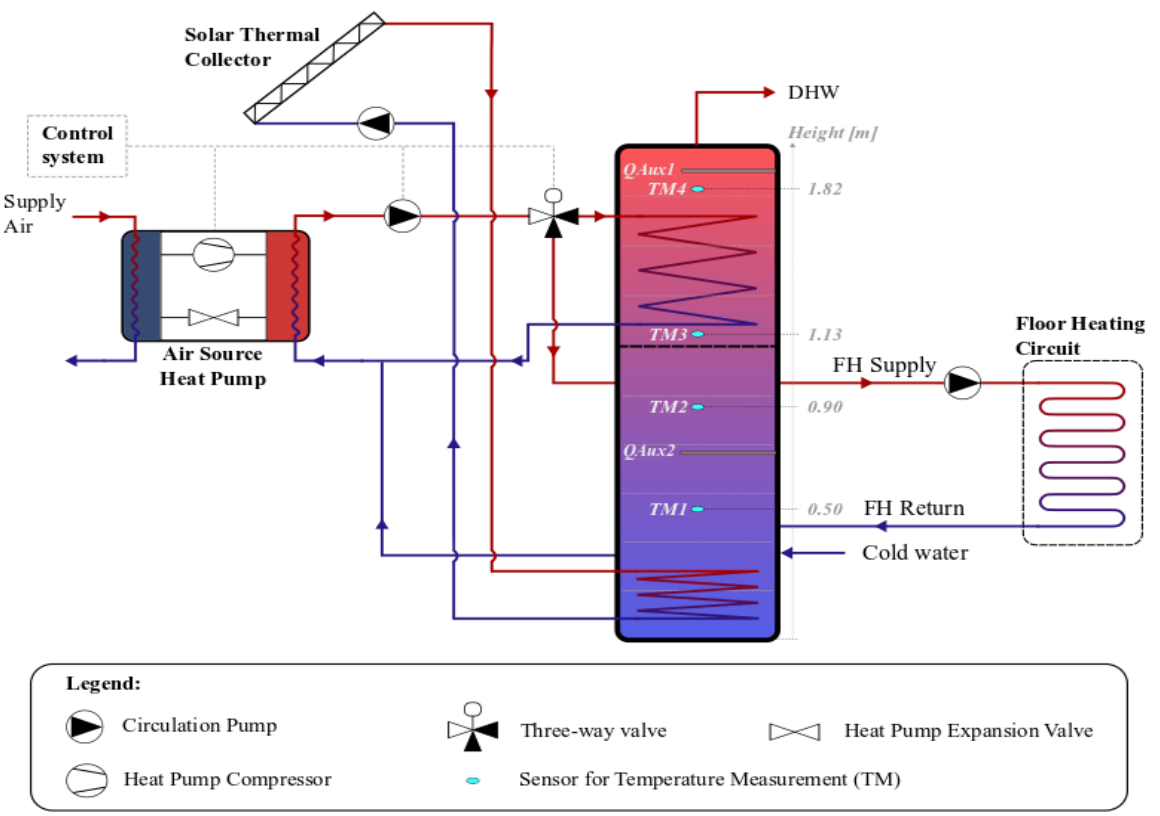

Figure 47. Simplified layout of the energy system of the Living Lab (Clauß and Georges, 2019)

A detailed description of the system is provided in Clauß et al. (2019 b) and the heat pump is described more detailed in Clauß and Georges (2019). The heat pump control algorithm is based on the temperature measurements from sensors located inside the water storage tank. Both the SH and DHW parts of the tank have two sensors to enable a charging according to a hysteresis. It is emphasized here that the control of any auxiliary heater should be clearly defined for bivalent heat pump systems, as they can have a strong impact on the total heating electricity use of the system. In this study, the temperature set-points for starting the operation of the auxiliary heaters are set to be 3 K below the start temperature of the heat pump. In that way, the auxiliary heater starts operating only if the heat pump cannot cover the heat demand.

Figure 48: Technical room in the test building, Living Lab (Source Anne J. Bruland).

4.3.7 Results

The main objectives are the reduction of (1) the operational costs (CSP control), (2) the yearly CO_2 emissions to operate the heating system (CSC control) and (3) the energy use during peak hours (CSS control). These controls are compared to a business-as-usual control scenario where the set-points are kept constant (BAU).
The results for each control are evaluated based on their respective objective function. Results are presented for a modulating heat pump system (MHP), for an on-off heat pump system (OHP) and for direct electric heating, where SH is covered by electric radiators and DHW heating by an electric resistance heater.

4.3.7.1 Demand response measures for both DHW and SH

Figure 49 shows the influence of the three control scenarios (CSP, CSC and CSS) on the annual electricity use for heating during peak, pre-peak and after-peak periods for a modulating heat pump system (Figure 49 (a) and (b)) and for direct electric heating (Figure 49 (c) and (d)). In general, all scenarios, except for CSC for direct electric heating, lead to an increased electricity use for heating. The investigated strategies reduce the energy use for heating during peak hours, except for CSP for the modulating heat pump system.

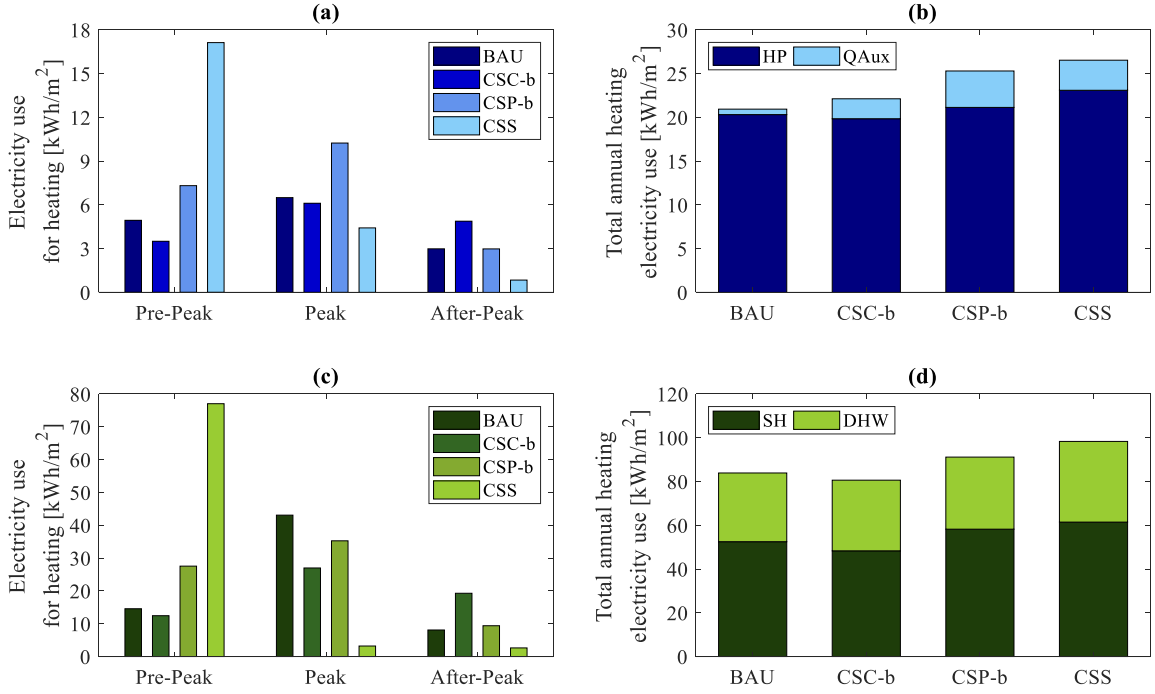

Figure 49. Electricity use for heating of the ZEB for modulating heat pump (a,b) and direct electric heating (c,d) (Clauß et al., 2019 b)

CSS is very effective for load shifting away from peak hours, but, as it simply moves the electricity use from peak to pre-peak hours, it may create new peaks. The annual heating electricity use is increased for all three control strategies for the modulating heat pump system, which is not only due to longer periods with higher temperature set-points (for CSP and CSS), but also due to an increased use of the electric auxiliary heater (for all three control strategies). In comparison, for the case of direct electric heating, the total annual heating electricity use is increased for CSP and CSS but decreased for CSC. The reduction is due to extended periods with lower temperature set-points, meaning that the total heating needs for the building are also lower than in the business-as-usual (BAU) case.
In this study, controlling the heat pump using CSP leads to an increased heating electricity use during peak hours because of the strict prioritization of DHW heating. Extended periods for DHW heating by the heat pump lead to a more frequent use of the electric auxiliary heater to charge the SH tank since the heat pump is not able to heat both. Furthermore, increased temperature set-points in the water storage tank (i.e. DHW and SH parts) lead to higher thermal losses from the water tank.

4.3.7.2 Influence of DHW prioritization on auxiliary heater operation

The strict prioritization of DHW heating by the heat pump has proven to significantly influence the overall system performance of a bivalent mono-energetic heat pump system due to an increased use of the electric auxiliary heater for SH. In further investigations, the price-based control strategy (CSP) is applied to a modulating (MHP) and an on-off heat pump (OHP) to perform demand response for DHW heating only or for SH only. This is done to compare with the previous case where demand response was applied to both DHW and SH.

Figure 50 compares the electricity use for the MHP and the OHP for the CSP cases. It distinguishes between the electricity use for the heat pump itself (HP) and the electric auxiliary heater (Q_{Aux}). The demand response scenarios are compared to a reference case (MHP-BAU and OHP-BAU) where constant temperature set-points for DHW and SH are applied throughout the whole year.

"The DR strategies work very well for DHW heating if DHW and SH are generated by two separate heating systems. For a bivalent heat pump system producing both DHW and SH, the deterioration in system efficiency is mainly due to the strict prioritization of DHW during times of simultaneous DHW and SH demand."

Applying demand response to DHW heating and SH causes the highest share of electricity from auxiliary heaters, Q_{Aux} (cases MHP-CSP and OHP-CSP). This is due to longer periods for charging the DHW tank when temperature set-points are increased. This also implies that the SH tank is charged less frequently by the heat pump so that the electric auxiliary heater is operated more often to cover the SH needs.

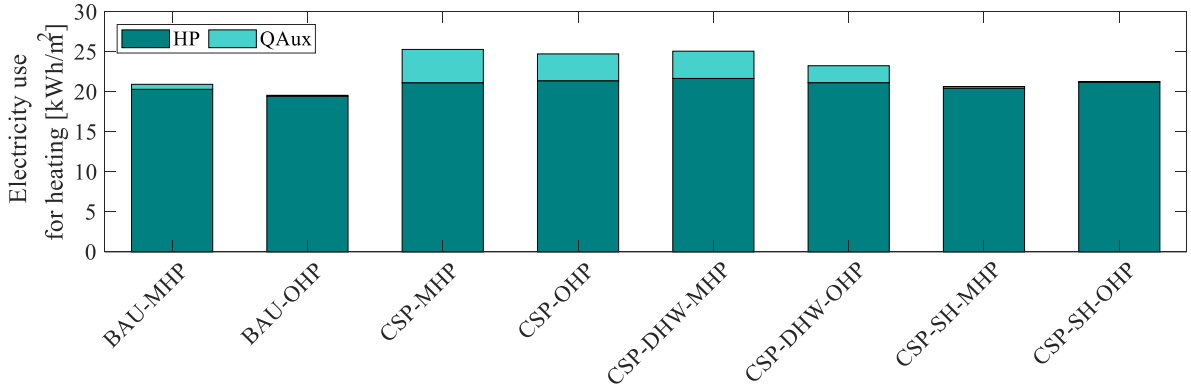

Figure 50. Electricity use for heating for the MHP and OHP for the different DR scenarios.

If CSP is applied to DHW heating only (cases MHP-CSP-DHW and OHP-CSP-DHW), the auxiliary heater is operated slightly less frequently compared to the baseline MHP-CSP and OHP-CSP. It is shown in Figure 50 that the heating electricity use is only slightly increased if the CSP is applied to SH only (MHP-CSP-SH and OHP-CSP-SH), thus confirming that the DHW prioritization is the primary cause for an increased electricity use for heating. A detailed discussion of the results is presented in Clauß and Georges (2019). The deterioration of the DR measure with a bivalent heat pump system is mainly due to the strict prioritization of DHW during times of simultaneous DHW and SH demand. It has been shown in Clauß et al. (2019 a) that the DR strategies work very well, if only applied to a separate DHW heater (without coupling to the space-heating).

4.3.7.3 Modelling complexity of the local heat pump controller

Heat pump systems and their control are usually modelled in a simplified manner in building performance simulation tools. A real modulating heat pump is typically controlled by a PI-controller to meet a required set-point temperature. However, the parameter tuning of the PI-controller can be time-consuming. Therefore, different modelling complexities for the heat pump controller are studied to investigate its effect on energy-related and heat pump-related key performance indicators (KPI). Six different cases for the local heat pump controller are investigated. Among others, a comparison of the system behaviour is done for a heat pump controlled by a PI-controller, a P-controller, or if an on-off control is used (Clauß and Georges, 2019).

In summary, it has been found that the model complexity affects the short-term behaviour of the heat pump system. A simplified local heat pump controller is not able to capture short-term dynamics correctly. Controller tuning is recommended regardless of any control strategy for demand response. It has been found that, even though the energy-related KPIs do not vary significantly amongst the six investigated cases, the heat pump-related KPIs (such as the number of heat pump cycles per year or the average heat pump run time) vary significantly for the studied cases.
Therefore, the modelling complexity of the heat pump system should not be overlooked for demand response studies.

4.3.7.4 Flexibility potential for the introduced PRBCs for the case of Norway

Table 18 presents an overview of the flexibility potential for the investigated control strategies applied to both space-heating and DHW. The control strategies use electricity spot prices and $CO_{2eq.}$ intensities for the electricity mix in the Norwegian bidding zone NO3 (Trondheim). It is mentioned here that the results and thus the flexibility potential would be different for other bidding zones or countries.

"The implemented PRBCs are more favourable in countries with higher fluctuations in spot price and $CO_{2eq.}$ intensity."

Cost savings are achieved for one scenario: CSC in combination with direct electric heating. This case leads to satisfactory results because it has long periods with lowered temperature set-points throughout the whole year, so that the heating needs are lower than the needs for the BAU case and thus cost and emission savings can be achieved. For all other cases, potential cost and emission savings are outweighed by the additional electricity use for heating to charge the thermal storages during times of low costs or low $CO_{2eq.}$ intensities. As an example, the operational costs are increased by about 20% for the CSP in combination with the modulating ASHP.
For the case of direct electric heating, costs are also slightly increased, showing that not only the DHW prioritization of the heat pump has an effect on the overall costs, but also the fluctuations of the spot price. In fact, the implemented PRBCs are more favourable in countries with higher fluctuations in spot price and $CO_{2eq.}$ intensity. These two signals do not fluctuate enough throughout the day for the case of Norway. It has been tested that the performance of the PRBCs is significantly better in bidding zones with higher price fluctuations, like in Denmark.

"In the Norwegian context, the reduction of the energy use during peak hours and especially the peak power is important. The schedule-based control has been designed to address this issue. Results showed that this control is very efficient to reduce the heating energy use during peak hours."

Most important in the Norwegian context is the reduction of energy use and especially the peak power demand during peak hours. The schedule-based control strategy (CSS) has shown to be very efficient for reducing the heating energy use during peak hours. This works very well for a direct electric heating system (Figure 49 (c)), whereas the effect is less pronounced for a bivalent mono-energetic MHP system, where the reduction in electricity use is significantly less pronounced due to the complexity of the heat pump control.

Table 18: Flexibility potential for the investigated demand response scenarios applied to space heating and DHW.

	Modulating air-source heat pump				**Direct electric heating**			
	BAU	CSC	CSP	CSS	BAU	CSC	CSP	CSS
Cost savings	-	✗	✗	✗	-	✓	✗	✗
CO_2 savings	-	✗	✗	✗	-	✓	✗	✗
Peak shifting	-	✓	✗	✓	-	✓	✓	✓

4.3.8 Conclusions

Heat pump systems are a competitive and mature technology. They offer the possibility to deploy the demand side flexibility provided by buildings. This report summarizes the findings from three studies investigating the control of heat pump systems to activate the energy flexibility of Norwegian residential buildings.
It has been shown that Norway is a special case in the European power grid since (1) the electricity generation is almost fully based on hydropower and (2) the lowest $CO_{2eq.}$ intensities usually occur simultaneously with the highest daily electricity spot prices. However, a main concern regarding the Norwegian electricity grid is the capacity of the distribution grid. Congestion problems can be caused by too high power demand on the grid, especially during very cold days during typical peak hours.

4.3.9 Summary

Regarding the flexibility potential of predictive rule-based controls (PRBC) for heat pump systems in Norwegian residential buildings, this chapter has shown that

- Schedule-based control is very effective for load shifting towards grid off-peak hours, but at the risk of creating new peaks in off-peak hours.
- Price-based and $CO_{2eq.}$ intensity-based controls fail to decrease operational energy costs or $CO_{2eq.}$ emissions in Norway, respectively,
- Sufficiently high hourly and/or daily fluctuations in electricity prices and hourly $CO_{2eq.}$ intensities are necessary to benefit from these two demand response measures,
- The DHW prioritization over space-heating (SH) has a strong influence on the operation of the electric auxiliary heater for bivalent mono-energetic heat pump systems. This strongly impacts the performance of the PRBC.
- When DHW is produced by a dedicated heating unit (meaning that SH and DHW are generated by two separate systems), the investigated PRBC applied to DHW managed to reduce the energy costs, $CO_{2eq.}$ emissions and peak power using the current Norwegian grid conditions.

Regarding the modelling complexity of local heat pump controllers, it has been shown that

- The modelling complexity is important when analysing the short-time behaviour of the heat pump system (< 15 minutes),
- Realistic controller behaviour cannot be captured in detail by strongly simplified models,
- Controller tuning is recommended regardless of the applied demand response control strategy.
- In real implementation, predictive controls are applied on the supervisory control level in the building. The resulting set-point temperature is then applied in the local controllers (here PI-controls adjusting the compressor power to meet the set-point temperature). Many modelling studies assume that model predictive control (MPC) can directly control the compressor power, which is most often not true. Our study shows that the dynamic behaviour of the local controller is also important and should not be neglected.

4.3.10 Recommendations for further work

Future work should focus on the following aspects

- Investigate different price (penalty) signals with higher daily and hourly fluctuations
- Improve the fine-tuning of the PRBC, e.g. the determination of thresholds (HCT and LCT in Figure 45)
- Investigate more advanced controls, such as model-predictive control (MPC)
- Investigate different hydraulic layouts (e.g. 4-pipe/2-pipe tank connections, floor heating/ radiator, air-source/ground-source heat pump)
- Investigate design guidelines for heat pump systems that consider energy flexibility
- Design alternative controls of the auxiliary heaters to minimize their operation during demand response

4.4 Design of capacity-control heat pump

Within the framework of the Annex 49, various system configurations and controls for NZEB with heat pumps are investigated.
The current European Performance of Buildings Directive (EPBD, 2018) stipulates that all new buildings must be nearly zero energy buildings by the beginning of 2021. In Switzerland, this requirement is implemented with the introduction of the new building regulations MuKEn 2014 (EnDK, 2018). In order to achieve the new legal standard, it can be assumed that the already frequent use of heat pumps will increase.
With decreasing building loads and high fluctuations by higher impact of solar gains, a part load operation can gain importance, since the heat pump can react more flexible to changing building loads. Furthermore, also the electric power is affected by the capacity control, which enables to better match the heat pump operation to on-site PV yields.
Moreover, speed-controlled heat pumps, which show promising efficiency in part load operation are increasingly entering the market. Figure 51 show the COP-characteristic in dependency of the part load and the compressor control. For inverter controlled units, in particular with DC inverter, the part load COP is significantly higher than in full load conditions. Thus, one could conclude, that a deliberate over-dimensioning of the heat pump to avoid full load operation and maximize part load operation may be a good design approach to optimize the COP during operation.

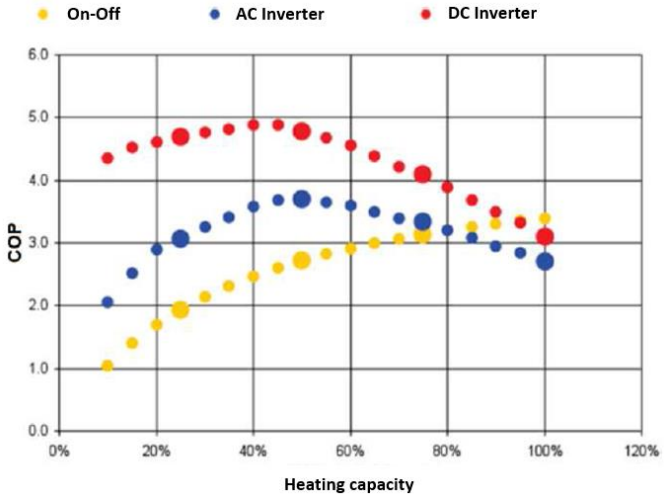

Figure 51: COP in dependency on the part load factor for on-off and different inverter controls (source: Lamanna)

Thus, for a future highly efficient building operation in Switzerland, also the speed-controlled heat pumps must be well designed and integrated into the building. Thus, the design and control of speed controlled heat pumps for NZEB application has been investigated by simulations of a single family house.

4.4.1 Boundary conditions

4.4.1.1 Building definition

NZEBs are already well introduced in the new built residential sector, in particular in single-family houses. Therefore, a single family house is chosen for this study. The building has an energy reference area of 200 m² spread over two floors. The unheated basement is not accounted to the energy reference area, but it is located entirely inside the thermal insulation perimeter. The building has no connection to an underground car park and does not contain a garage. The insulation layer is located outside the supporting structure or between the supporting structure on the pitched roof. With the exception of the pitched roof, all components are of solid construction. The building is oriented to the south. The roof faces east and west and is equipped with a 3.5 kW_p solar photovoltaic system for each direction. The building contains a mechanical ventilation system with heat recovery and a floor heating.

The heating demand according to SIA380/1 (2016) is 23 kWh/(m²a), which is within the limits of MuKEn 2014 (EnDK, 2018). The location of the building is Zurich (weather data set Meteoschweiz). The heat pump uses outside air as a heat source.

4.4.1.2 NZEB definition

In this study, the complete energy consumption of the building services as well as the household electricity is included in the balancing. The PV electricity produced is also included in the balance at 100%. A delivered energy of 0 kWh/(m²a) is used as the limit value for the annual balance. Thus, an NZEB is achieved. Since it is an all-electric building which uses only electricity as delivered energy no energy weighting factors have been applied, implying a symmetric weighting of generated and consumed electricity.

4.4.2 Scientific methodology

For the comparison of different control strategies and design variables, parameter studies by simulations of the defined building and its HVAC system have been performed.

4.4.2.1 Simulation model

The simulations are carried out on the Matlab-Simulink (Mathworks, 2017) simulation platform with the CARNOT Toolbox 6.1 (Solar Institute Juelich, 2018) as coupled dynamic building and system simulation.
Since the whole building has a high thermal inertia the temperatures of each room are considered as equal. Therefore, only one zone for the entire building is considered.

4.4.2.2 Heat pump model

As there is no existing accessible speed controlled heat pump model for the Matlab-Simulink environment, a new model has been developed. The model is based on performance maps of marketable heat pumps taken from manufacturer data and literature (De Coninck et al., 2014), see Figure 52 left and Figure 52 right. Different heat pump data were used to evaluate how strong the result depends on the performance map of the heat pump. These performance maps are implemented as look-up tables. The control also uses these tables to ensure that the heat pump is running at the most efficient operating point. All heat pump data used for the modelling are based on inverter controlled heat pumps.

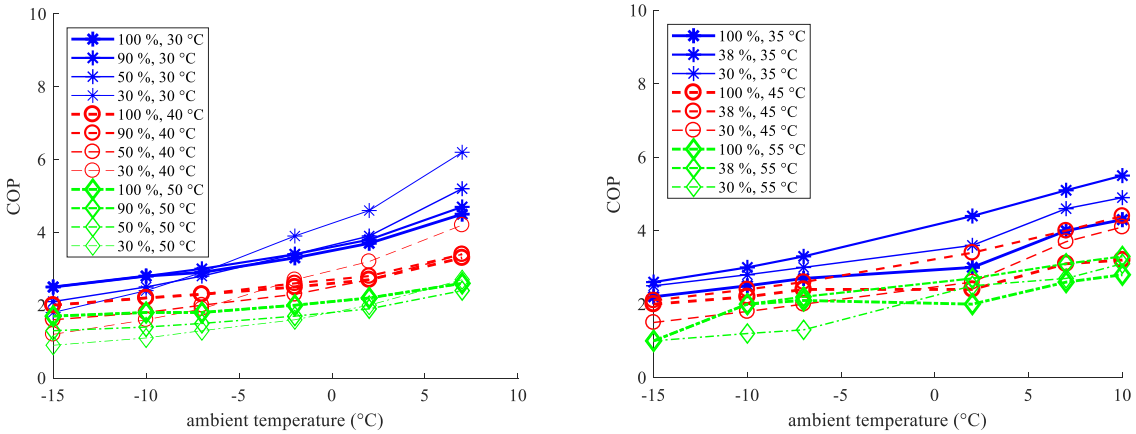

Figure 52: Performance maps of two heat pumps HP1 and HP2 used for the investigation

4.4.3 Results obtained

4.4.3.1 Speed controlled heat pump vs. on/off controlled heat pump

Figure 53 left shows the COP for space heating and domestic hot water (DHW) operation determined by annual simulations. The simulations differ only in the modulation stage of the heat pump. For on/off control, the modulation level is always 1. For speed control, the modulation level is selected which produces the highest COP or the modulation level which can produce the required heating capacity. Here, the term heating capacity refers to the thermal power at the condenser side of the heat pump.

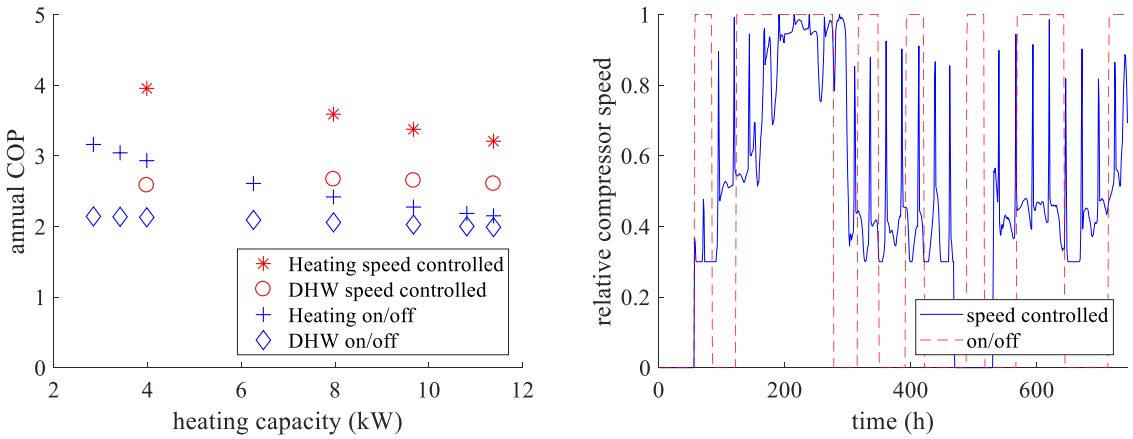

Figure 53: Speed controlled HP1 vs. on/off controlled HP1 and relative compressor speed of HP1

Figure 53 right shows the modulation levels in January. The short peaks of the speed-controlled heat pump can be traced back to domestic hot water operation. It is clear that a speed controlled heat pump achieves a higher COP for heating and DHW operation. Thereby, the degree of improvement depends strongly on the characteristic of the heat pump. Another reason for the better COP in space heating mode is the lower number of starts, as the temperature can be kept constant by modulation. This also promotes thermal comfort in the building. Furthermore, it also prevents the supply temperatures from rising as a result of a too high heating capacity. Figure 53 right also shows that there is no need of a heating buffer storage, because with a speed controlled heat pump the consecutive running times without a heating buffer storage are several hundred hours.

Despite the desired heating capacity has been kept constant in DHW mode, the heat pump is also modulated in order to produce the required heating capacity at best COP conditions and consequently also achieves a higher COP in DHW mode. During times when the space heating mode is not active it would also make sense to run the heat pump at the most efficient compressor speed. During winter time, however, the optimised DHW operation may be limited by needed running time of the heat pump for space heating operation to keep comfortable indoor temperatures.

4.4.3.2 Sizing of the heat pump

Figure 54 shows the annual performance factors as a function of the heating capacity. The heat pump is the only heat generator. The points shown can all meet the requirements for the room and hot water temperature. According to the hydraulic system STASCH 2 taken from the STASCH design guideline (Gabathuler et al., 2002), the heat pump should be designed to a heating capacity of 5.5 kW. The performance maps used for the two heat pumps were scaled with a factor for variation. The efficiencies of the two heat pumps have not been changed.

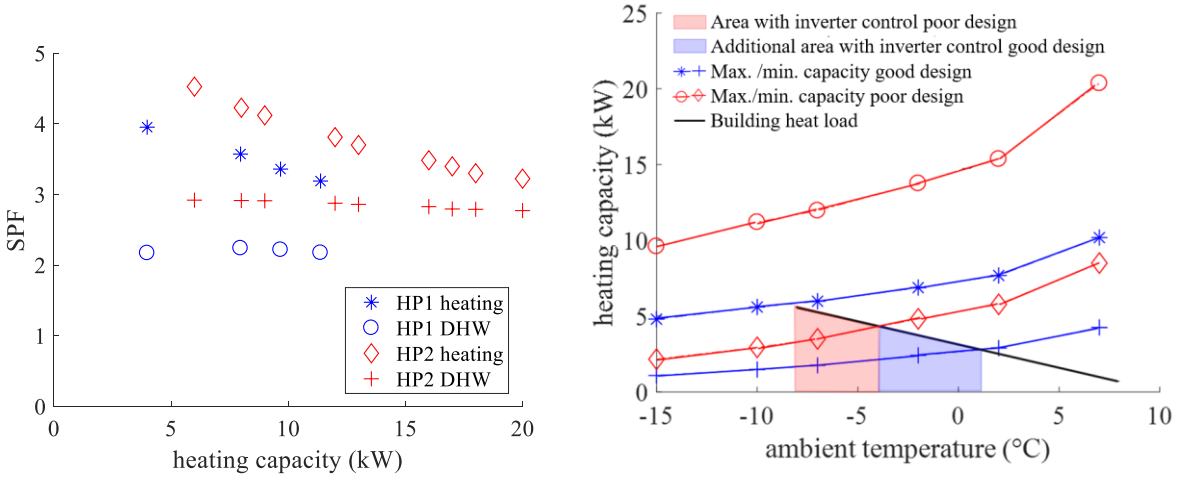

Figure 54: Influence of sizing of the HP on SPF (left) and plot of performance map at 30 °C of HP1 (right)

It can be seen that efficiency decreases with increasing heating capacity. This has the following reason: Due to the oversizing of the heat pump, it already starts cyclic operation at higher heat loads. This is also illustrated in Figure 54 right with a plot of the performance map of heat pump 1. The decrease of the building heat load is depicted idealised as linear black line dependent on the ambient temperature in Figure 54 right. With oversized design of twice the building design heat load the building load curve (black line) crosses the lowest capacity that can be achieved with the inverter control (red line with diamond markers), which is typically at about 30% of the capacity, and the cyclic operation starts already at an ambient temperature of -4 °C (red area in Figure 54 right). On the other hand, with a design according to the design heat load of the building, cycling starts significantly later above an ambient temperature of 2 °C, as shown by the crossing of the lowest capacity (blue line with plus markers) with the building load curve. That means, that between -4 °C and 2 °C (blue area in Figure 54 right), a temperature range, which has a high frequency during the year, inverter control and thus the better part load COP can be additionally used with the smaller design, while with oversizing, the heat pumps is already in cyclic operation in this temperature range.
Therefore, the smaller heat pump is more efficient. In Figure 54 right only the temperatures are considered for the heating curve. But obviously solar radiation is also influencing the heating demand.
The design according to STASCH is in principle still correct even for net zero energy buildings with low heating loads. The design, though, tends to be somewhat too large, as no gains are taken into account. In terms of efficiency, oversizing can help to generate more operating hours with high efficiency. The losses in cyclic operation are, however, decreasing the efficiency. In the simulations, the losses due to cyclic operation are weighted higher than the efficiency gains. However, no start-up data was available for the heat pumps. In addition, the supply temperatures also increase due to the excess heating capacity in cyclic operation, which reduces efficiency. For this reason a deliberately oversizing should be avoided.

4.4.3.3 Control strategy and flexibility of the building

To evaluate how the efficiency is influenced by the control strategy, four rather simple control strategies have been compared:

- Constant supply temperature:
  The heat pump is controlled in such a way that the desired supply temperature is reached. For this purpose, the required heating capacity is calculated as enthalpy balance with set point of the supply temperature and the return temperature. If the COP of the heat pump is better at a higher speed, this operating point is selected.
- Constant return temperature:
  With this control, the return temperature is kept constant. The required heating capacity is calculated with the set point of the return temperature. The heat pump is also operated at an operating point which produces a higher capacity, in case of higher efficiency.
- Constant supply temperature, maximal running time:
  The control is analogous to the control constant supply temperature. Only the most efficient operating point of the performance map is not used, but always the operating point, which supplies the required heating capacity.
- Constant return temperature, maximal running time
  The control is analogous to the control constant return temperature. However, the heat pump is always operated in such a way that the required heating capacity is reached.

For all strategies the mass flow is kept constant.
It can be seen that a slightly higher efficiency is achieved with a constant supply temperature than with a constant return temperature. This does not meet expectations, as the lower supply temperature should be achieved with a constant return temperature. However, it should be noted that a constant return temperature leads to a higher supply temperature at the design point, as otherwise the mean temperature in the underfloor heating system is too low at low heating capacity. This results in slightly higher supply temperatures. However, this problem could certainly be solved with a more advanced control system.
Figure 55 shows also that in this case, with the performance map, the COP is higher with a control strategy, which achieves the longest running time.

Thus, it is more efficient to run the heat pump at the exact capacity that the building needs than at the capacity which would be most efficient for the heat pump itself. This is due to the fact that the heat pump has more on and off cycles due to the heating capacity surplus. In addition to that the supply temperature increases in times of surplus heating capacity of the heat pump compared to the building load. This increase leads to a lower efficiency of the heat pump. For further work an optimised control should already take this supply temperature increase and the cycling losses into account and thereby always run at the operation point which leads to the highest efficiency of the whole system. For the next step the most efficient control strategy was taken and improved regarding the reduction of the delivered energy from the grid. Therefore, the simulation was carried out in Figure 8 with including PV production in the control strategy. The heat pump thus runs earlier than necessary, both for heating and domestic hot water, when the production of the PV system exceeds the consumption of the building to a certain extent.

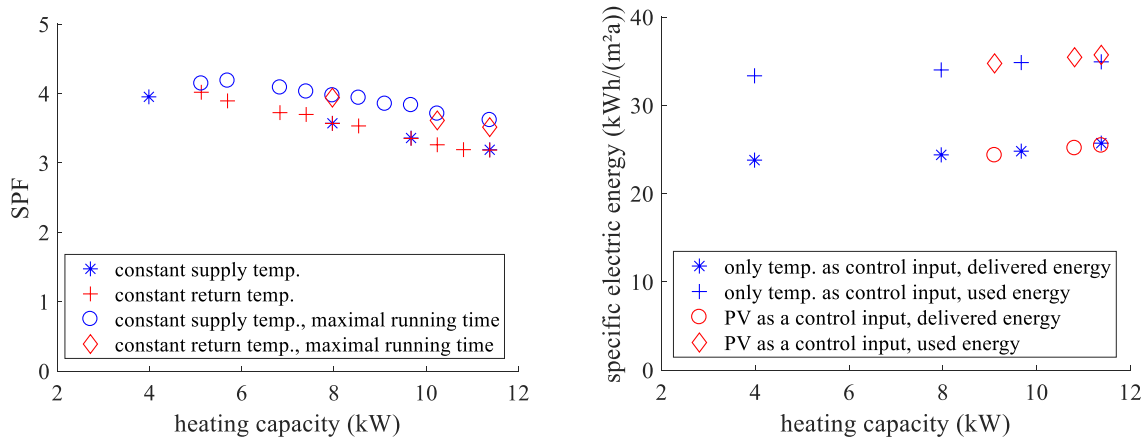

Figure 55: Comparison control strategies for HP2 and Electrical energies of different control strategies for HP2

It can be seen that the imported electrical energy decreases with the regulation according to PV electricity. This reduces the PV production impact on the grid. This is generally regarded as positive, as a growing share of renewable energies is expected to lead to a higher fluctuation in production. In the simulated case, however, the heating demand increases because the average room temperature increases due to the earlier activation of the heat pump during heating operation. In addition, the heat pump is also switched-on if this is not necessary at all with the standard control, since the building heats up anyway as a result of the solar irradiation. During DHW operation, and storage losses also increase due to a higher average temperature in the storage tank. The higher start-up frequency of the heat pump results in even more cyclic losses. On the other hand, there are higher source temperatures due to increased operation during daytime. Moreover, in this case, the reduction of the delivered electric energy from the grid is also comparably low due to the two different orientations of the photovoltaic installation. The heat pump can be used to reduce the interactions with the electricity grid or to have an electricity grid supportive operation mode. A speed controlled heat pump has the advantage that, if desired, it can use a smaller PV output over a longer period of time. However, the actual flexibility of operation seems to be defined by the heat consumers (building and DHW tank). While flexible operation is easier to achieve with the DHW tank, user acceptance must also be guaranteed in the case of the building thermal comfort. The larger heat capacity is naturally in the thermal inertia of the building. Due to the high efficiency of the heat pump and the low consumption of net zero energy buildings, the PV production peaks are also difficult to absorb. Electric mobility offers higher potential in this respect.

4.4.4 Conclusion

The simulations carried out show that the recommendations according to the design guideline STASCH are in principle still applicable also for efficient buildings with low heating loads like net zero energy buildings. Furthermore, it was clearly shown that a significantly more efficient operation can be achieved with a speed controlled heat pump compared to an on-off control.

The preferable design size is approximately in the range of the STASCH design. A strong over-dimensioning of the heat pump leads to a lower efficiency. The best results were achieved when the heat pump always delivers the required heating capacity and thus achieves the longest possible running time. To decrease the delivered energy from the grid the speed controlled heat pump can be used. However, how effective it can be done depends strongly on the boundary condition. To further investigate how flexible a building is with a speed controlled heat pump, it has to be looked at other metrics. The approach of the IEA EBC Annex 67 (Gronborg Junker et al., 2018), which is penalizing grid interactions differently over time, seems to be a good approach in this sense. A heating buffer storage tank is not required for a system with a speed controlled heat pump.

The evaluation of the control strategies yielded the result that by a room temperature based control a higher performance of the heat pump can be reached.

Speed controlled heat pumps lead to the problem, that it is hard to tell which heat pump is the more efficient one. Or at least more data have to be considered. However, for numerous speed controlled heat pumps this data are not publicly accessible.

For domestic hot water operation, an efficient operation is achieved by adapting the desired heating capacity to the maximum COP, which occurs in part load operation. In this case, the design size of the heat pump does not affect the efficiency.

All simulations were carried out for single family houses. However, it can be assumed that the general statements are also valid for multi-family houses.

5 Integration with building envelope/structure – TABS

The work documented in the following was mostly carried out in the project solSPONGEhigh "High solar fraction through thermally activated building elements in urban environments" at the Institute of Thermal Engineering at Graz University of Technology. The final report of the mentioned project (Heimrath, Lerch, Mach, Ramschak and Fink, 2018) contains detailed information on all boundary conditions and assumptions and the simulation variants performed. Within the framework of the Austrian participation in IEA Annex 49, additional simulations were carried out for the coupling of an air-to-water heat pump with a photovoltaic system, which are documented here with the main assumptions.

5.1.1 Introduction

One way to increase the heat storage capacity of a building is to use the building construction. All solid building components such as ceilings, walls and foundations are basically capable of storing heat as a sensitive heat capacity, i.e. by increasing the temperature. This process is called thermal activation of building elements. In combination with solar thermal or solar electric systems, a high level of solar fraction of the energy demand in the building can be achieved, which allows for an extensive supply of renewable energy or, if a heat pump is used, a low level of electrical energy consumption from the grid.
The aim of the research project solSPONGEhigh was an analysis of this approach using detailed dynamic simulations. Different system concepts for heating and domestic hot water preparation were defined for three reference buildings, a single-family house, an apartment building and a production hall. In addition to small thermal buffer storage units, these system concepts essentially include thermally activated components (floor ceilings) as heat storage and heat distribution systems. Building-integrated solar thermal or solar electric systems, combined with heat pumps, serve as the energy source. The system concepts were numerically modelled in different configurations, supplemented with control concepts and used to cover the heat demand of the reference buildings with different heat demand levels.

5.1.2 Boundary Conditions

5.1.2.1 Climate

The city of Graz was chosen as the locations for the thermal building and system simulations. An average climate data set (over 10 years) was generated with the software Meteonorm (Meteotest, 2015) ($T_{ambient,avg}$ = 10.7 °C; heating degree days 3102 Kd; global radiation on the horizontal 1206 kWh/(m²yr); diffuse radiation on the horizontal 616 kWh/(m²yr). Figure 56 shows the graphic evaluation of the used climate data set of Graz.

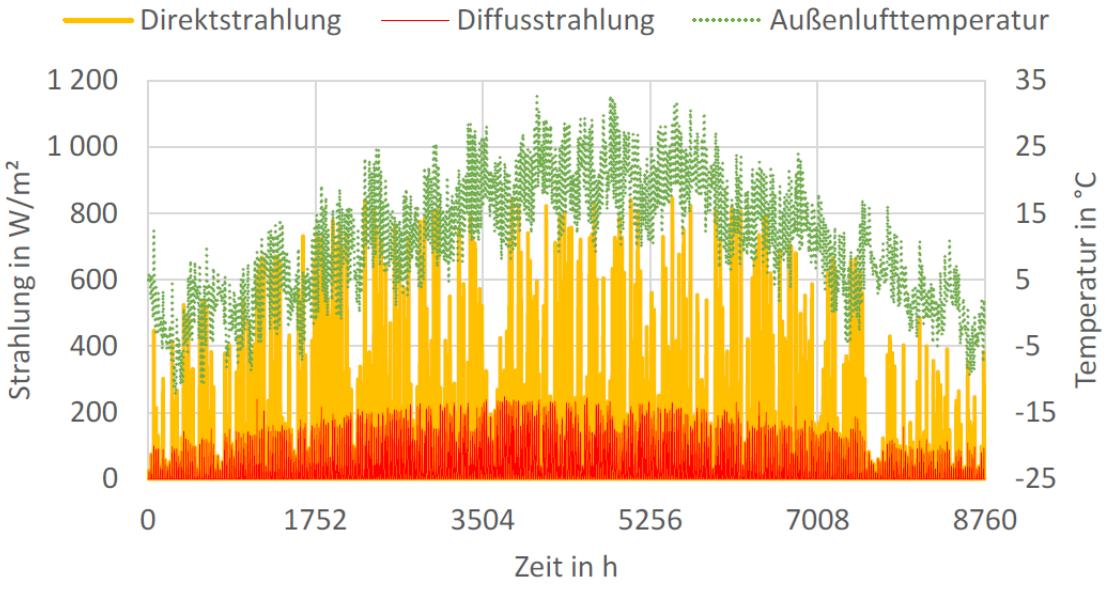

Figure 56: Average climate data set of Graz, generated with Meteonorm (Meteotest, 2015)

5.1.2.2 Building

Based on a module with a usable area of 30 m², a single-family house (Figure 57), a multi-family house and a production hall, each with two heat demand levels, were modelled in the simulation environment TRNSYS 17 (Solar Energy Lab, 2017). The heat demand level "Low Energy Building" (LEB) meets the current standard of thermal insulation for new buildings in Austria and the heat demand level "Nearly Zero Energy" (NZE) is equivalent to the heat consumption of a passive house.

Single family house (SFH)

4 Modules

Heated floor area = 120 m²

Net Volume = 336 m³

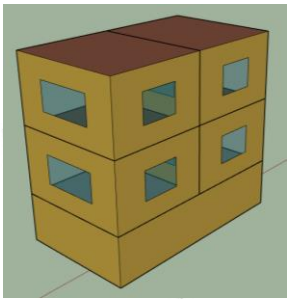

North	East	South	West
Outer wall area [m²]			
87.2	38.2	87.2	38.2
Window area [m²]			
4.2	3.6	18	3.6

Figure 57: Reference single family house

For the work and variants described here, the single-family house with the heat demand level "Nearly Zero Energy" was used, with the following assumptions regarding the U-values of the components:

- U-Value exterior wall (25 cm bricks, 20 cm EPS): 0.171 W/(m²K)
- U-value interior wall (25 cm bricks): 1.160 W/(m²K)
- U-value roof (25 cm concrete, 30 cm XPS): 0.128 W/(m²K)
- U-value suspended ceiling (25 cm concrete, 10 cm insulation, 8 cm screed): 0.389 W/(m²K)
- U-value window: 0.59 W/(m²K) (g-value window: 0.584)

5.1.2.3 Internal loads and domestic hot water demand

The building was configured with specific internal loads for occupancy, electrical lighting and equipment. The specific energy input is approx. 80 kWh/(m²yr), which corresponds to an average load of 9.14 W/m². For domestic hot water (DHW) a tap profile was defined with a total heat demand of 2966 kWh/yr. The tap temperature for hot water was defined with 45 °C (corresponds to 50 l/(dPers) at 45 °C, 4 persons).

5.1.3 System configurations

System A in Figure 58 represents the reference heat supply system. In this system, the complete heat demand is covered by an air-to-water heat pump (AWP). To cover the heat requirement for DHW, a storage tank with a volume of 0.35 m³ is installed. DHW preparation is done via a fresh water module.

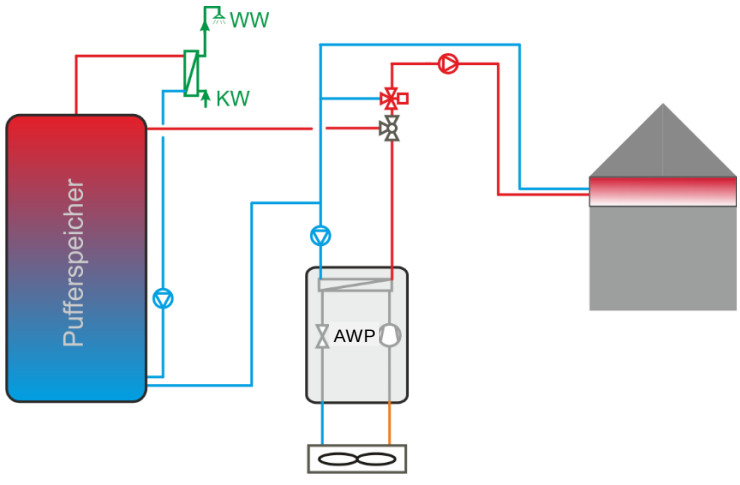

Figure 58: System A – Reference system with AWP

The building is heated exclusively and directly by the AWP. As with systems B and C, the AWP is dimensioned for monovalent operation so that no second heat source or backup system is required. The AWP has an output of 4.3 kW at operating condition A-12/W35. In the SolSPONGEhigh project the heat pump was dimensioned to cover the heating load of the defined heating demand level "Low Energy Building" (LEB). This same size was also used for the NZE heating demand level used here.
In solSPONGEhigh a single speed compressor was assumed. Within the framework of the present project, a variant with a variable speed compressor was also considered for system C (see section 5.1.5).

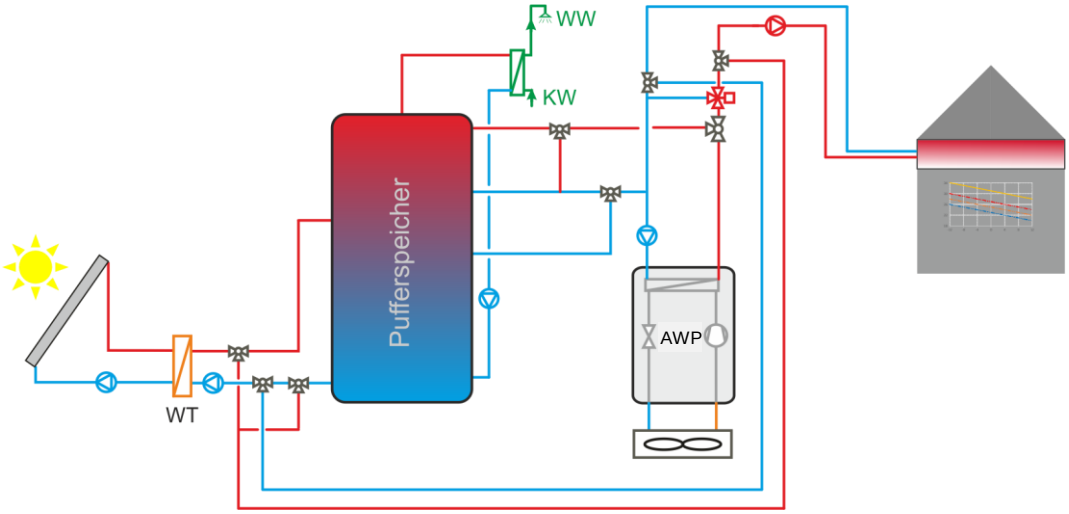

Figure 59: System B – Solar thermal heat supply with AWP and solar charging of the concrete core

In the next step, the heat supply system was extended by a solar thermal system in concept B (Figure 59). Compared to system A, the storage tank has a larger volume of 1 m³ due to the additional storage volume required to integrate the solar thermal system. Primarily, the room is heated with solar heat from the storage tank and only in times when the storage does not have a sufficient temperature level to heat the building the AWP is used for charging the concrete core of the floor slabs.
In order to increase the solar yield of the thermal collector and the solar fraction, the hydraulic system was designed in such a way that the building can be heated directly by the solar thermal system, as shown in Figure 59. Due to the low temperature level required for charging the concrete core compared to the storage tank, the solar collectors can be operated with a higher efficiency and at times of low irradiation.

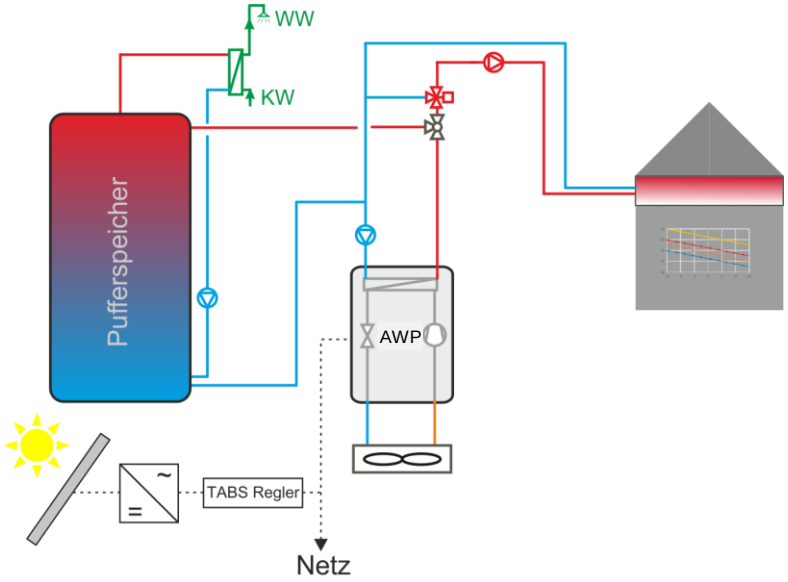

Figure 60: System C – Solar electric system with AWP and solar charging of the concrete core

System C was defined as a solar electric heat supply system (Figure 60). Instead of the thermal solar system a photovoltaic (PV) system is installed here. The only difference to system A described above (Figure 58) is the additional photovoltaic system. The electricity generated by PV is used to operate the AWP, the excess electricity is fed into the grid. In order to increase the solar fraction and reduce energy consumption from the grid, the control system was optimized.
The aim was to increase the PV self-consumption by thermal activation of the building's floor slabs. Depending on the electricity consumption of the heat pump and the PV yield, the floor slabs are charged to a higher temperature level.

5.1.4 Thermal component activation (TABS) and charging control

The used concept of thermal activation is shown in Figure 61. The existing floor slabs with a thickness of 250 mm, which contain a centrally arranged pipe layer with a pipe spacing of 200 mm, are activated.

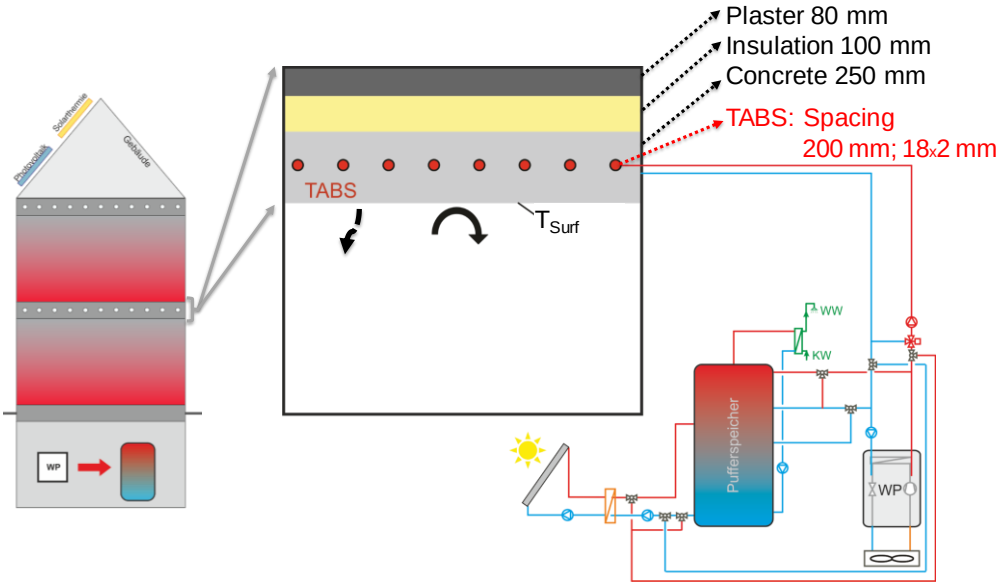

Figure 61: TABS-arrangement in the building and construction of the floor slabs

On the basis of the evaluation of simulation results of different control strategies examined for the charging of the concrete core (charging cycles, comfort), it was found that a good way to control the heating of the room is by means of the temperature sensor T_{Surf} on the surface of the concrete ceiling (Figure 61). The used temperatures for the heating of the room are determined depending on the outside air temperature. The corresponding temperature levels depend on the average value of the outside air temperature of the previous 24 hours (Figure 62).

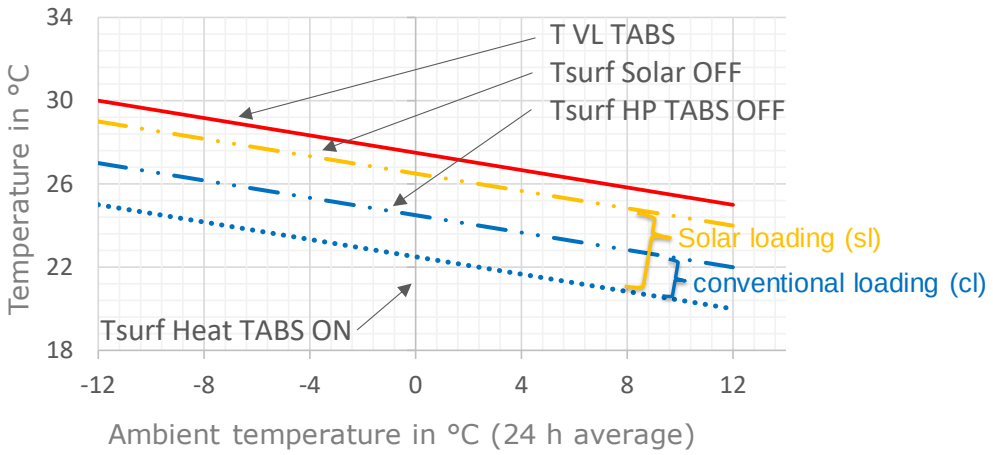

Figure 62: Control of the TABS charging: switching temperatures dependent on the outside temperature

Figure 62 shows that the heating flow temperature ($T_{VL,TABS}$) varies between 30 °C (at -12 °C) and 25 °C. The charging of the TABS is started as soon as the temperature at the surface (T_{Surf}) drops below $T_{Surf,Heat,TABS,ON}$. The floor slab is then heated by the heat pump until the temperature $T_{Surf,HP,TABS,OFF}$ is reached at the temperature sensor T_{Surf} (conventional loading "cl"). If there is sufficient solar radiation, the ceiling is additionally heated up to the control temperature $T_{Surf,Solar,OFF}$ (solar loading "sl"), measured at the temperature sensor T_{Surf}.

5.1.5 Control options with PV (System C)

In addition to the variants analysed in solSPONGEhigh, additional control options were considered for system C.

5.1.5.1 Time window for DHW charging (Win)

Here charging of the DHW zone of the storage tank is not possible all day, as in the other variants, but only in a fixed time window from 10:00 to 16:00. This means that DHW charging tends to be carried out when photovoltaic electricity is available on the one hand and the outside temperature and thus efficiency is higher on the other. Due to the available storage volume of 350 l, it should be possible to bridge the remaining time without recharging the storage tank.

5.1.5.2 Variable speed compressor, power adjustment heat pump to PV (nHP)

In this variant a variable speed compressor (20 to 100%) is used. When PV yield is available, the compressor speed is adjusted so that the power consumption of the heat pump corresponds to the available PV surplus.

5.1.5.3 Performance figures

In order to enable an evaluation of the various system concepts considered in the simulations, energetic performance figures were defined.

An important figure is the **specific heating demand (q_{RH})** of the building. The specific heating demand is calculated by dividing the heat supplied to the building (Q_{RH}) by the gross floor area of the building ($A_{BGF}=A_{NGF}/0.8$). This figure is interesting due to the different charging strategies (temperature levels of the building storage masses) of the thermally activated building components, since the influence on the heat consumption of the building can be shown.

$$q_{RH} = \frac{Q_{RH}}{A_{BGF}} = \frac{\int \dot{Q}_{RH}\ dt}{A_{BGF}}\ [kWh/m^2] \qquad \text{Eq. 5.1}$$

The **total electricity consumption of the system ($W_{el,tot}$)** is calculated from the power consumption of the heat pump, the pumps, the electrical heater and the control system, minus the electricity supplied by the photovoltaic system ($\int P_{el,PV,EV}\ dt$). The household electricity consumption was not considered in solSPONGEhigh. Thus $W_{el,tot}$ corresponds to the amount of energy obtained by the heating system from the grid $W_{el,grid}$.

$$W_{el,tot} = \int (P_{el,tot} - P_{el,PV,EV})\ dt = W_{el,grid} \quad [kWh] \qquad \text{Eq. 5.2}$$

Especially for combined systems (heat pumps with solar thermal or PV systems), the **system seasonal performance factor (SPF_{sys})** is an important performance figure. It is calculated by dividing the useful heat consumption (Q_{Useful}) (space heating Q_{RH} & domestic hot water Q_{DHW}) by the total electricity consumption of the system ($W_{el,tot}$).

$$SPF_{sys} = \frac{Q_{Useful}}{W_{el,tot}} = \frac{\int (\dot{Q}_{RH} + \dot{Q}_{DHW})\ dt}{\int (P_{el,tot} - P_{el,PV,EV})\ dt} \quad [-] \qquad \text{Eq. 5.3}$$

5.1.6 Results

The simulation results are presented and discussed on the basis of the above mentioned performance figures in Figure 63. For system A, a SPF_{sys} of 2.84 is achieved, which means an electricity consumption from the grid $W_{el,grid}$ of 1875 kWh.
For the variant with a solar thermal system (System B, Figure 59) conventional loading (cl) with a 20 m² of solar thermal collectors the electricity consumption from the grid can be reduced by 56% to 830 kWh. If the solar loading (sl) is activated, $W_{el,grid}$ remains almost unchanged, but SPF_{sys} increases from 6.4 to 7.7. This is due to the fact that the heat demand increases due to solar loading, which according to the definition in Eq. 4.3 also leads to an increase of SPF_{sys}. Only taking into account the figure SPF_{sys} for the evaluation of a system is therefore not meaningful, since it does not provide any information about the electricity consumed from the grid and thus the electricity costs.
If the collector surface is increased to 40 m² in system B, the electricity consumption from the grid drops further to approx. 696 (cl) and 604 (sl) kWh. Although these additional savings correspond to 16 and 28%, the savings are relatively low in absolute numbers [kWh] given the doubling of the collector area.

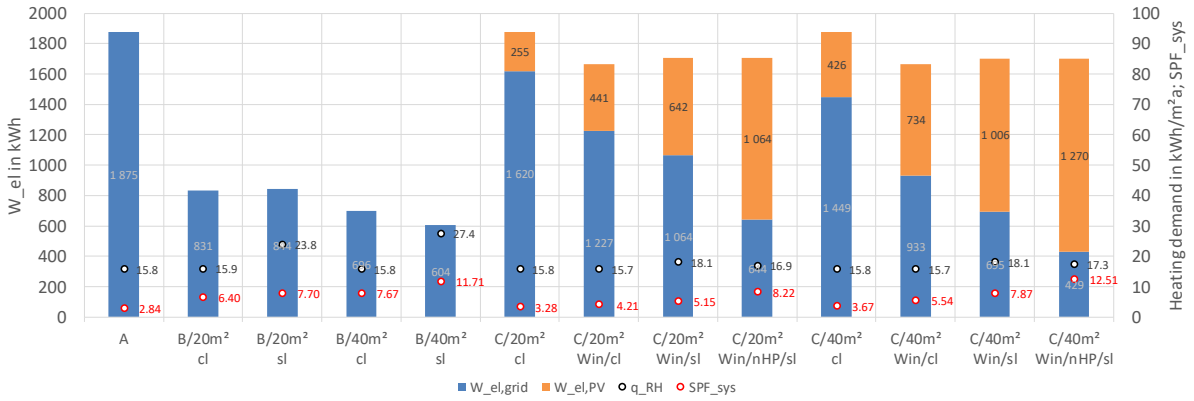

Figure 63: Simulation results for systems A, B and C, for 20 and 40 m² collector area, conventional loading (cl) and solar loading (sl)

System C was also simulated with 20 and 40 m² collector area (PV) and for four variants with regard to the control. With conventional loading (cl), $W_{el,sys}$ is 1620 kWh for 20 m² PV and 1449 kWh for 40 m². Here the heat pump and the PV system are operated in parallel, which means that the heat pump only uses PV electricity, if it happens to be operated when PV yield is available.
If a time window is used for DHW charging (Win), the electricity drawn from the grid can be reduced to 1227 (-24 %) with 20 m² and 933 kWh (-36 %) with 40 m², because DHW charging only takes place at times when PV yield is potentially available. The simulation results have shown that this time limitation for DHW charging does not cause any loss of comfort concerning the hot water temperature. In cases, where only a smaller storage volume is available for DHW, comfort could be ensured by an "emergency charging" option (e.g. charging also outside the time window from a temperature threshold lower than the threshold that is otherwise used).
As in system B, $W_{el,sys}$ decreases further to 1064 (20 m²) and 695 (40 m²) kWh with additional solar loading of the TABS (sl). If, as a last additional measure, a variable speed compressor with a corresponding control is used (nHP), $W_{el,sys}$ can be reduced to 644 with 20 m² and 429 kWh with 40 m² of PV. This corresponds to a saving of 66 and 77 % respectively compared to the system without PV (system A).
These results show that when a heat pump is coupled with a PV system (system C), the PV share in the energy supply can be significantly increased (and the grid consumption can be reduced) by simple control measures. With the same collector surface used, slightly better results can be achieved with PV than with solar thermal collectors. For this reason, the use of PV as a whole currently appears more attractive than solar thermal, primarily because of the relatively low investment costs, but also because of the possibility of feeding surplus energy into the grid.

As mentioned above, the simulations did not take the household electricity consumption into account. On the one hand, this would lead to less PV energy being available for the heat pump, but on the other hand, it would result in an overall higher self-consumption of PV and substitution of grid electricity.

5.1.7 Conclusions and outlook

The project solSPONGEhigh and the work carried out in the present project show that the thermal activation of building components can be combined very well with the use of solar thermal or solar electric energy generation in buildings. Especially in buildings with a very low heat demand, the main part of the heat supply can be covered by solar energy.
The focus of the reported work was on systems for space heating and preparation of domestic hot water. However, the thermal activation of building components also offers an excellent possibility for space cooling, as it enables a potentially comfortable extraction of heat from the interior spaces due to the large available surfaces. The developments concerning the climate change as well as the rapid spread of decentralized, often inefficient cooling devices clearly show that systems for cooling buildings are in demand and that the demand for systems enabling sustainable cooling will probably continue to increase. For a comprehensive analysis of the performance of thermal activation of building components, space heating and DHW preparation should be supplemented by cooling aspects in further work. There is a demand for system and control concepts that enable both heating and cooling on the basis of solar decentralised energy generation.

6 Conclusions

IEA HPT Annex 49 has performed in-depth analysis of energy concepts, heat pump integration and operation as well as design and control for the application in nZEB, mainly linked to real monitoring projects. This report summarises the results of the detailed studies in connection to these long-term monitorings of real-world operation of heat pumps in different types of nZEB and further case studies not linked to the monitoring performed within the Annex 49.

Optimisation of system

Meeting ambitious nZEB or plus energy targets can still be a challenge, in particular in larger buildings with limited space for on-site energy production and requires optimised building concepts and operation. By accompanying modelling and simulation system configurations and performance can be optimised. By the link to monitoring projects a real world model validation is enabled. Thus, the created "digital twin" can be used for in-depth investigation and further optimisation of the running operation. At UIBK validated system models of the main components have been developed and used for evaluation of component behaviour, e.g. of the desuperheater, and evaluation of variants of the system configuration. Further investigations will be performed in order to continuously optimise the system operation. Furthermore, it could be confirmed by the model, that an nZEB balance can be reached.

Control/Energy Flexibility

Another focus was set on control and heat pump integration for energy flexibility, in particular for the integration of the heat pump with thermal and electric storage by smart controls in order to increase self-consumption of on-site generated PV electricity. Therefore, electric battery storages as well as flexible user operation by load shifting are suited, but also the conversion of surplus electricity into heat denoted as power2heat and storage in thermal water storages for the space heating, cooling and DHW operation, but also the building thermal mass is suited. Case studies have been performed for the plus energy single family house Berghalde and the Herzo Base terraced houses. In the solSPONGEhigh project high solar fraction of solar PV or solar thermal installations have been confirmed for the storage in thermally activated building structures.

Control/grid integration

With nZEB as energy producing buildings also the integration in the energy system in terms of electrical and thermal grids is becoming a more and more important feature of building operation. Building should be operated in synergy with the connected grids and should be able to react the connected grids' needs. At NTNU it has been confirmed that heat pumps in residential buildings are suited to be used for load shifting, however, with the risk of creating new peaks. Due to the specific Norwegian boundary conditions, price-based and $CO_{2eq.}$-intensity based controls fail to decrease operational costs or CO_2 emissions. Higher fluctuations would be required to these predictive rule-based control strategies.

Flexibility, control and design

Furthermore, the flexibility aspect could also become a design criterion, if also an economic incentive would exist to invest in larger systems with more flexibility potential, which could be accessed by distributed smart controls. However, in many market there is currently no economic trade-off to invest in flexible system technology.

Design of capacity-controlled heat pumps

Depending on the inverter type variable speed heat pumps have significantly better part load COPs than in full load. Thus, a deliberate over-sizing could be thought to lead to higher overall performance due to longer part load operation instead of full load. However, due to already existing oversizing by common design rules, a further deliberate larger design would lead to higher on-off cycling. Best performance was achieved in the case study with a slightly undersized heat pump based on a STASCH design guidelines.

7 Acknowledgment

IEA HPT Annex 49 is a co-operative research project on heat pump application in nearly Zero Energy Buildings in the framework of the Technology Collaboration Programme (TCP) on Heat Pumping Technologies (HPT) of the International Energy Agency (IEA). This report is based on the contributions of all participants in the Annex 49 and the constructive and co-operative discussions during the project as well as the contributed results are highly appreciated.

The support and funding of the IEA HPT Annex 49 by the Swiss Federal Office of Energy (SFOE) is highly appreciated and gratitude is expressed to the programme managers of the SFOE heat pump research Dr. Carina Alles and Stephan Renz for advice and support in the IEA HPT Annex 49 and the Swiss national contributions.

The financial supports from the Austrian Ministry for Transport, Innovation and Technology and the Austrian Research Promotion Agency (FFG Project Nr. 864143) through the IEA Research Cooperation to this work are gratefully acknowledged.

The project COOLSKIN (FFG Project-Nr. 848871) was funded by the Austrian Climate and Energy Fund and was carried out as part of the Energy Research Programme 2014.

The project solSPONGEhigh (FFG Project-Nr. 845182) was funded by the Austrian Ministry for Transport, Innovation and Technology (bmvit).

The participation in the IEA Annex 49 as well as this research and the monitoring of the buildings was funded by the German Federal Ministry for Economic Affairs and Energy (BMWi) and the research initiative ZukunftBau and the Federal Institute for Research on Building, Urban and Spatial Development (the BMVBS and BMUB). Thanks to all building owners and operators for their help and support as well as for providing measurement data and information about the monitored buildings.

The Norwegian authors would like to thank the Norwegian Research Center on Zero Emission Neighborhoods in Smart Cities (FME ZEN) as well as ENOVA for their support

8 Abbreviations

Abbreviation	Meaning	Remark
A-HP	Air heat pump	
ANN	artificial neural network	
AS	Air source	
Aux	Auxiiary	
AWP	Air-to-water heat pump	
BAU	Business as usual	
BC	Boundary condition	
BPS	Building Performance Simulation	
BS	Buffer storage	
CND	Condenser	
COP	Coefficient Of Performance	
CSC	Control Strategy $CO_{2eq.}$-intensity	
CSP	Control strategy price	
CSS	Schedule based control strategy	
CV	Coefficient of Variation	
DC	Direct Current	
DHW	Domestic hot water	
DR	Demand response	
DSH	Desuperheater	
DSM	Demand Side Management	
EL	electric	
EPBD	Energy Performance of Buildings	EU Directive
Err	error	
EU	European Union	
EVP	Evaporator	
GS	Ground source	
HC	heat control	
HCT	High control temperature	
HD	Heat demand	
HP	Heat pump	
HPT	Heat Pumping Technologies	IEA TCP
HVAC	Heating, Ventilation and Air-conditioning	
IWT	Institut für Wärmetechnik	
KPI	key performance indicator	
LCF	load cover factor	
LCT	Low control temperature	
LEB	low energy building	
LEH	Low energy house	
MFB	Multi-family building	
MFH	Multi-family house	
MHP	modulating heat pump	
MILP	Mixed integer linear programming	
MPC	Model predictive control	
Msr	measured	
MuKEn	Model ordinance of the cantons in Energy	
MVHR	mechanical ventilation heat recovery	
NS	Norge Standard	
NTH	Neue Heimat Tirol	
nZE	nearly Zero Energy	
nZEB	nearly Zero Energy Building	

Abbreviation	Meaning	Remark
NZEB	Net Zero Energy Builiding	
OHP	on- off controlled heat pump	
PRBC	Predictive Rule based control	
PE	Primary energy	
PEB	Primary energy demand	
PER	Primary Energy Renewable	
PH	Passive house	
PHPP	Passive House Planning Package	Passivhaus-Projektierungs-Paket
PID	Proportional-integral-differential control	PID Regelung
PV	Photovoltaic	
PVC	Photovoltaic optimized control	
PV/T	photovoltaic/thermal	
RE	Renewable energy	
ref	reference	
RBC	Rule based control	
RES	Renewable Energy Sources	EU Directive
RMSE	Random Mean Square Error	
SC	Space cooling	
SCF	supply cover factor	
SFH	Single family house	
SH	Space heating	
SIA	Swiss society of engineers and architects	
sim	Simulated	
SOS	special ordered set	
SPF	Seasonal performance factor	
ST	Solar thermal	
TA	treated area	Konditionierte Fläche
TABS	Thermally activated building system	
THN	Technische Hochschule Nürnberg	
UIBK	Universität Innsbruck Baukonstruktion	
VSD	Variable speed drive	

9 Referenced Literature

Betzold, C., Bordin, S., Dentel, A., Harhausen G. 2021. Control strategies for modulating heat pumps in a plus energy building, Proceedings 13th IEA Heat Pump Conference, Jeju, April 2021 (Paper accepted for publication)

Betzold, C., Dentel, A. and Bordin, S., 2020. Entwicklung und Implementierung von Betriebsführungsstrategien in einem Plusenergiegebäude. 8. Deutsch-Österreichische ibpsa Konferenz BauSIM 2020. (Paper accepted for publication)

Betzold, C., Dentel, A. 2019. PV Optimized Control of Modulating Heat Pumps regarding PV Self-Consumption, Proceedings IBPSA Building Simulation 2019, 2.-4.Sept. 2019, Rome

Bockelmann, F., Fisch, N.M., Kley, Ch., Wilken, Th. 2015. Betriebsstrategien für EnergiePLUS-Gebäude am Beispiel der Berghalde, final report Forschungsinitiative Zukunft Bau des Bundesinstitutes für Bau-, Stadt- und Raumforschung (Aktenzeichen: SWD–10.08.18.7-13.33), TU Braunschweig Institut für Gebäude- und Solartechnik, 2015

Bockelmann, F., Fisch, N. M. 2019. „Dezentrale, modulare Stromspeicher zur Eigenstromsteigerung in EffizienzhausPLUS Gebäuden“, Abschlussbericht, Forschungsinitiative Zukunft Bau des Bundesinstitutes für Bau-, Stadt- und Raumforschung (Aktenzeichen: SWD–10.08.18.7-16.34), TU Braunschweig Institut für Gebäude- und Solartechnik

Clauß, J., Stinner,S., Solli,S., Lindberg, K. B., Madsen, H., Georges,L. 2019a.Evaluation Method for the Hourly Average CO2eq. Intensity of the Electricity Mix and Its Application to the Demand Response of Residential Heating," Energies, vol. 12, no. 7, p. 1345, Apr. 2019.

Clauß, J., Stinner,S., Sartori, I., Georges,L. 2019b. Predictive rule-based control to activate the energy flexibility of Norwegian residential buildings: Case of an air-source heat pump and direct electric heating," Appl. Energy, vol. 237, pp. 500-518, Mar. 2019.

Clauß, J., Georges, L. "Model complexity of heat pump systems to investigate the building energy flexibility and guidelines for model implementation," Appl. Energy, vol. 255, no. 113847, 2019.

De Coninck, R., Helsen, L. 2016. Quantification of flexibility in buildings by cost curves - Methodology and application," Appl. Energy, vol. 162, pp. 653-665, 2016.

De Coninck, R., Baetens, R., Saelens, D., Woyte, A., Helsen, L. 2014. "Rule-based demand side management of domestic hot water production with heat pumps in zero energy Neighbourhoods, Journal of Building Performance Simulation, 271-288

Dentel, A. and Betzold, C., 2017. Control Strategies for Geothermal Heat Pump Systems in Combination with Thermal and Electrical Storage Units. Building Simulation 2017

Dott, R., Haller, M. Y., Ruschenburg, J., Ochs, F., Bony, J. 2013. The Reference Framework for System Simulations of the IEA SHC Task 44 / HPP Annex 38 - Part B: Buildings and Space Heat Load, Muttenz, Institute of Energy in Building, FHNW

EN 442. 2015. Radiators and convectors. European Committee for Standardization, June 2015, Brussels

EN ISO 13370. 2017. Thermal performance of buildings heat transfer via the ground – calculation methods. *European Committee for Standardization*, June 2017, Brussels

EnDK. 2018. Model energy prescription of the cantons, Edition 2014 of January 9 2015, updated in 2018 due to new standards, Conference of Energy Directors (EnDK) of the cantons, April 20, 2018, Berne

European Parliament. 2018. Directive (EU) 2018/844 of the European Parliament and of the Council of 30 May 2018 amending Directive 2010/31/EU on the energy performance of buildings and Directive 2012/27/EU on energy efficiency, Journal of the European Union, L 156/75, 19.6.2018, Brussels, EU

Equa Simulation Technology AB .1999. IDA Simulation Environment. Version 2.11, Reference manual, Sundbyberg, Sweden, www.equa.se

Franzoi, N. 2020. Simulation-based optimization of a heating system in a high-performance building. Master's thesis.

Gabathuler, H.R., Mayer, H., Afjei, Th. 2002. Standardschaltungen für Kleinwärmepumpen-anlagen, Teil 1: STASCH Planungshilfen, Final report SFOE, Diessenhofen

Gervind, P, Ruud, S., Petterson, U., Björkman, J. .2011. Erfarenhetsåterföring från Hamnhuset - Uppföljande mätningar av energianvändningen och termisk komfort i ett lågenergihus (In Swedish) – Experience feedback from Hamnhuset – Follow-up measurements of energy use and thermal comfort in a low-energy house, SP Rapport 2011:79, Borås, Sweden.

Gronborg Junker, R., Ghasem Azar, A., Amaral Lopes, R., Byskov Lindberg, K., Reynders, G., Relan, R., Madsen, H. 2018. Characterizing the energy flexibility of buildings and districts, Applied Energy (225), 175-182.

Haghighi, M. M. 2013. Controlling Energy-Efficient Buildings in the Context of Smart Grid?: A Cyber Physical System Approach," University of California at Berkeley, 2013.

Heimrath, R., Lerch, W., Mach, T., Ramschak, T., Fink, F. (2018): Hohe solare Deckungsgrade durch thermisch aktivierte Bauteile im urbanen Umfeld – solSPONGEhigh; Projektbericht im Rahmen des Programms Haus der Zukunft, im Auftrag des Bundesministeriums für Verkehr, Innovation und Technologie; Berichte aus Energie- und Umweltforschung 20/2018

Hengel, F., Heinz, A. Rieberer, R. 2016. Performance analysis of a heat pump with desuperheater for residential buildings using different control and implementation strategies. Applied Thermal Engineering 105, 256–265.

Khilström, P. 2016. Optimering av pumpdrift i Skanska Deep Green Cooling (In Swedish), Uppsala Tekniska Universitet, Sweden (Master's Thesis).

Killian, M., Kozek,M. 2016. Ten questions concerning model predictive control for energy efficient buildings," Build. Environ., vol. 105, pp. 403-412

Kley, Ch. 2018. Untersuchungen zur Steigerung der Eigenstromnutzung in EnergiePLUS – Gebäuden, Dissertation, IGS, TU Braunschweig

Kristjansdottir, T. F. et al. 2018. Is a net life cycle balance for energy and materials achievable for a zero emission single-family building in Norway?, Energy Build., vol. 168, pp. 457-469, 2018.

Magni, M., Ochs, F. Bonato, P. D'Antoni, M. Geisler-Moroder, D. de Vries, S. Loonen, R. Maccarini, A. Afshari, A., Calabrese, T. 2019. Comparison of simulation results for a reference office building - analysis of deviations for different BES tools. In *IBPSA Proceedings*, Volume 16. University of Innsbruck.

Meteotest, 2015. Meteonorm, Global Meteorological Database for Engineers, Planner and Educations, Berne

The Mathworks. 2017. Matlab-Simulink. 2017. Release 17a

Monteleone, W. 2019. Modelling and dynamic simulation of a groundwater heat pump with desuperheater installed in a Passivhaus based on monitoring data. Master's thesis.

Ochs, F., Dermentzis, G., Feist, W. 2014. Minimization of the residual energy demand of multi-storey passive houses energetic and economic analysis of solar thermal and PV in combination with a heat pump. Energy Procedia 48, 1124–1133.

Ochs, F., Dermentzis, G., Monteleone, W. 2019. Simulation-assisted optimization of the HVAC system of NZE multi-family buildings. In IBPSA Proceedings, Volume 16. University of Innsbruck.

SIA 380/1. 2016. Space heating demand, Swiss society of Engineers and Architects, Zurich

Siegele, D., Leonardi, E., Ochs, F. 2019. A new Matlab Simulink Toolbox for dynamic building simulation with BIM and hardware in the loop compatibility. In IBPSA Proceedings.University of Innsbruck.

Solar-Institute Juelich. 2018. Carnot toolbox ver. 6.3, 10/2018 for Matlab Simulink R2018b. Solar-Institut Jülich, FH Aachen

Solar-Institute Juelich. 2017. CARNOT Toolbox 6.1. Retrieved 11 12, 2019, from https://de.mathworks.com/matlabcentral/fileexchange/68890-carnot-toolbox

Solar Energy Lab. 2017. TRNSYS - A Transient System Simulation Program – Trnsys, Version 17.2.004, Univ. of Wisconsin

SVEBY. 2009. Brukarindata för energiberäkningar i bostäder (in Swedish), projekt rapport

Ylmén, P., & Persson, J. 2017. Monitoring of Pilot Sites. Grant agreement: ENER/FP7/285173/NEED4B

Yuan, T. et al. 2017. Thermodynamic and economic analysis for ground-source heat pump system coupled with borehole free cooling, Energy and Buildings, 155.

Zhou, Z. et al. 2016. The energy-saving effects of ground-coupled heat pump system integrated with borehole free cooling: A study in China. Applied Energy 183.

Heat Pump Centre
c/o RISE - Research Institutes of Sweden
PO Box 857
SE-501 15 BORÅS
Sweden
Tel: +46 10 516 5512
E-mail: hpc@heatpumpcentre.org

www.heatpumpingtechnologies.org

Report no. HPT-AN49-4

www.heatpumpingtechnologies.org